Analysis and Estimation of Effective Built-In Temperature Difference for North Tangent Slabs

Data analysis from the Palmdale, California Rigid Pavement Test Site

Draft Report Prepared for the California Department of Transportation

by:

Shreenath Rao and Jeff Roesler

University of Illinois
Urbana, IL 61801

Pavement Research Center
Institute of Transportation Studies
University of California Berkeley
University of California Davis

May 2004

TABLE OF CONTENTS

LIST OF FIGURES

LIST OF TABLES

1.0 INTRODUCTION

As part of the California Department of Transportation (Caltrans) Long Life Pavement Rehabilitation Strategies (LLPRS), a high early strength hydraulic cement was field tested using the Heavy Vehicle Simulator (HVS). This fast-setting hydraulic cement concrete (FSHCC) was designed to gain enough strength to allow it to be opened to traffic within 4 hours of placement. The objective of the HVS tests was to evaluate the performance of this concrete under the influence of simulated loads along with pavement design features such as dowels, tied concrete shoulder, and a wide truck lane that had not previously been implemented in California.

Two full-scale test pavements, each approximately 700 ft. (215 m) in length, were constructed on State Route 14 about 5 miles (8 km) south of Palmdale, California using FSHCC. The South Tangent was constructed along State Route 14 southbound and was used to conduct a fatigue evaluation of the FSHCC with three thicknesses of PCC [4, 6, and 8 in. (100, 150, and 200 mm)]. The North Tangent test sections, constructed on State Route 14 northbound, were 8-in. (200-mm) nominal thickness PCC over a 4-in. (100-mm) nominal thickness cement-treated base and included several design features: asphalt concrete shoulders, PCC shoulders with dowels, and widened lanes with dowels). Design details of these sections are outlined in Roesler et al. and in du Plessis.(*1, 2*) These sections were constructed and evaluated using the HVS over a 2-year period.

Prior to fatigue testing of these slabs, many of them were monitored over 24-hour cycles without any applied load (with and without a temperature control box). The slabs were also monitored over 24-hour cycles under the influence of 9,000-lb. (40-kN) dual-wheel rolling load (with and without a temperature control box). These sections were also loaded from 4,500 lb. to 18,000 lb. (20–80 kN), in increments of 2,250 lb. (10 kN) using the HVS dual-wheel rolling load

within 1 to 2 hours and with the temperature control box. All loads were applied bi-directionally at low speeds [approximately 6 MPH (10 km/h)].

This report presents analyses of the daily movement of the slabs observed over 24-hour cycles, particularly corner and edge deflections under the loaded and unloaded condition, with and without the temperature control box, and uses them to evaluate curling in the slab and estimate the effective built-in temperature difference in the slab. For analysis purposes, particularly in estimation of stresses, damage, and cracking, this effective built-in temperature difference in the slab can be used to represent the combined effects of nonlinear built-in temperature gradients, irreversible shrinkage, and creep. A brief summary of the sections used in the analyses is shown in Table 1.

Table 1 Properties of Sections Included in Analyses

Section	Slab Thickness, in. (mm)	PCC Density, pcf (g/ml)	Joint Spacing: Left-Test Slab-Right, ft. (m)	Dowels?	Shoulder Type	Slab Width, ft. (m)	Crack Location, Slab @ ft. (m)
535FD	8.64 (219)	154 (2.47)	13.5-12.2-17.6 (4.11-3.72-5.36)	No	AC	12.0 (3.66)	Right @ 7.5 (2.29)
537FD	8.38 (213)	143 (2.29)	19.0-12.9-12.0 (5.79-3.93-3.66)	Yes	Tied PCC	12.0 (3.66)	Left @ 6.3 (1.92)
538FD	8.70 (221)	149 (2.37)	19.2-12.9-12.3 (5.85-3.93-3.75)	Yes	Tied PCC	12.0 (3.66)	Left @ 9.7 (2.96)
539FD	7.99 (201)	151 (2.42)	19.2-12.6-12.2 (5.85-3.84-3.72)	Yes	Widened lane w/AC	14.0 (4.27)	Left @ 10.0 (3.05)
540FD	8.78 (223)	151 (2.42)	19.2-12.5-12.5 (5.85-3.81-3.81)	Yes	Widened lane w/AC	14.0 (4.27)	Left @ 9.9 (3.02)
541FD	9.59 (244)	149 (2.37)	19.4-12.8-12.0 (5.91-3.90-3.66)	Yes	Widened lane w/AC	14.0 (4.27)	Left @ 10.2 (3.11)

1.1 Description of Curling

Curling in concrete slabs is a combination of 5 nonlinear components:

1. Temperature gradient through the slab: During daytime, the top of the PCC slab is typically warmer than the bottom, resulting in a positive temperature gradient through the slab. During nighttime, the top of the PCC slab is typically cooler than the

bottom, resulting in a negative temperature gradient through the slab. Several field studies have shown that these temperature gradients are nonlinear and that the daily fluctuation in temperature is greater at the surface than at the bottom of the slab.(*3–5*) Air temperature, solar radiation, cloud cover, and precipitation affect temperature gradients in concrete slabs.

2. Moisture gradient through the slab: The moisture content in concrete affects the reversible concrete shrinkage. The surface of the slab [the top 2 in. (50 mm) is typically only partially saturated compared to the bottom, which is usually saturated.(*6*) Differences in concrete moisture content will cause the slab to curl upward. These moisture gradients are affected by atmospheric relative humidity and weather phenomena such as rainfall, snow, etc., and design factors such as pavement layer materials (permeable base versus poorly draining soil layers).
3. Built-In Temperature Gradient: PCC paving is typically performed during daytime in warmer months of the year. During daytime paving, the top of the slab is warmer than the bottom of the slab at the concrete set time. Since the PCC slab sets under this condition, the flat slab is associated with the temperature gradient it had at the time it set. When the temperature gradient in the slab is zero, the slab curls upward rather than remaining flat. Thus, an effective negative temperature gradient is "built into" the slab, and is referred to as the "built-in construction temperature gradient." The built-in temperature gradient is affected by air temperature and weather conditions during set and curing conditions.
4. Differential Drying Shrinkage: Drying shrinkage is defined as "the reduction in concrete volume resulting from a loss of water from the concrete after hardening"(*7*)

and is caused principally by the contraction of the calcium silicate gel when the moisture content of the gel is decreased.(*8*) Significant irreversible drying occurs in a concrete pavement to a shallow depth [approximately 2 in. (50 mm)].(*6, 9, 10*) The shrinkage at the surface is affected by early-age curing conditions. The drying shrinkage at the bottom of the slab is significantly lower due to the high relative humidity in the pores.

5. Creep: A portion of the fixed curling in the slab (built-in temperature gradient + differential drying shrinkage) may be recovered through the creep of the slab caused by restraints from shoulder and adjacent slabs as well as slab self weight.(*11, 12*) Creep mechanisms reduce shrinkage strain in restrained concrete by at least 50 percent.(*13*)

The five factors listed above are summarized in Table 2. The total amount of curling in a slab due to a combination of the above factors can be represented as a temperature difference—the total effective linear temperature difference (TELTD), ΔT_{tot}:

$$\Delta T_{tot} = \Delta T_{tg} + \Delta T_{mg} + \Delta T_{bi} + \Delta T_{shr} - \Delta T_{crp} \quad \textbf{(1)}$$

where,

ΔT_{tg} = Temperature difference between top and bottom of a slab equivalent to (i.e., producing similar response to) non-linear vertical temperature gradients in the slab.

ΔT_{mg} = Temperature difference between top and bottom of a slab equivalent to (i.e., producing similar response to) non-linear vertical moisture gradients in the slab.

ΔT_{bi} = Temperature difference between top and bottom of a slab equivalent to (i.e., producing similar response to) non-linear construction temperature gradient "built into" the slab.

ΔT_{shr} = Temperature difference between top and bottom of a slab equivalent to (i.e., producing similar response to) irreversible differential drying shrinkage between top of the slab and bottom of the slab.

ΔT_{crp} = Portion of ΔT_{bi} and ΔT_{shr} recovered through the long-term creep of the slab.

Table 2 Five Components of Curling in Concrete Pavement Slabs

Cause of Slab Curling	Frequency (Best Description)	Comments
Temperature Gradient	Daily variation + weather	Result of differential temperature changes through the slab and affected by day/night fluctuations in air temperature, solar radiation, and weather phenomena
Moisture Gradient	Seasonal variation + weather (e.g., rainfall)	Result of differential changes in slab moisture/humidity and affected by atmospheric humidity, weather phenomena, and drainage
Built-In Temperature Gradient	Fixed	Result of temperature gradients during concrete set and affected by air temperature and weather phenomena during set and curing conditions
Differential Drying Shrinkage	Fixed + short-term (majority develops during early-age)	Result of the irreversible differential loss of water in concrete and consequent contraction upon hardening and affected by early-age curing conditions
Creep	Long-term change	Recovery of fixed curl due to restraint and slab self weight

These components are affected by material properties of the slab such as coefficient of thermal expansion, thermal conductivity, permeability, etc., and depend on mix design parameters such as aggregate type, cement content and type, water content, admixtures, etc.(*14-17*)

The result of an elongation of the top of the slab relative to the bottom of the slab due to curling is a convex curvature, which is equivalent to a void beneath the middle of the slab (Figure 1a). The result of a contraction of the top of the slab relative to the bottom of the slab is a concave curvature, which creates voids beneath the edges and corners of the slab (Figure 1b).

Poblete et al. observed that curling of a concrete slab in the field was restrained by the shoulder and adjacent slabs (through aggregate interlock, load transfer devices, and tie bars) and through non-uniform friction between the base layer and concrete slab.(*18*) This restraint can vary from one location of the slab to another resulting in asymmetric concave curling of the slab as shown in Figure 1c.

The cumulative effect of built-in temperature gradient, shrinkage, and creep can be defined as an effective built-in temperature difference, ΔT_{ebi} (EBITD). The EBITD is a linear temperature difference between the top and bottom of a concrete slab that produces the same deflection response as the cumulative effects of non-linear built-in temperature gradient and non-linear shrinkage gradient reduced over time by creep.

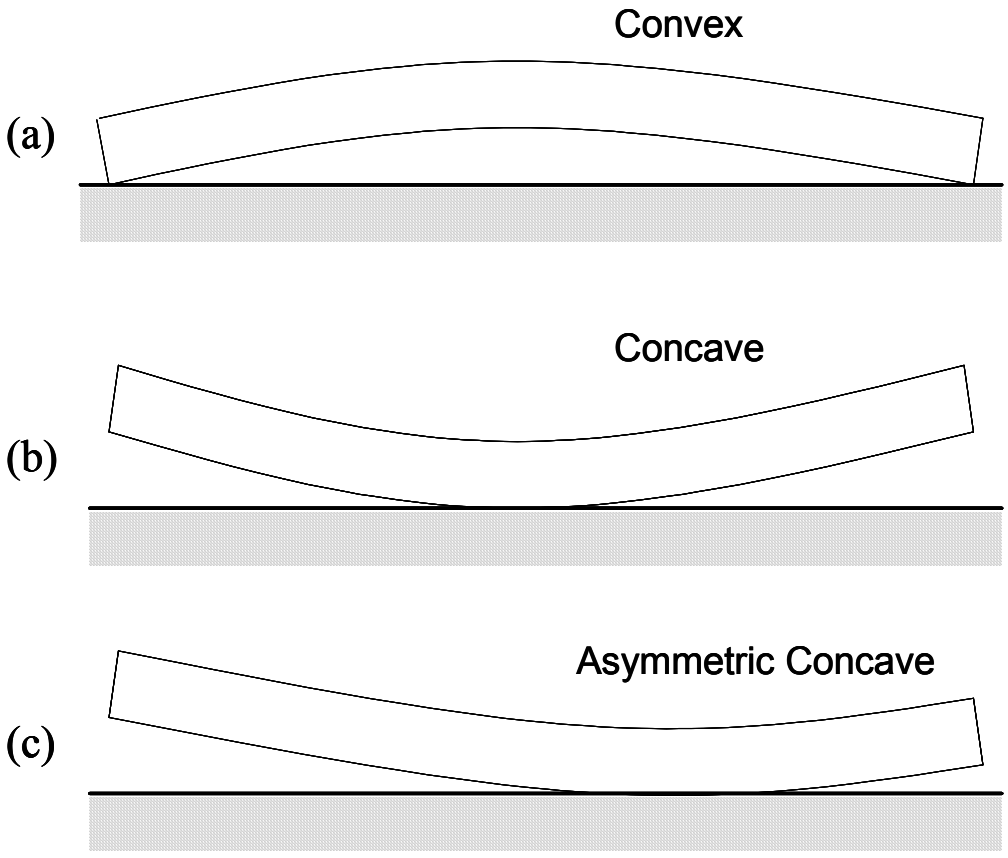

Figure 1. Slab shapes deformed by curling (cross-sectional view).

$$\Delta T_{ebi} + \Delta T_{bi} + \Delta T_{shr} - \Delta T_{crp} + \Delta T_{mg} \quad \textbf{(2)}$$

The value of ΔT_{mg} need not be included in this equation if it can be estimated or determined independently. For the Palmdale data, this term can be ignored because it is a minor factor for short term testing in desert climate. Combining Equations 1 and 2:

$$\Delta T_{tot} = \Delta T_{tg} + \Delta T_{ebi} \quad \textbf{(3)}$$

$$TELTD = \Delta T_{tg} + EBITD \quad \textbf{(4)}$$

1.2 Field Data Collection

The data collected at two-hour intervals included vertical temperature profile measured using thermocouples, midslab edge and corner surface deflections measured using Joint Deflection Measuring Devices (JDMDs), and vertical deflections (interior slab location) at multiple depths of the pavement structure measured using Multi-Depth Deflectometers (MDDs). Type K thermocouples were taped and spaced on wooden dowels at 0, 4, and 8 in. (0, 200, and 400 mm) in order to measure the temperature profile in the concrete slab. The thermocouple stacks were placed at the following four locations on each test section: in the sun (TC/sun), in the shade (TC/shade), in the temperature control box (TC/box), and near the k-rail (TC/k-rail). The JDMDs and MDDs were Linear Variable Displacement Transducers (LVDTs) used to measure vertical displacements under rolling wheel and temperature loadings. Details of the data acquisition system and instrumentation of each section are included in References (*1, 2, 19*).

2.0 ANALYSIS OF 9,000-LB. (40-KN) LOADED CORNER AND MIDSLAB EDGE DEFLECTIONS OVER A 24-HOUR CYCLE

Several North Tangent sections were loaded over a 24-hour cycle with a rolling 9,000-lb. (40-kN) dual-wheel half-axle HVS load. These 24-hour loaded tests were conducted to evaluate the intraday response of the test slabs to daily temperature fluctuations and were performed on Sections 535FD, 537FD, 538FD, 539FD, 540FD, and 541FD. All of these sections except for Sections 538FD and 541FD were tested over one 24-hour cycle with the temperature control box and over another 24-hour cycle without the temperature control box. Sections 538FD and 541FD were tested for one 24-hour cycle without the temperature control box.

2.1 Data Analysis Procedure

Deflections resulting from the rolling 9,000-lb. (40-kN) dual-wheel HVS load were measured during testing using JDMDs as described in the previous section. Corresponding vertical temperature profile data in the slab were collected using thermocouples embedded in the concrete slab as described in the previous section. The deflection and temperature data were collected approximately every two hours over the 24-hour cycle. A finite element program ISLAB2000 (*20*) was used to perform the analysis as follows:

1. An EBITD between the top of the slab and the bottom of the slab was assumed and added to the measured temperature difference to obtain the assumed TELTD (Equation 4). The analysis was performed separately for the shade thermocouple, the box thermocouple, and the k-rail thermocouple. Although the measured gradients in the slab are typically nonlinear, for computational ease they were assumed linear. This assumption does not significantly affect the results [< 2 to 4ºF (< 1.1 to 2.2ºC)] because when the temperature control box is used, the temperature differences and

the degree of nonlinearity is small and when the box is not used, the assumption affects only 2 to 3 of the 12 data points within the 24-hour cycle, the results of which are averaged out. The extent of the nonlinearity on the affected 2 to 3 points is small because of the shade provided by the HVS.

2. ISLAB2000 was used to calculate the slab deflections due to the 9,000-lb. (40 kN) load and TELTD for each of the two-hour time interval for the specific concrete slab geometry and layer properties.
3. For each two-hour time interval, a residual was calculated based on the difference in measured versus predicted deflection.
4. An iterative procedure was used to calculate the value of the EBITD that minimized the sum of square of the residuals over the 24-hour cycle:

$$R_i = \left(\delta_p - \delta_M\right)_i \quad \textbf{(5)}$$

where,

R_i = Residual corresponding to two-hour time interval *i*

δ_p = Deflection predicted using ISLAB2000 for assumed EBITD and specific concrete slab geometry and layer properties.

δ_M = Field deflections measured using JDMDs.

The above process was performed on both slab corners and the midslab edge for all test sections. Because the temperature at the surface of the slab is not known, each of the calculations was performed for the following two cases:

1. Assume that the top thermocouple sensor is located at the surface of the slab. The slab temperature difference is the difference in temperatures between the top sensor and the bottom sensor.

2. Assume that the top thermocouple sensor is located 8 in. (200 mm) from the bottom of the slab (the distance between the top sensor and the bottom sensor as installed on the wooden dowels). Because many of the test slabs are thicker than 8 in. (200 mm), the temperature at the surface of the pavement is estimated using nonlinear extrapolation using the temperatures at the top and the midslab sensors. The slab temperature difference is the difference between this extrapolated temperature and the temperature at the bottom sensor.

For slabs with high negative TELTD, loaded slab deflections can be used to calculate the TELTD and consequently the EBITD in the slab as described above. Figure 2 shows a plot of the slab deflections under the 9,000-lb. (40-kN) load (calculated using ISLAB2000) versus TELTD in the slab for Section 535FD. At low magnitude negative or positive TELTD, the loaded corner deflection is not sensitive to TELTD and thus cannot be used to estimate TELTD. In these cases, this procedure cannot be used to estimate EBITD for these slabs. In these situations, the corner of the slab (or edge of the slab) comes in contact with the base under the action of the load. When the slab is in contact with the base, the corner deflections do not depend on the total temperature difference in the slab. However, at higher negative TELTD, the slab corner (or edge) does not come in contact with the base and the predicted corner deflections are proportional to the TELTD in the slab (or total curl of the slab). The results of the analysis are summarized below for each section individually.

2.2 Section 535FD

The layout of the section and the locations of the sensors are shown in Figure 3.(*2*) The deflections measured by the JDMDs over the 24-hour cycle without the temperature control box

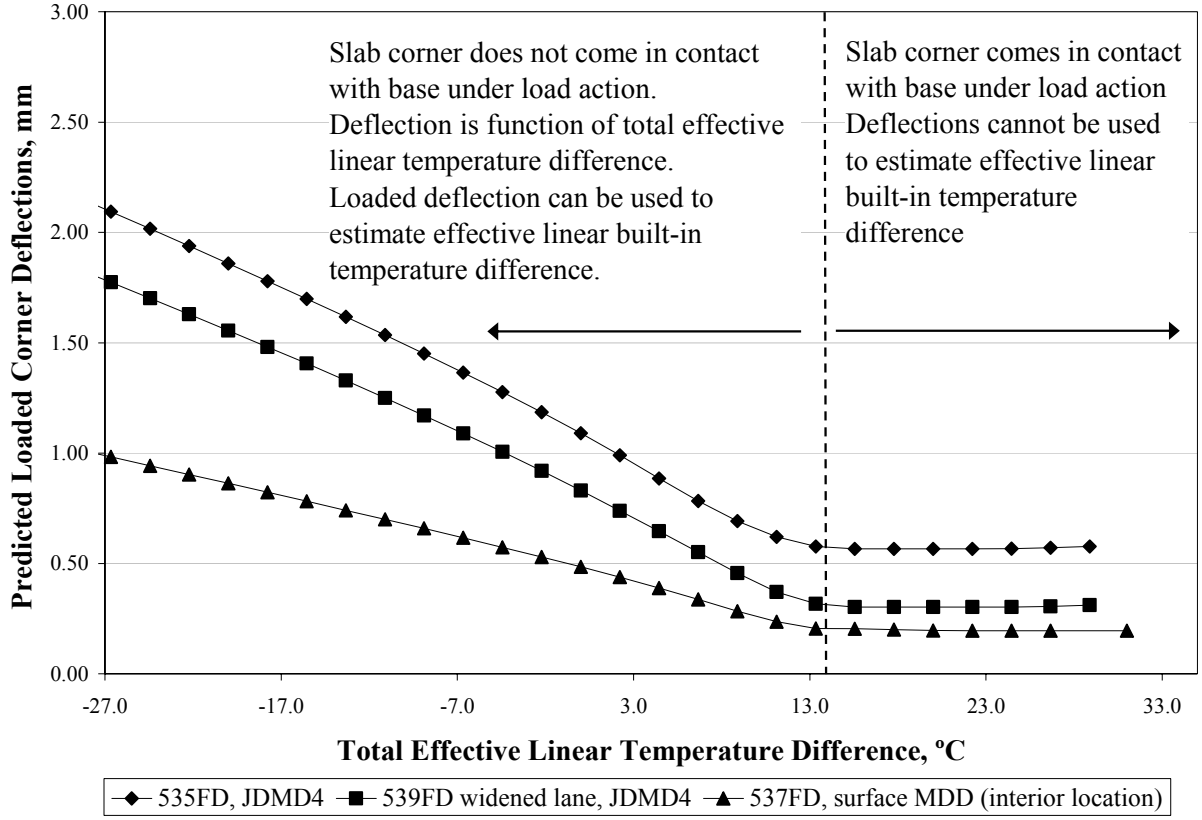

Figure 2. Predicted loaded slab deflections under influence of 9,000-lb. (40-kN) dual wheel for Section 535FD (JDMD4, slab corner deflection, slab corner loading), Section 537FD (interior MDD location deflection, slab corner loading), and widened lane Section 539FD (JDMD4, slab corner deflection, interior loading) as a function of total effective temperature difference.

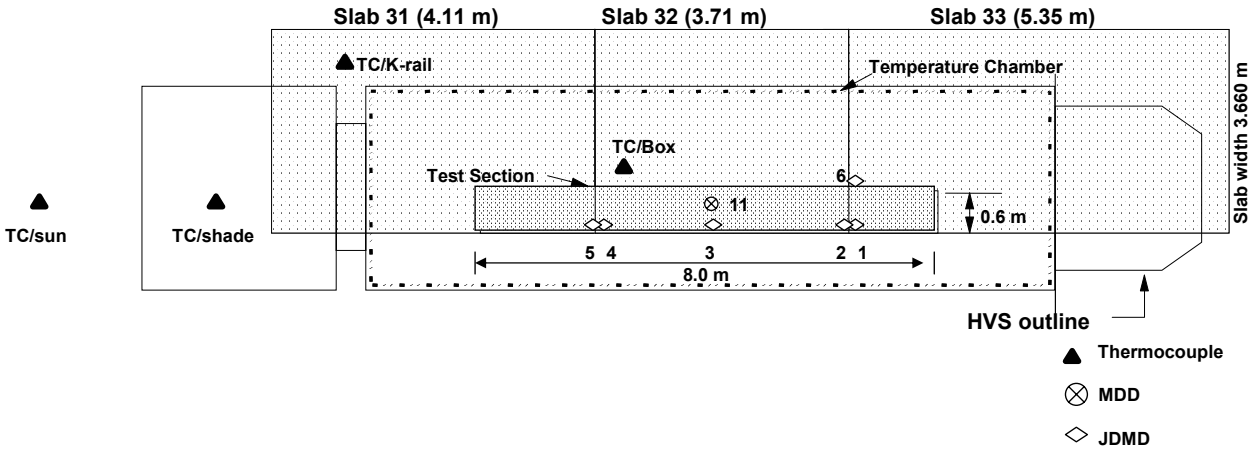

Figure 3. Instrumentation layout of Section 535FD.(*2*)

relative to the flat slab condition. The corresponding temperature differences are shown in are shown in Figure 4. The deflections measured by the MDDs over the same 24-hour cycle are shown in Figure 5. These deflections were measured relative to the unloaded slab and not Figures 6 and 7. Figure 6 shows the measured temperature difference between the top sensor and the bottom sensor. Figure 7 shows the estimated temperature difference between the top of the slab and the bottom of the slab extrapolated using the known temperatures at the 3 sensors. The slab corners and edge deflected less under positive temperature differences. Although JDMD2 and JDMD4 were two corners of the same slab, the loaded deflections were significantly different from each other. Some of this difference is a result of the asymmetry of the slab configuration, but much of it is due to discrepancies in EBITDs arising from difference in restraints between the two slab corners.

The MDD deflections shown in Figure 5 correspond to an interior location—midslab wheelpath [1 ft. (30 cm) from shoulder joint]. MDD1-1 corresponds to the deflection of the concrete slab, while MDD1-2 corresponds to that of the base course. MDD1-3 and MDD1-4 correspond to subbase and subgrade deflections, respectively. As expected, MDD1-1 deflects in tandem with the midslab edge deflection (JDMD2 from Figure 4) and deflects less under positive temperature differences. However, the deflections in the base, subbase, and subgrade are significant only when the temperature difference is positive resulting in contact of the slab with the base. This is the reason for the opposing deflection trends of MDD1-1 versus MDD1-2 through MDD1-4. When the temperature difference in the slab is negative or small, the slab does not come in contact with the base and MDD1-2 through MDD1-4 only register a small amount of elastic deformation, not affected by temperature difference in the slab.

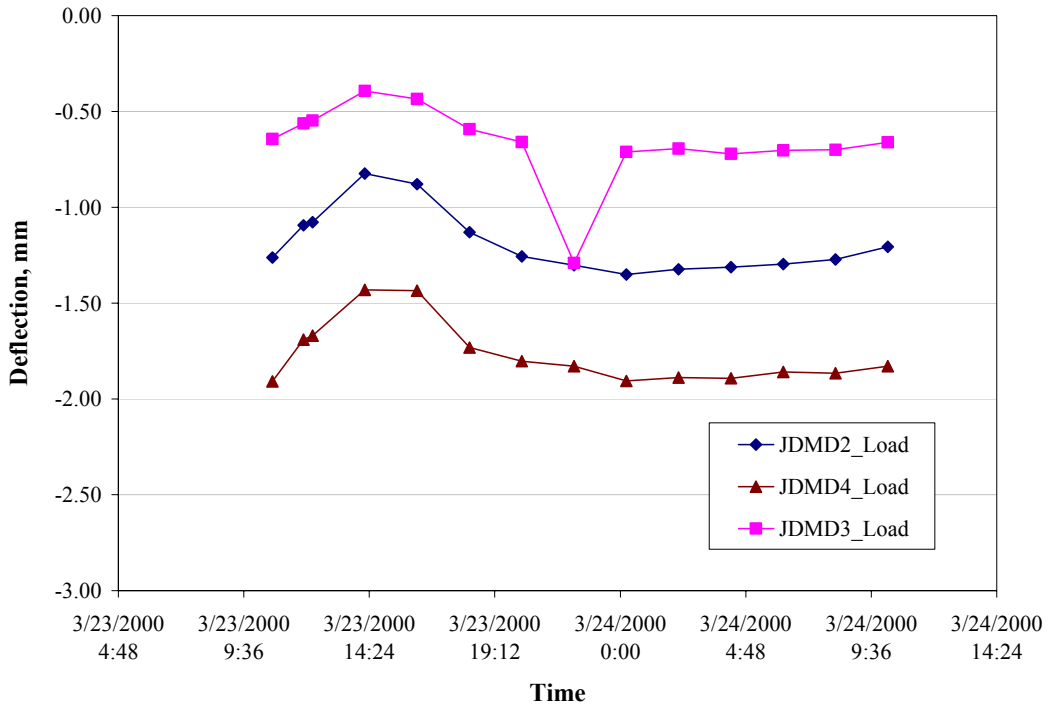

Figure 4. Corner (JDMD2 and JDMD4) and edge (JDMD3) deflections for Section 535FD without temperature control box.

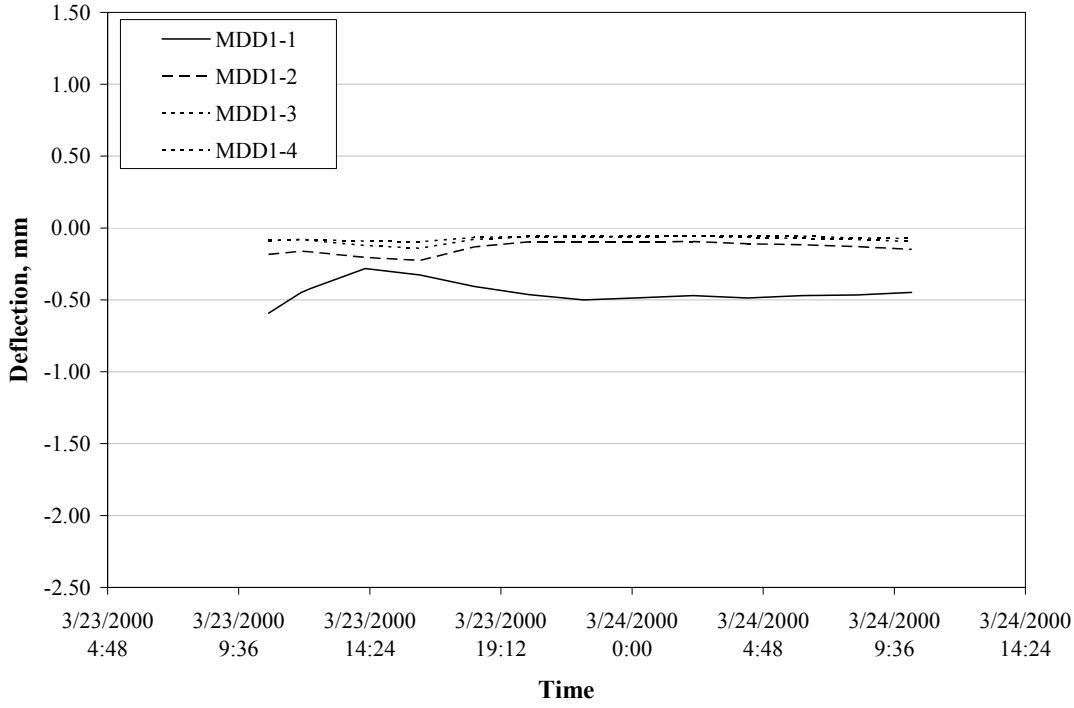

Figure 5. MDD deflections for Section 535FD measured over a loaded 24-hour cycle without temperature control box.

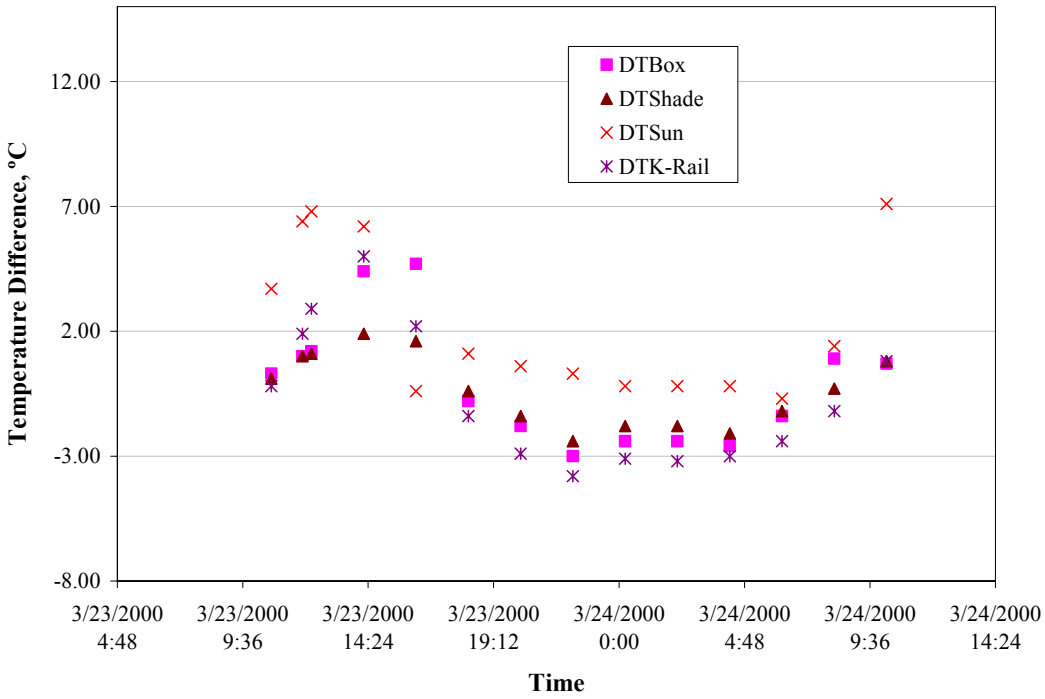

Figure 6. 24-hour temperature difference between the top sensor and the bottom sensor for Section 535FD measured using thermocouple assemblies at various locations (without temperature control box).

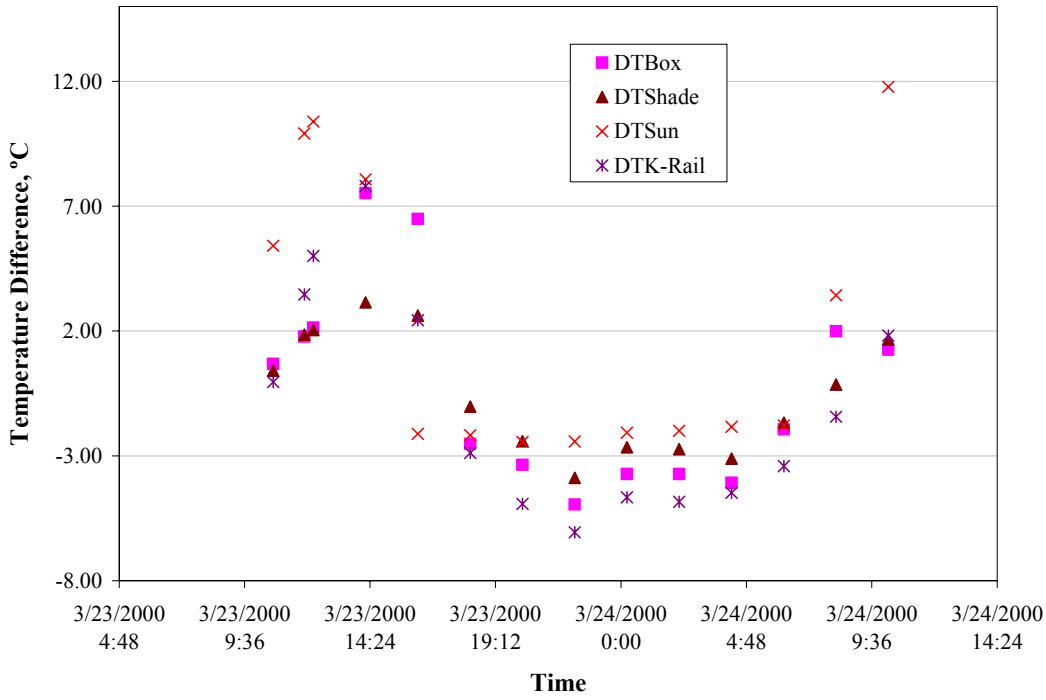

Figure 7. 24-hour temperature difference between the top of the slab and the bottom of the slab for Section 535FD estimated using extrapolation and data collected using thermocouple assemblies at various locations (without temperature control box).

The slab deflections under the 9,000-lb. (40-kN) load with the temperature control box in place are shown in Figure 8 for Section 535FD. The deflections measured by the MDDs over the same 24-hour cycle are shown in Figure 9. The corresponding temperature differences are shown in Figures 10 and 11. Even though the part of the slab corresponding to the JDMD locations was completely covered by the temperature control box, the JDMDs were affected by the temperature cycling of the exposed portion of the slab, with JDMD4 being the most effected.

As in the case of the loaded deflection measurements without temperature control, one corner of the slab (JDMD4) had higher loaded deflections than the other corner (JDMD2). Because of use of the temperature control box, positive temperature differences in the slab are small and the slab does not come in contact with the base at any time during the 24-hour period, resulting in small amount of uniform elastic deformation in MDD1-2 through MDD1-4, as seen in Figure 9.

The results of the analysis, the estimated EBITDs at three slab locations (left corner, right corner, and midslab), are shown in Table 3 using data collected with and without a temperature control box and using thermocouple data measured at various locations. Figures 12 through 14 show the residuals (difference between measured deflections and predicted deflections) as a function of various factors. The three figures show that the residuals are normally distributed about zero and are typically less than 10 percent of the measured deflections. The residuals also do not show any significant trend with temperature difference, measured deflection, or predicted deflection indicating true randomness and no other systemic cause for the difference between measured and predicted deflections.

The EBITD results for Section 535FD along with the initial cracking pattern are shown in Figure 15. As seen in the figure, the adjacent slab, slab 33, had early-age construction cracks

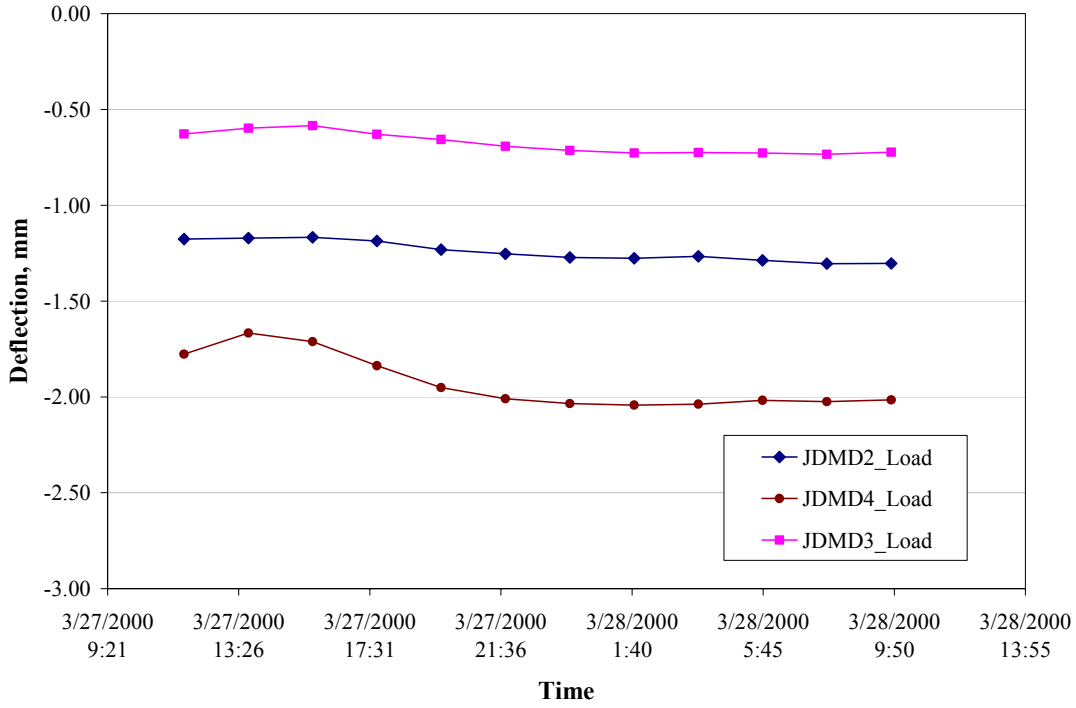

Figure 8. Corner (JDMD2 and JDMD4) and edge (JDMD3) deflections for Section 535FD with temperature control box.

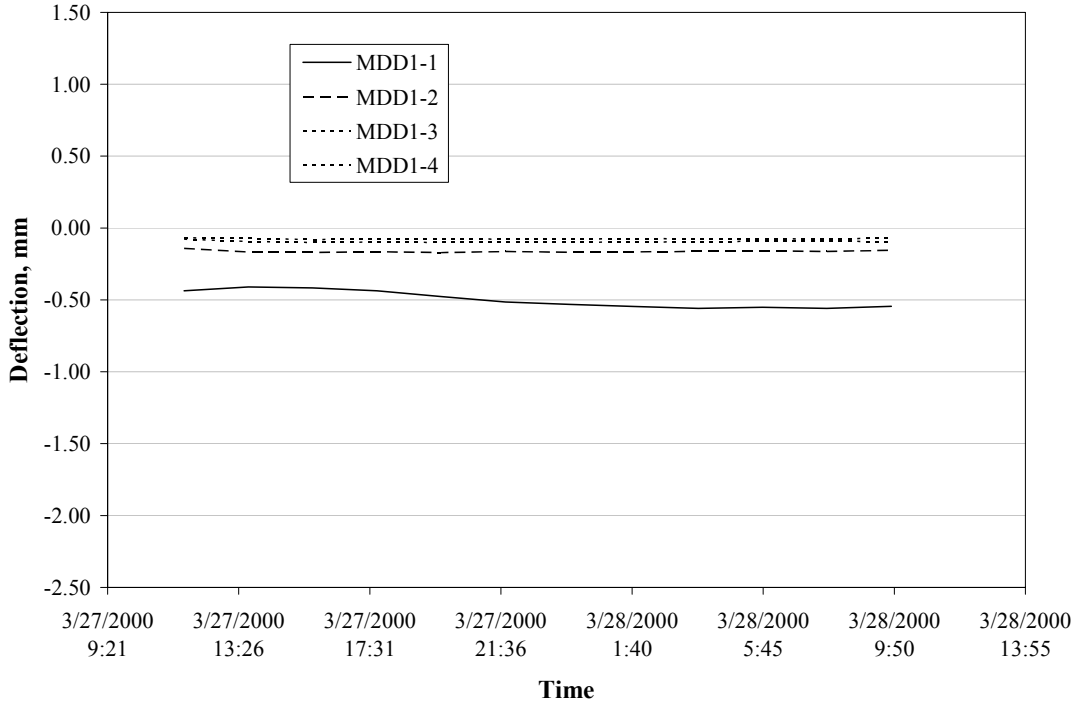

Figure 9. MDD deflections for Section 535FD measured over a loaded 24-hour cycle with temperature control box.

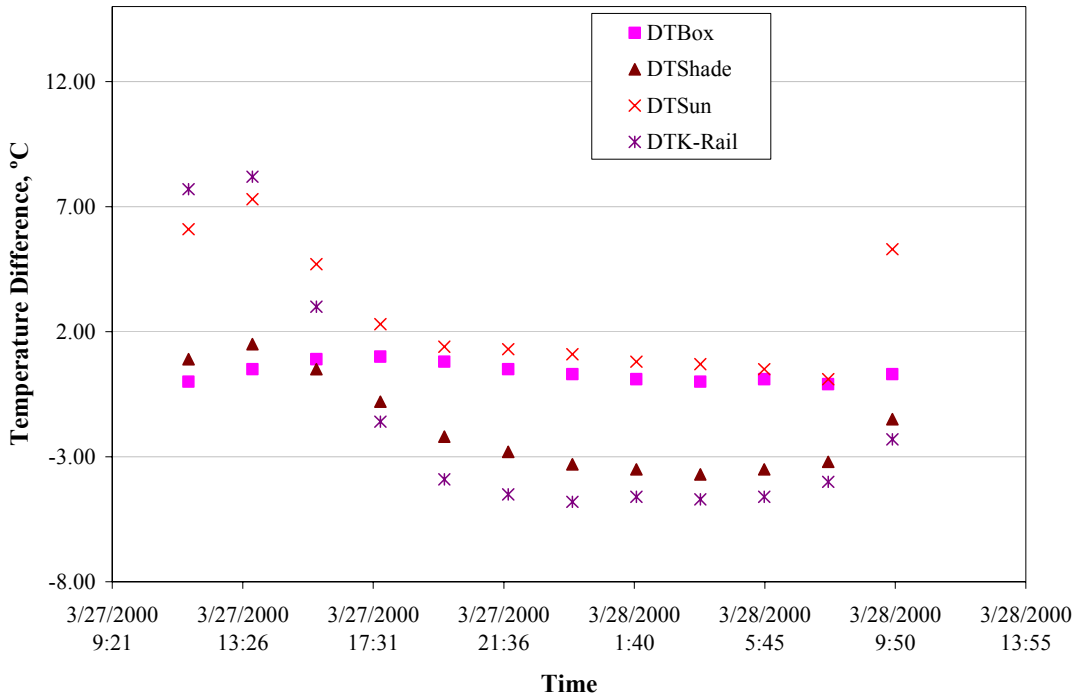

Figure 10. 24-hour temperature difference between the top sensor and the bottom sensor measured for Section 535FD using thermocouple assemblies at various locations (with temperature control box).

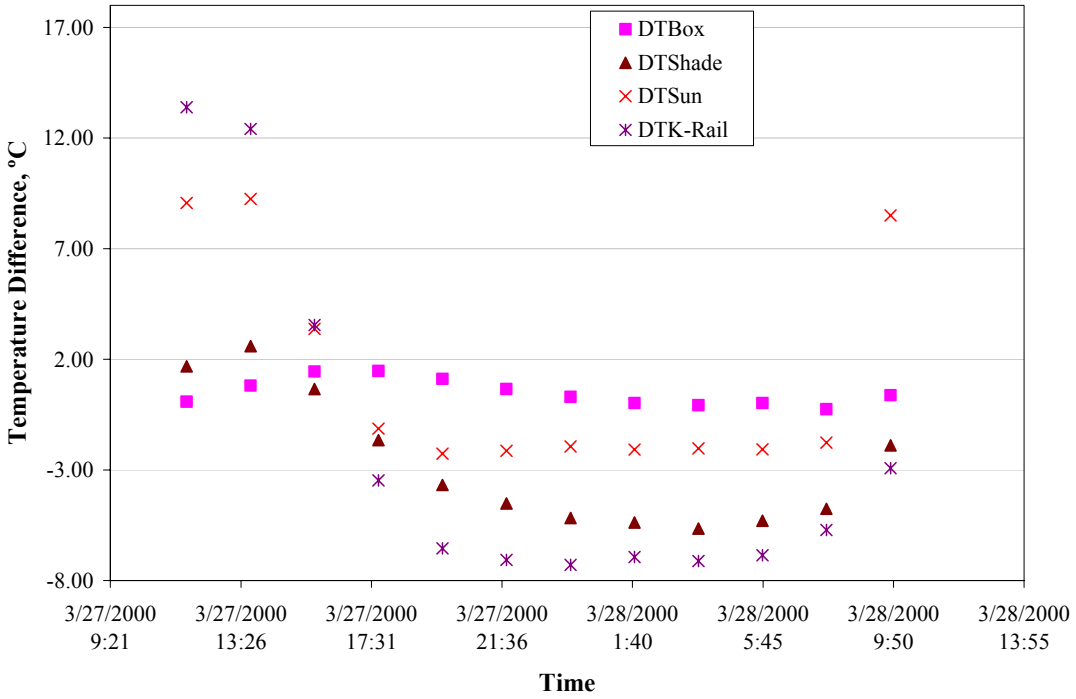

Figure 11. 24-hour temperature difference between the top of the slab and the bottom of the slab for Section 535FD estimated using extrapolation and data collected using thermocouple assemblies at various locations (with temperature control box).

Table 3 Estimated Effective Built-In Temperature Difference (EBITD) for Section 535FD at Three Locations

Location on Slab		EBITD at Slab Location for Thermocouple Location, Extrapolated and Measured, ºF (ºC)					
		Thermocouple at Box		Thermocouple in Shade		Thermocouple at K-Rail	
		Extrapolated	Measured	Extrapolated	Measured	Extrapolated	Measured
Left Corner (JDMD4)	No Box	-57 (-31.7)	-57.1 (-31.7)	-56.5 (-31.4)	-56.6 (-31.4)	-55.8 (-31.0)	-56.2 (-31.2)
	With Box	-65.5 (-36.4)	-65.3 (-36.3)	-59.7 (-33.2)	-61.4 (-34.1)	-61.2 (-34.0)	-62.3 (-34.6)
Right Corner (JDMD2)	No Box	-38.7 (-21.5)	-38.8 (-21.6)	-38.2 (-21.2)	-38.3 (-21.3)	-37.5 (-20.8)	-37.9 (-21.1)
	With Box	-42.5 (-23.6)	-42.2 (-23.4)	-36.7 (-20.4)	-38.4 (-21.3)	-37.7 (-20.9)	-39.3 (-21.8)
Midslab (JDMD3)	No Box	-36 (-20.0)	-36 (-20.0)	-35.5 (-19.7)	-35.5 (-19.7)	-34.8 (-19.3)	-35.1 (-19.5)
	With Box	-42.2 (-23.4)	-41.9 (-23.3)	-36.3 (-20.2)	-38 (-21.1)	-36.9 (-20.5)	-38.7 (-21.5)

Data was collected with and without a temperature control box and using thermocouple data measured at various locations.

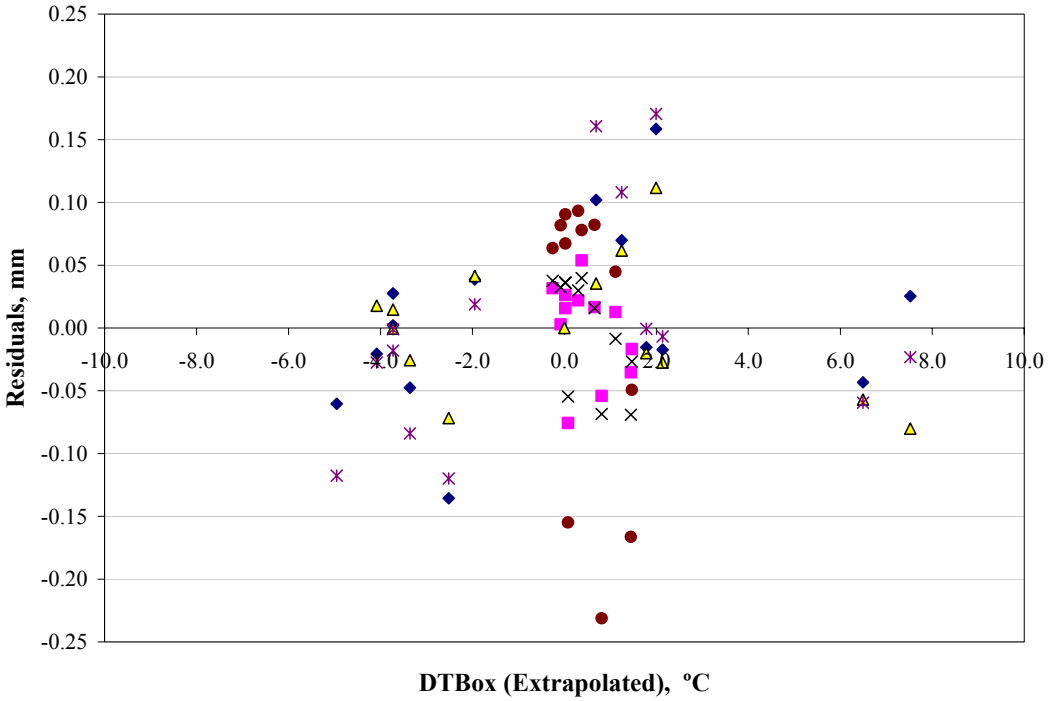

Figure 12. Residuals (difference in measured deflections and predicted deflections) as a function of extrapolated temperature difference (box) for JDMD2, JDMD3, and JDMD4 measured with and without the temperature control box for Section 535FD.

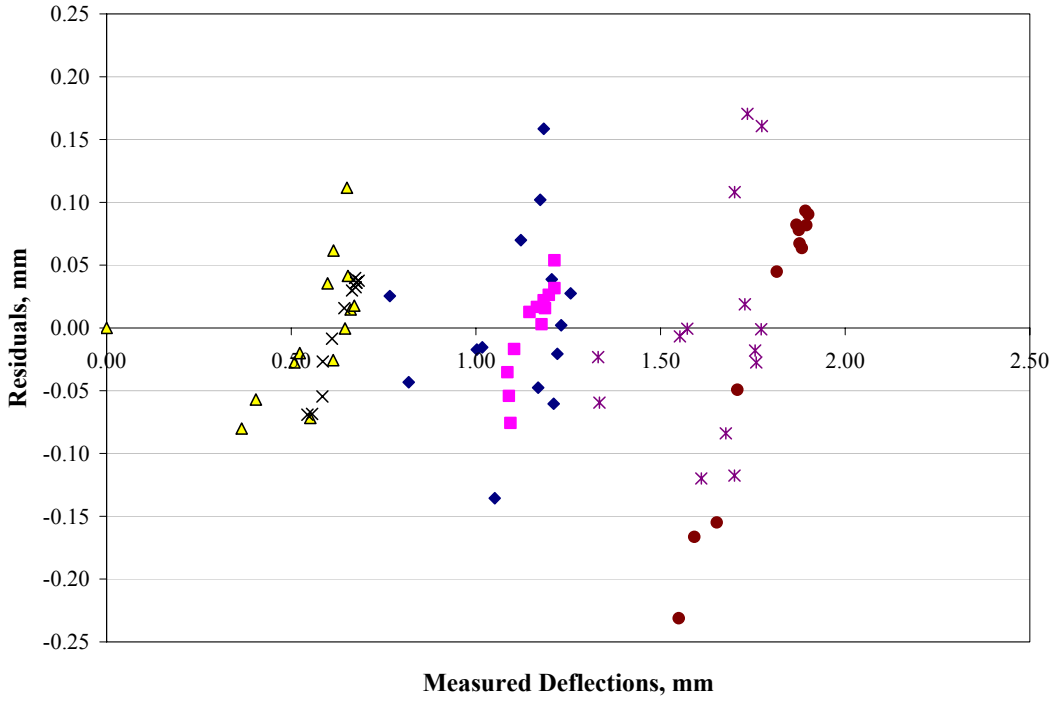

Figure 13. Residuals (difference in measured deflections and predicted deflections) as a function of measured deflections for JDMD2, JDMD3, and JDMD4 measured with and without the temperature control box for Section 535FD.

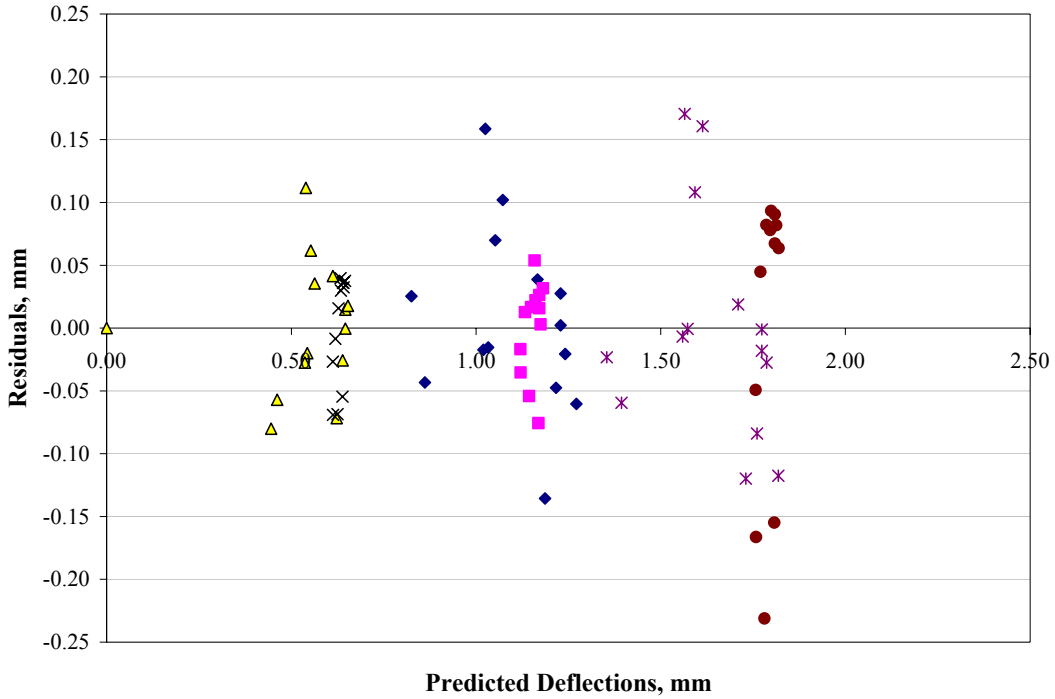

Figure 14. Residuals (difference in measured deflections and predicted deflections) as a function of predicted deflections for JDMD2, JDMD3, and JDMD4 measured with and without the temperature control box for Section 535FD.

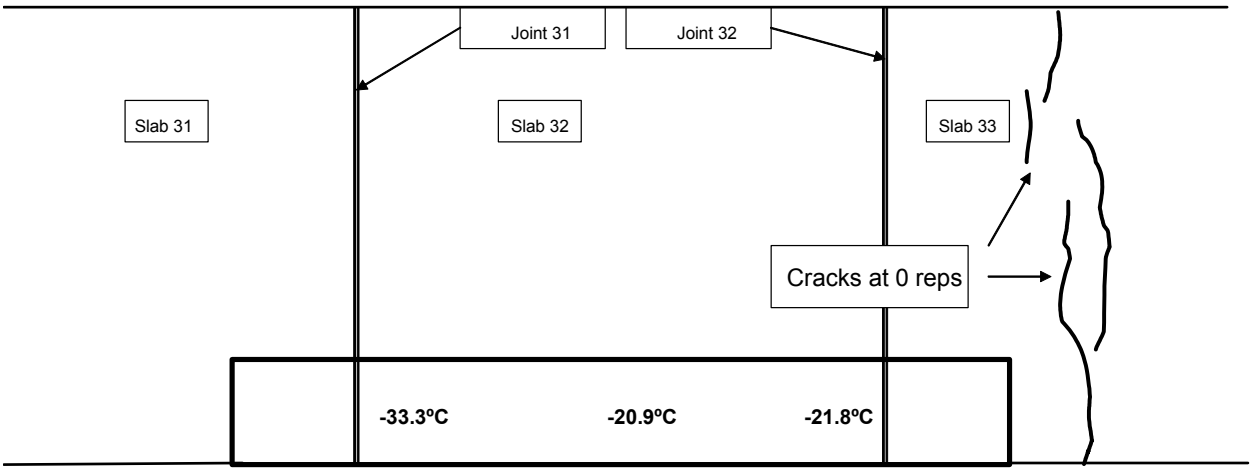

Figure 15. Crack pattern in slab (Section 535FD) prior to load application and estimated effective built-in temperature difference at three locations in the test slab.

prior to HVS loading. The crack patterns in the test slab and the adjacent slabs after loading with the HVS is shown in Figure 16. The corner break in the concrete slab corresponded to the side of the slab with the highest EBITD.

2.3 Section 537FD

The layout of Section 537FD and the location of the sensors are shown in Figure 17.(*2*) The deflections measured by the JDMDs over the 24-hour cycle without the temperature control box are shown in Figure 18. The deflections measured by the MDDs over the same 24-hour cycle are shown in Figure 19. The corresponding temperature differences are shown in Figures 20 and 21. As with Section 535FD, the slab corners and edge deflected less under positive temperature differences and the loaded deflections of JDMD2 and JDMD4 (two corners of the same slab) were significantly different from each other due to asymmetry of the slab

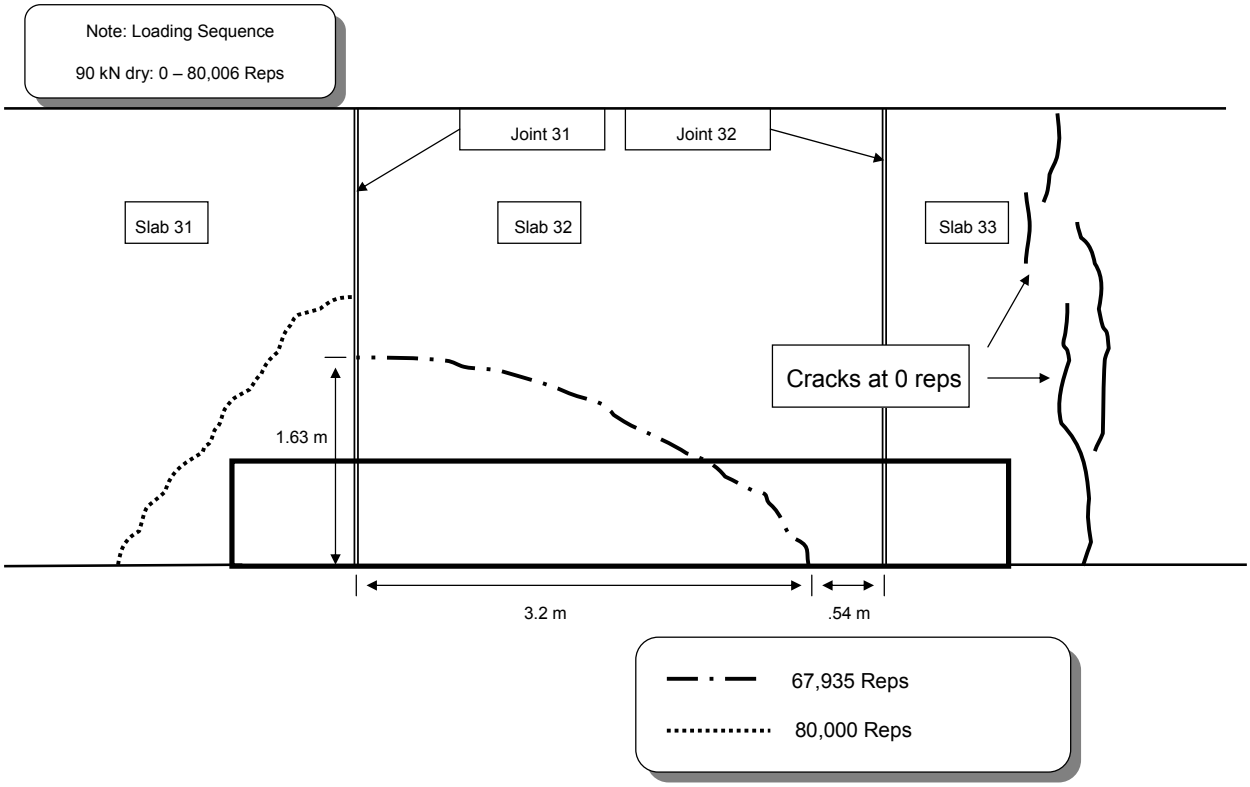

Figure 16. Crack pattern in slab (Section 535FD) after fatigue damage load application.(*2*)

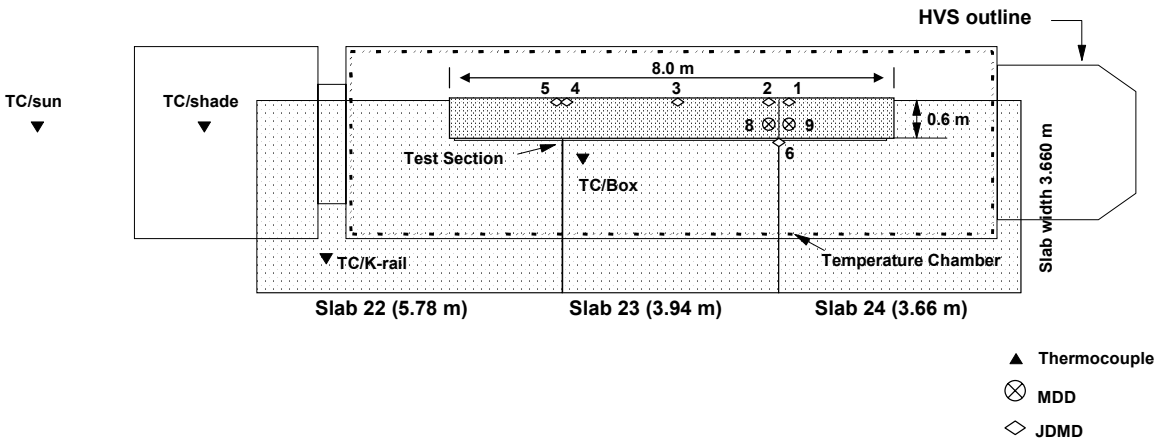

Figure 17. Instrumentation layout of Section 537FD.(*2*)

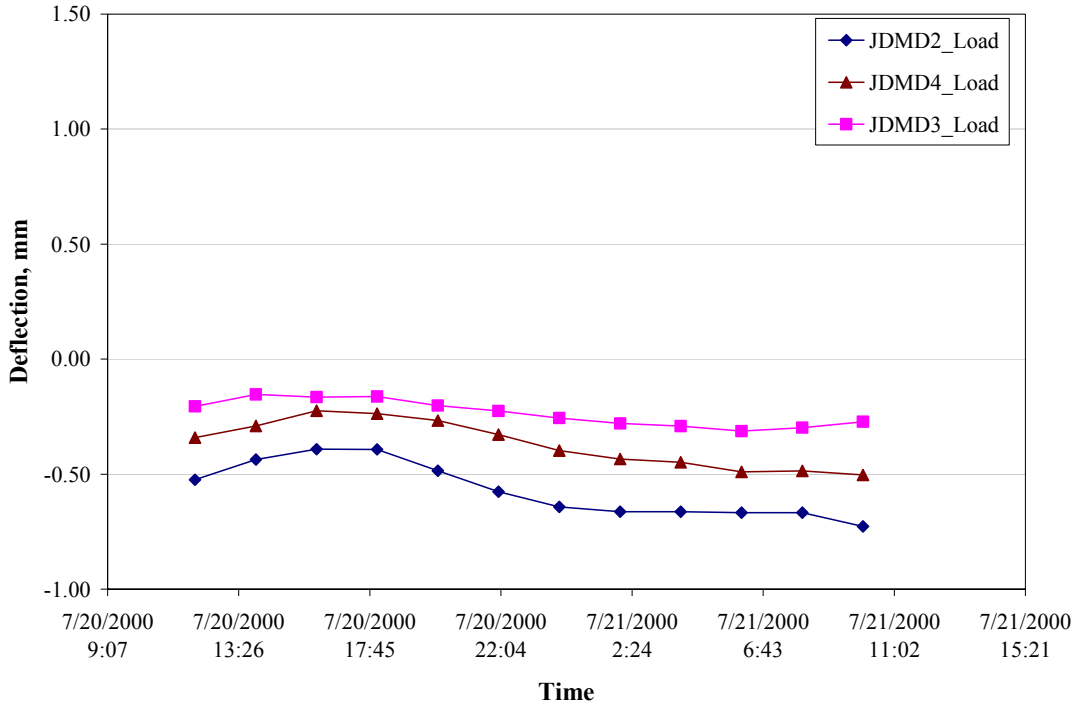

Figure 18. Corner (JDMD2 and JDMD4) and edge (JDMD3) deflections for Section 537FD without temperature control box.

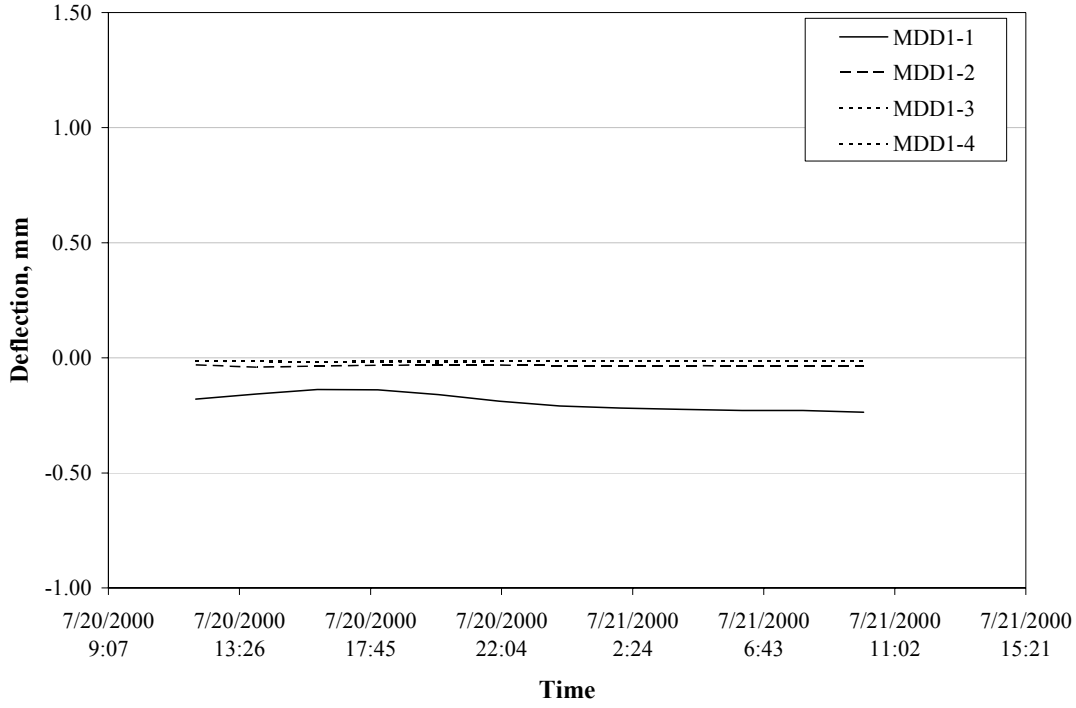

Figure 19. MDD deflections for Section 537FD measured over a loaded 24-hour cycle without temperature control box.

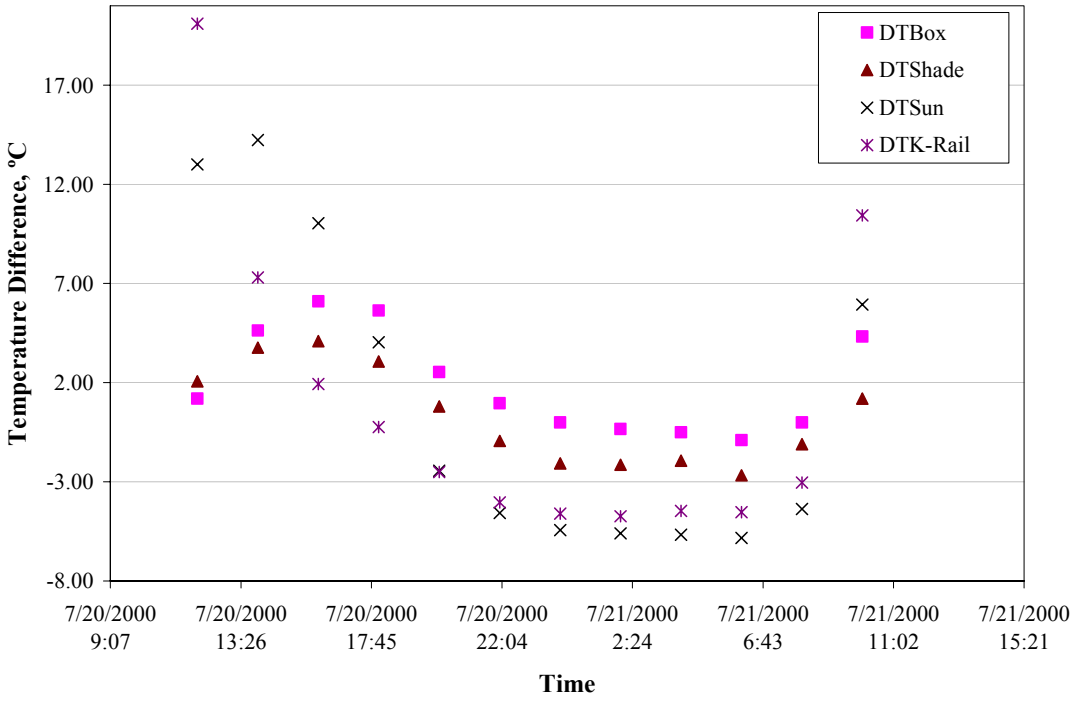

Figure 20. 24-hour temperature difference between the top sensor and the bottom sensor measured using thermocouple assemblies at various locations (without temperature control box) for Section 537FD.

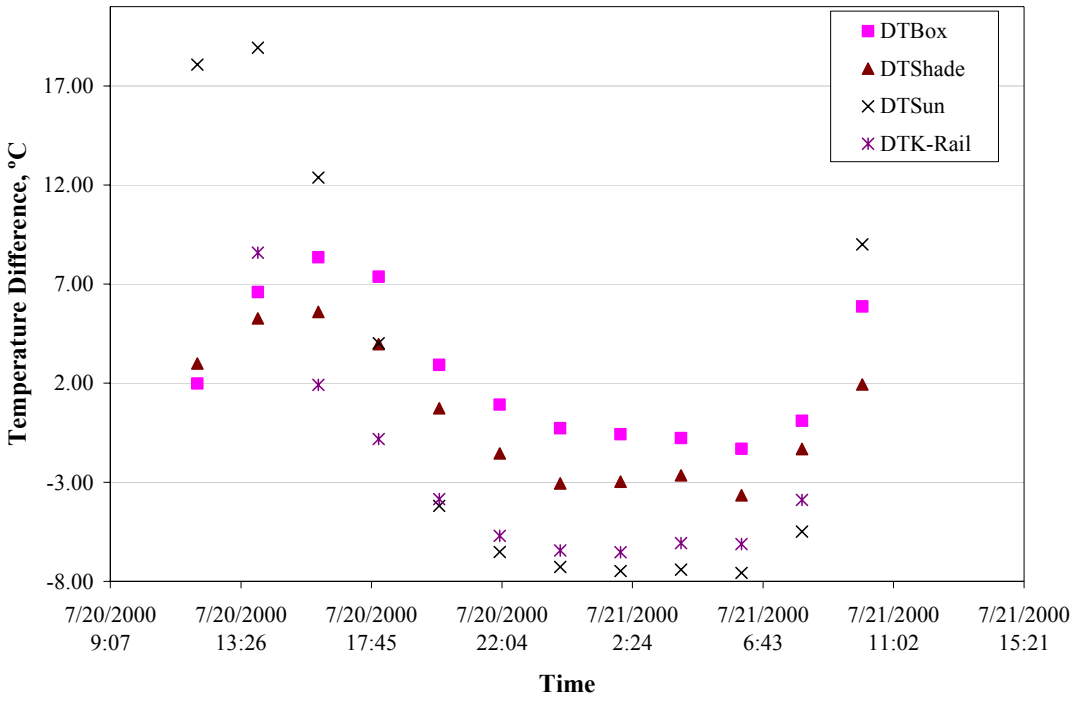

Figure 21. 24-hour temperature difference between the top of the slab and the bottom of the slab estimated using extrapolation and data collected using thermocouple assemblies at various locations (without temperature control box) for Section 537FD.

configuration and discrepancies in EBITDs arising from difference in restraints between the two slab corners.

The MDD deflections (Figure 19) correspond to an interior location—right corner wheelpath [1 ft. (30 cm) from the transverse joint and 1 ft. (30 cm) from the shoulder joint]. MDD1-1 corresponds to the deflection of the concrete slab, while MDD1-2 corresponds to that of the base course. MDD1-3 and MDD1-4 correspond to subbase and subgrade deflections, respectively. As expected, MDD1-1 deflects in tandem with the right corner deflection (JDMD2 from Figure 4) and deflects less under positive temperature differences. However, the slab does not come in contact with the base, and MDD1-2 through MDD1-4 only register a small amount of elastic deformation, which is unaffected by temperature difference in the slab.

The slab deflections under the 9,000-lb. (40-kN) load measured with the temperature control box are shown in Figure 22 for Section 537FD. The deflections measured by the MDDs over the same 24-hour cycle are shown in Figure 23. The corresponding temperature differences are shown in Figures 24 and 25. The inconsistency of the thermocouple readings inside the temperature control box over the 24-hour cycle suggests that the temperature control box was not functioning adequately during this period. The positive temperature differences in the slab, particularly at the right slab corner are small and the slab does not come in contact with the base at any time during the 24-hour period, resulting in small amount of uniform elastic deformation in MDD1-2 through MDD1-4 as seen in Figure 23.

The results of the analysis, the estimated EBITDs at three slab locations, are shown in Table 4. As described earlier and illustrated in Figure 2, when the slab is in contact with the base, the deflections do not depend on the total temperature difference in the slab. At low negative or positive TELTD, the slab comes in contact with the base and the loaded deflection is not sensitive to TELTD and thus cannot be used to estimate TELTD and consequently EBITD. For Section 537FD, this is the case at the left corner (JDMD4) and midslab (JDMD3). The EBITD at these two locations of Section 537FD is low negative or positive [> -9.0ºF (> -5.0ºC)]. In this report, "> -X" is used to denote a value that is less negative or positive and represents a slab location with a small negative (concave) curvature or a positive (convex) curvature.

Figures 26 through 28 show the residuals (difference between measured deflections and predicted deflections) as a function of various factors. The EBITD results along with the initial cracking pattern are shown in Figure 29. The crack patterns in the test slab and the adjacent slabs after loading with the HVS are shown in Figures 30. As with Section 535FD, the corner break in the concrete slab corresponded to the side of the slab with the highest EBITD.

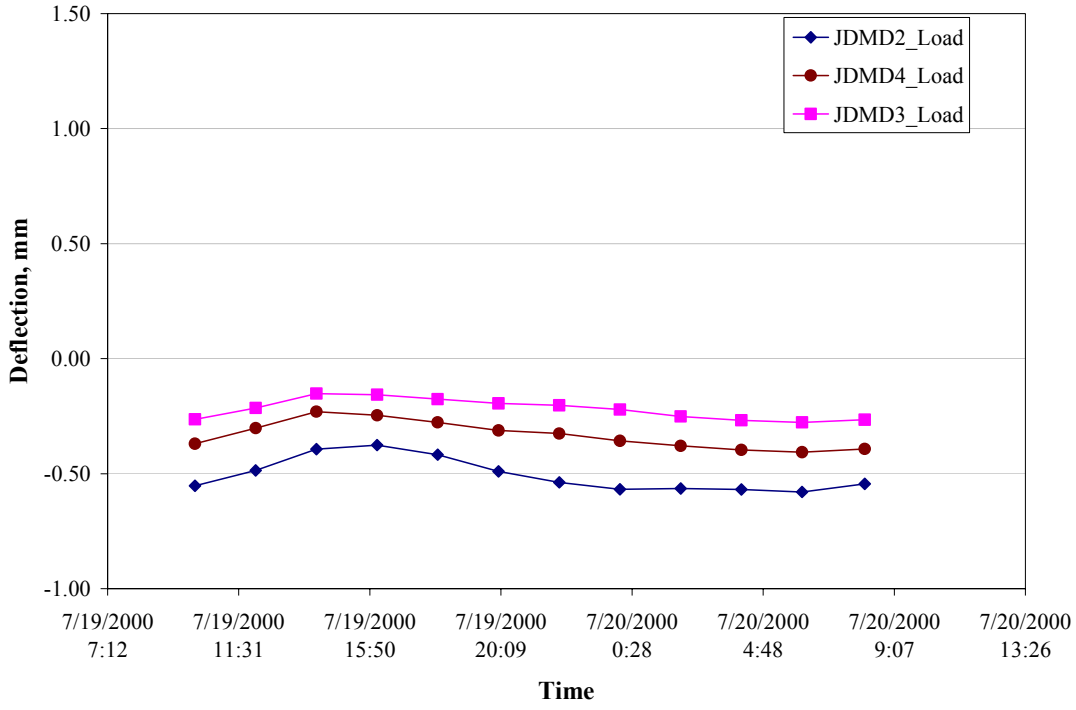

Figure 22. Corner (JDMD2 and JDMD4) and edge (JDMD3) deflections for Section 537FD with temperature control box.

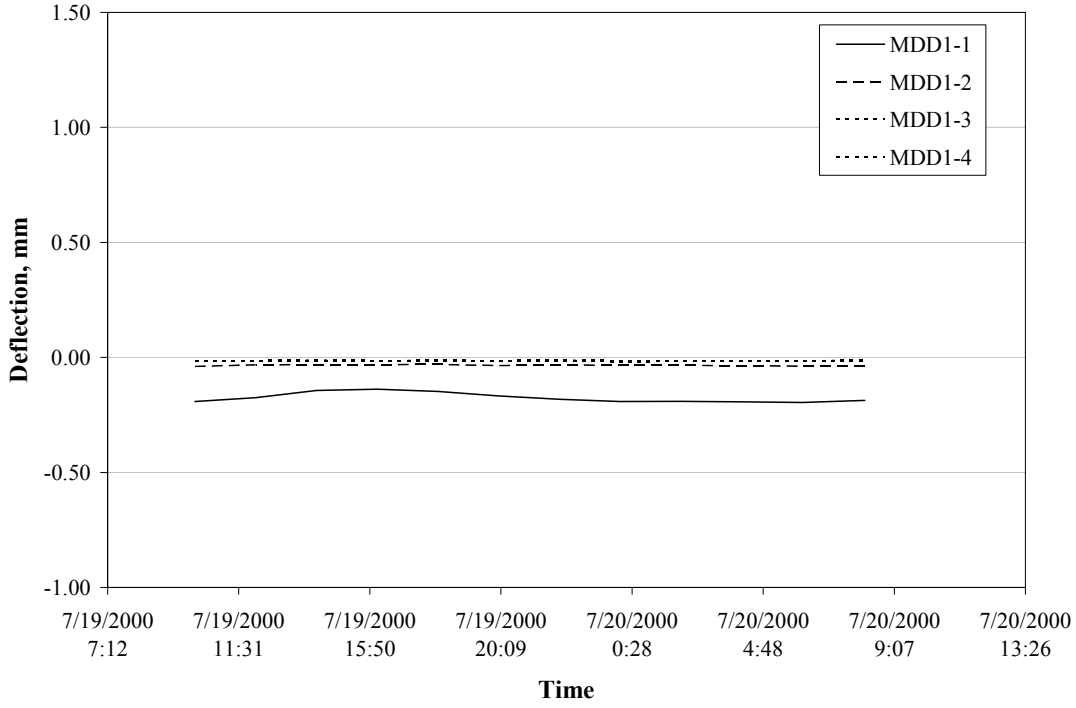

Figure 23. MDD deflections for Section 537FD measured over a loaded 24-hour cycle with temperature control box.

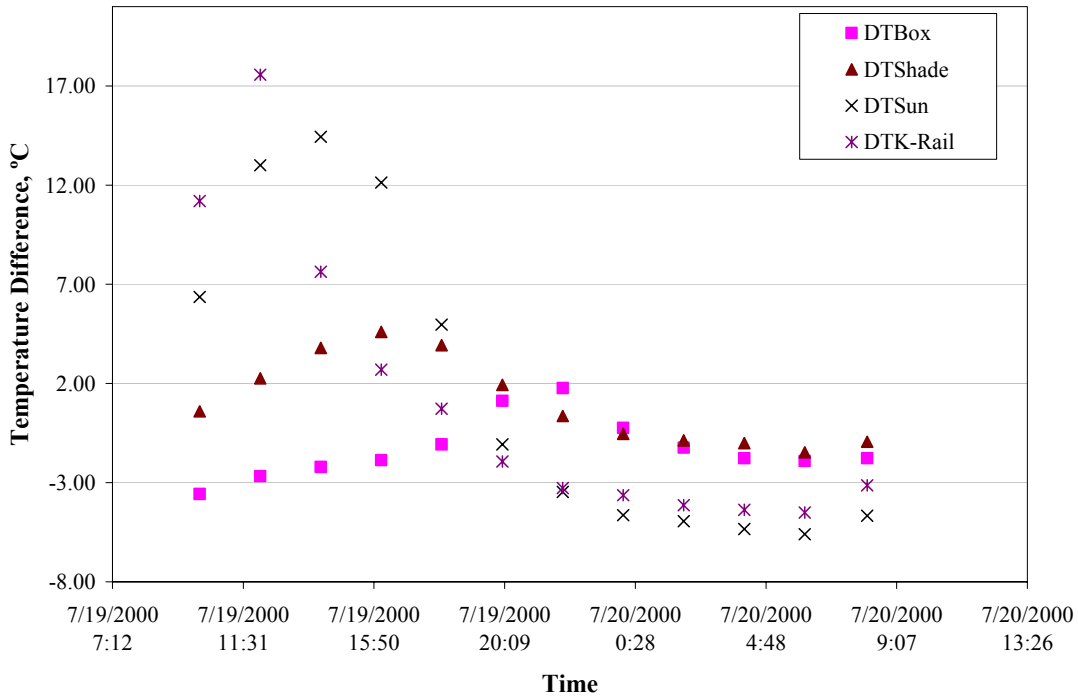

Figure 24. 24-hour temperature difference between the top sensor and the bottom sensor measured using thermocouple assemblies at various locations (with temperature control box) for Section 537FD.

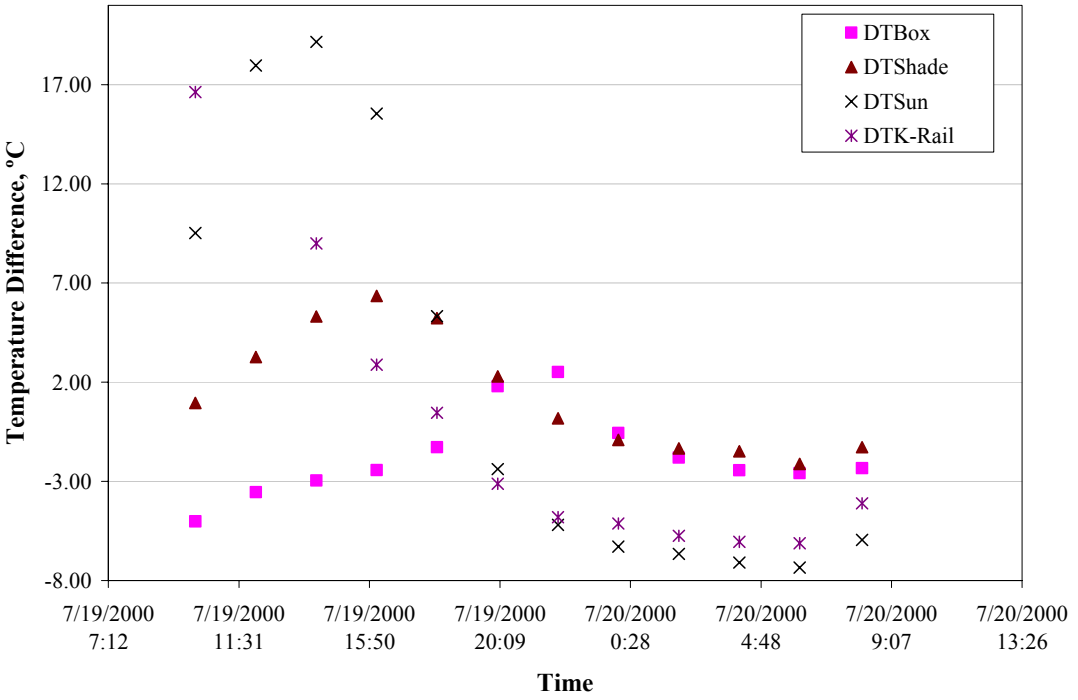

Figure 25. 24-hour temperature difference between the top of the slab and the bottom of the slab estimated using extrapolation and data collected using thermocouple assemblies at various locations (with temperature control box) for Section 537FD.

Table 4 Estimated Effective Built-In Temperature Difference (EBITD) for Section 537FD at Three Locations

Location on Slab		EBITD at Slab Location for Thermocouple Location, Extrapolated and Measured, ºF (ºC)					
		Thermocouple at Box		Thermocouple in Shade		Thermocouple at K-Rail	
		Extrapolated	Measured	Extrapolated	Measured	Extrapolated	Measured
Left Corner (JDMD4)	No Box	> -9.0 (> -5.0)	> -9.0 (> -5.0)	> -9.0 (> -5.0)	> -9.0 (> -5.0)	> -9.0 (> -5.0)	> -9.0 (> -5.0)
	With Box	> -9.0 (> -5.0)	> -9.0 (> -5.0)	> -9.0 (> -5.0)	> -9.0 (> -5.0)	> -9.0 (> -5.0)	> -9.0 (> -5.0)
Right Corner (JDMD2)	No Box	-13.7 (-7.6)	-14.6 (-8.1)	-19.1 (-10.6)	-18.7 (-10.4)	-13.1 (-7.3)	-15.3 (-8.5)
	With Box	-25 (-13.9)	-23.9 (-13.3)	-21.1 (-11.7)	-20.9 (-11.6)	-16.9 (-9.4)	-19.1 (-10.6)
Midslab (JDMD3)	No Box	> -9.0 (> -5.0)	> -9.0 (> -5.0)	> -9.0 (> -5.0)	> -9.0 (> -5.0)	> -9.0 (> -5.0)	> -9.0 (> -5.0)
	With Box	> -9.0 (> -5.0)	> -9.0 (> -5.0)	> -9.0 (> -5.0)	> -9.0 (> -5.0)	> -9.0 (> -5.0)	> -9.0 (> -5.0)

Data was collected with and without a temperature control box and using thermocouple data measured at various locations.

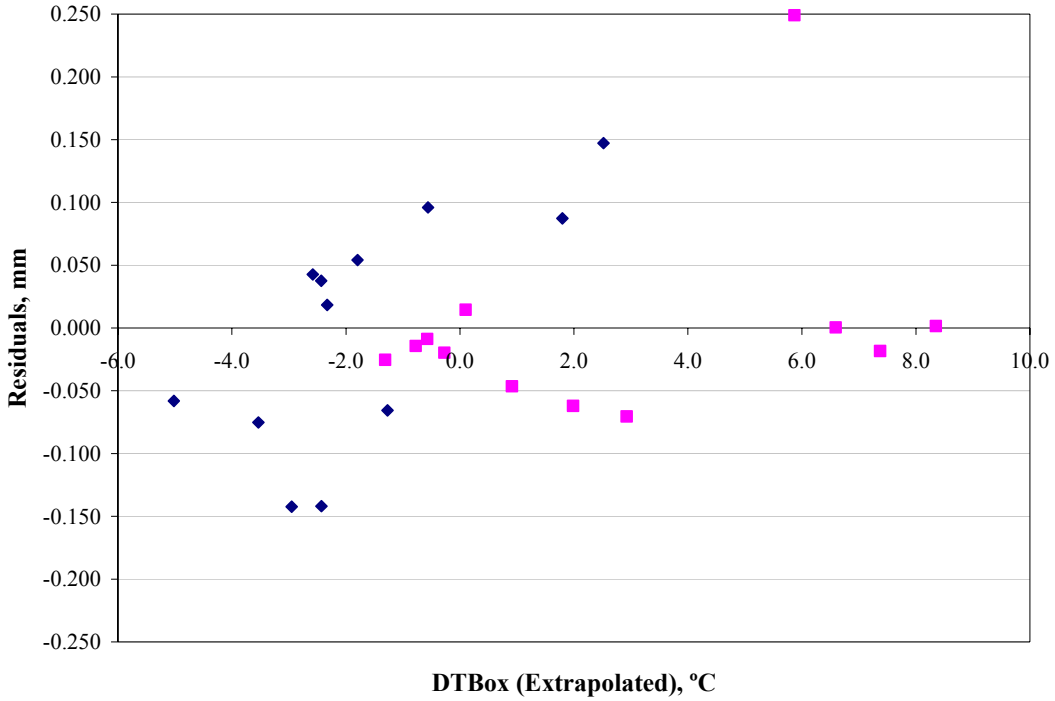

Figure 26. Residuals (difference in measured deflections and predicted deflections) as a function of extrapolated temperature difference (box) for JDMD2 measured with and without the temperature control box for Section 537FD.

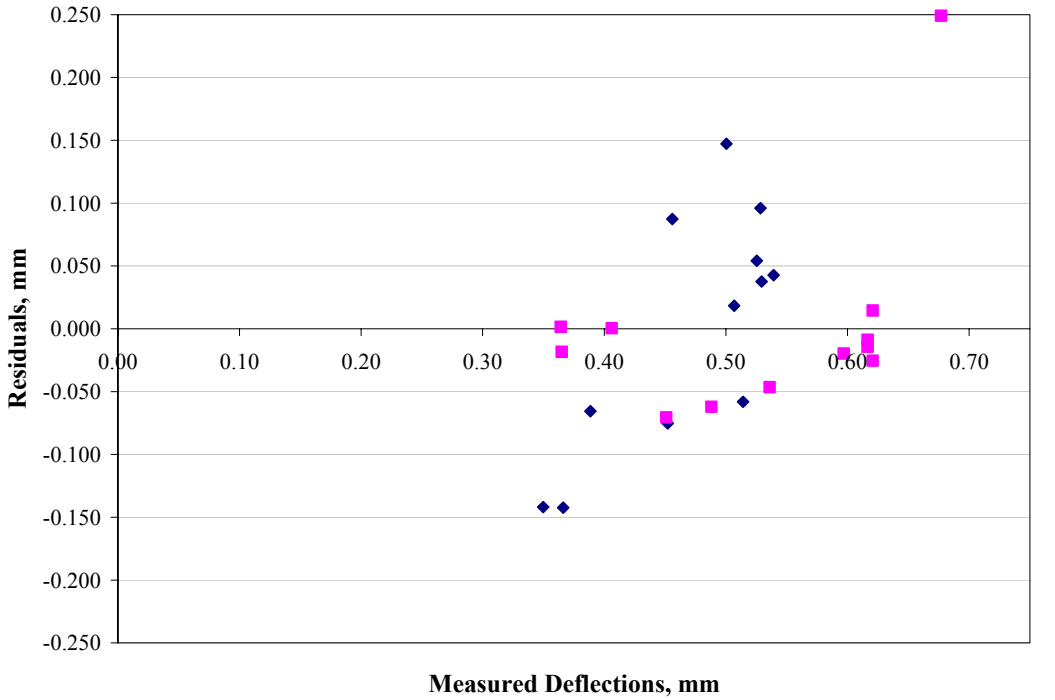

Figure 27. Residuals (difference in measured deflections and predicted deflections) as a function of measured deflections for JDMD2 measured with and without the temperature control box for Section 537FD.

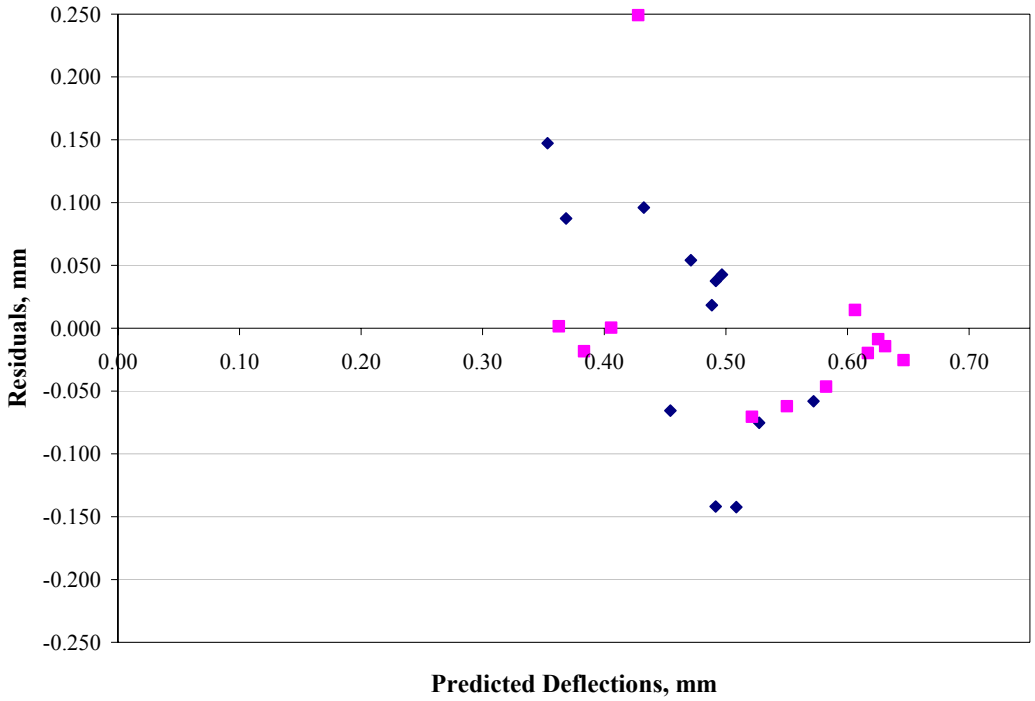

Figure 28. Residuals (difference in measured deflections and predicted deflections) as a function of predicted deflections for JDMD2 measured with and without the temperature control box for Section 537FD.

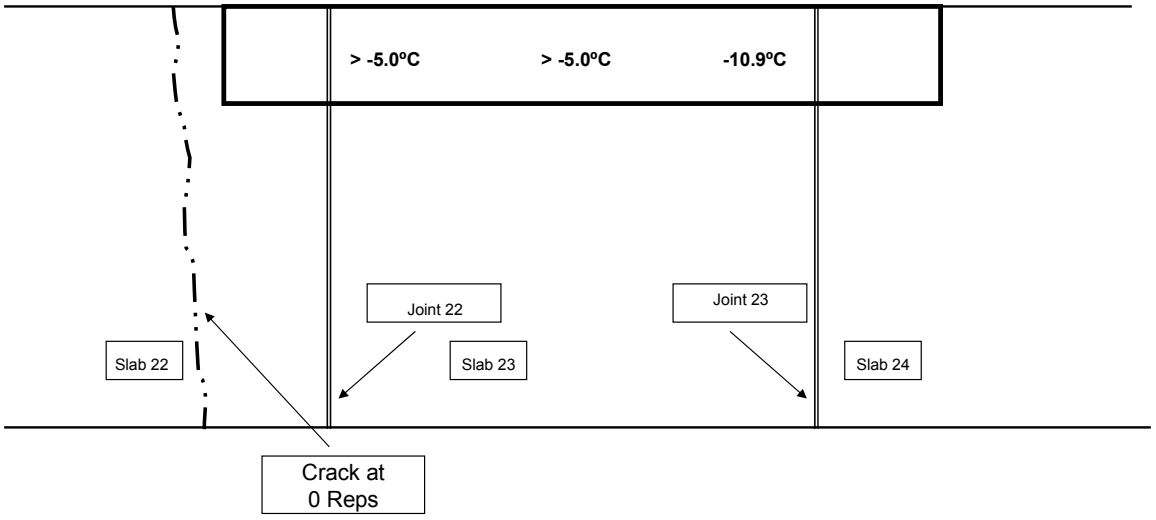

Figure 29. Crack pattern in slab (537FD) prior to load application and estimated effective built-in temperature difference at three locations in the test slab.

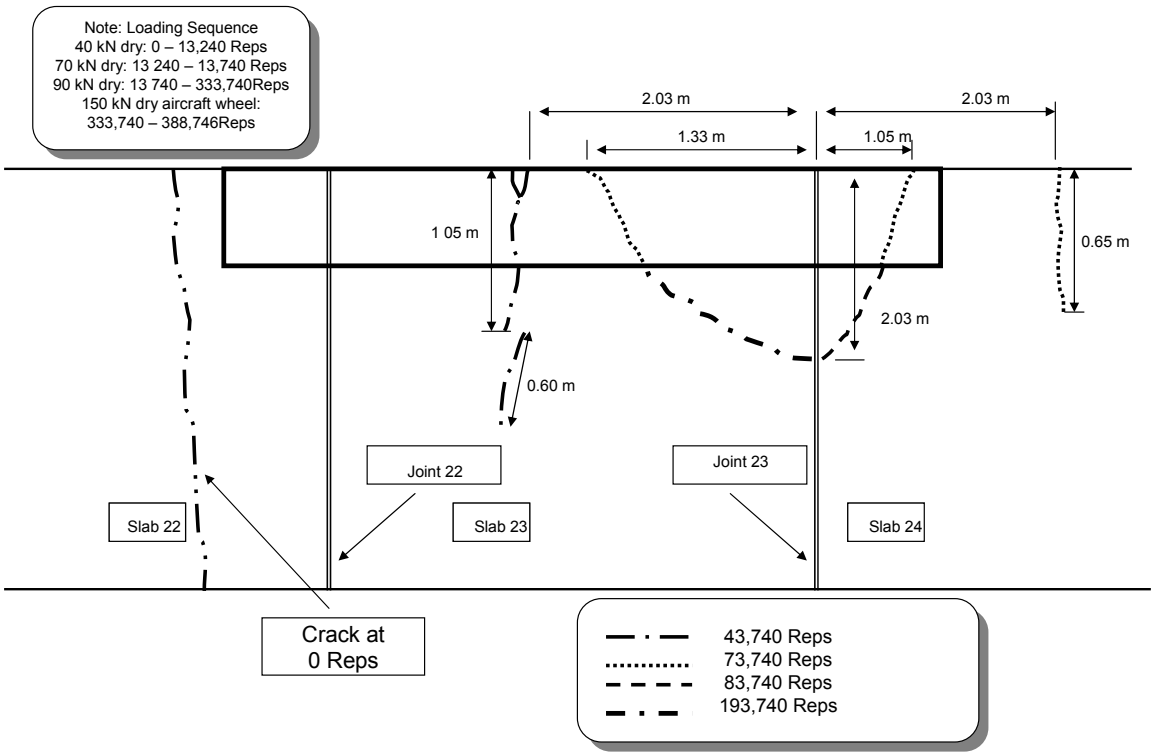

Figure 30. Crack pattern in slab (537FD) after fatigue damage load application.(*2*)

2.4 Section 538FD

The layout of Section 538FD and the locations of the sensors are shown in Figure 31.(*2*) The deflections measured by the JDMDs over the 24-hour cycle without the temperature control box are shown in Figure 32. No MDD data were collected for Section 538FD. The corresponding temperature differences are shown in Figures 33 and 34. 24-hour loaded deflection data with the temperature control box was not collected for Section 538FD.

As with Sections 535FD and 537FD, the slab corners and edge deflected less under positive temperature differences and showed differences between two corners of the slab. Midslab deflections (JDMD3) were very low as in the case of Section 537FD. This is a consequence of low EBITD at the midslab edge location and the slab coming in contact with the base when loaded at the midslab edge.

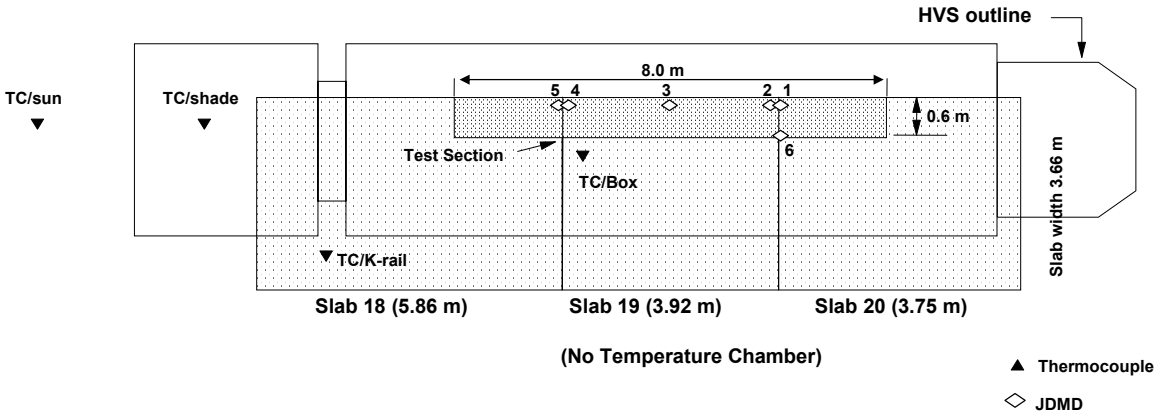

Figure 31. Instrumentation layout of Section 538FD.(*2*)

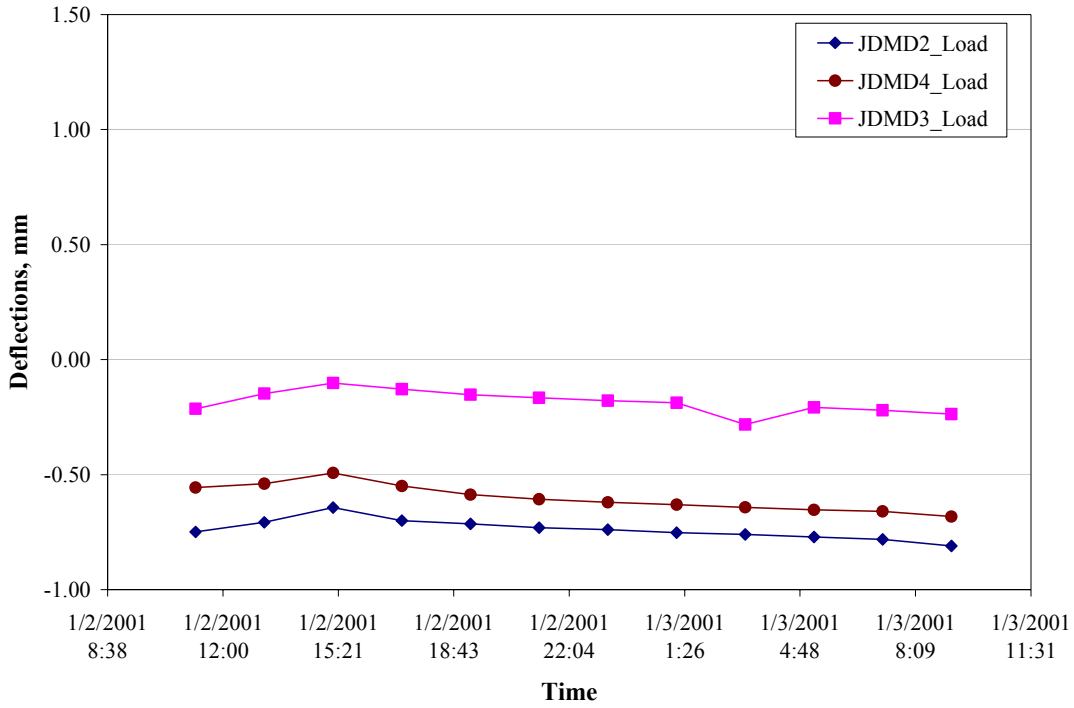

Figure 32. Corner (JDMD2 and JDMD4) and edge (JDMD3) deflections for Section 538FD without temperature control box.

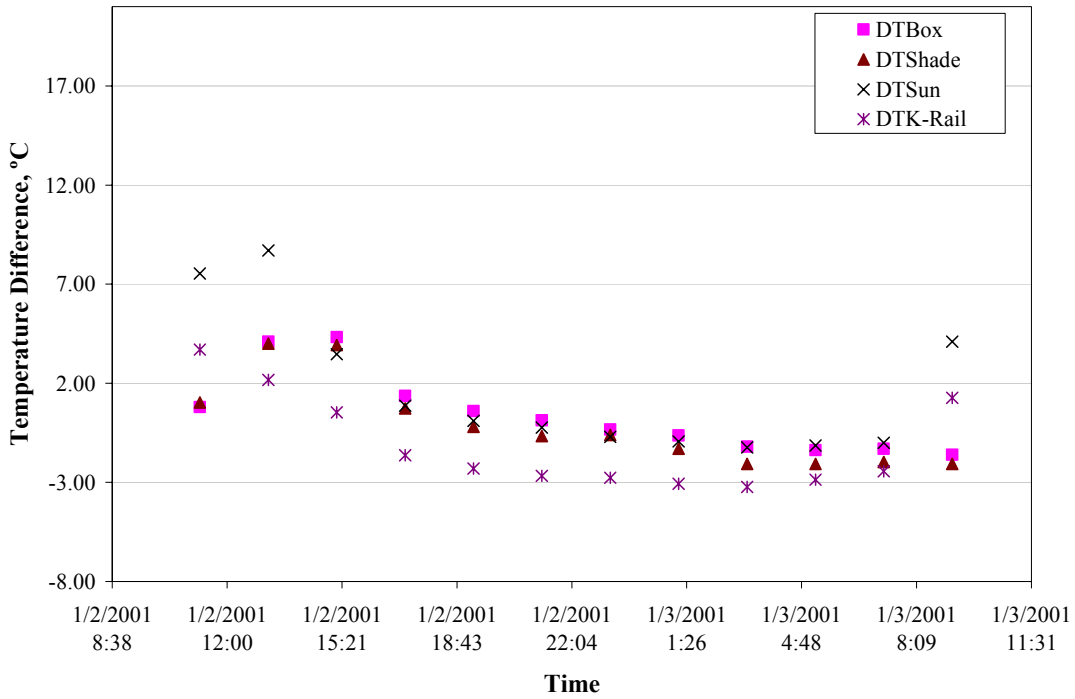

Figure 33. 24-hour temperature difference between the top sensor and the bottom sensor measured using thermocouple assemblies at various locations (without temperature control box) for Section 538FD.

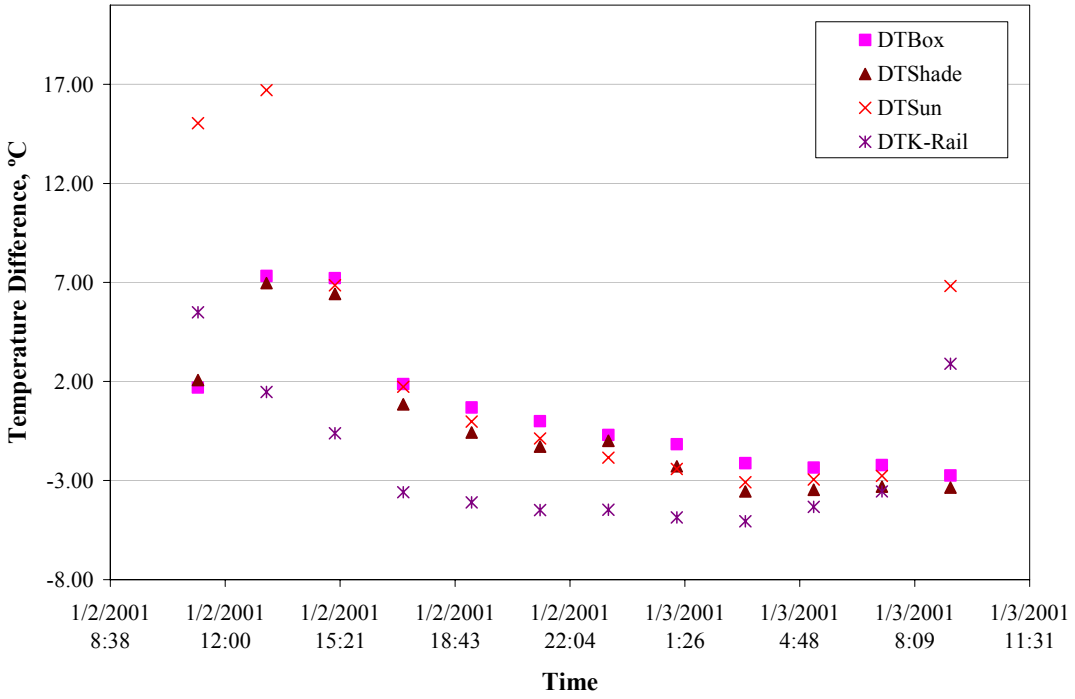

Figure 34. 24-hour temperature difference between the top of the slab and the bottom of the slab estimated using extrapolation and data collected using thermocouple assemblies at various locations (without temperature control box) for Section 538FD.

The results of the analysis, the estimated EBITDs at three slab locations, are shown in Table 5. When the slab is in contact with the base, the deflections do not depend on the total temperature difference in the slab. At low negative or positive TELTD, the slab comes in contact with the base and the loaded deflection is not sensitive to TELTD and thus cannot be used to estimate TELTD and consequently EBITD. For Section 538FD, this is the case at midslab (JDMD3) where the EBITD is low negative or positive [> -9.0ºF (> -5.0º)]. The low EBITD could be due to restraint caused by a tie bar (between PCC shoulder and test slab) in close proximity to the midslab test location.

Figures 35 through 37 show the residuals (difference between measured deflections and predicted deflections) as a function of various factors. The three figures show that the residuals are normally distributed about zero and are typically less than 10 percent of the measured deflections. The few outliers correspond to the daytime, when the temperature difference in the slab is large and positive, resulting in the slab coming in contact with the base (Figure 35). The residuals do not show any significant trend with temperature difference, measured deflection, or predicted deflection indicating true randomness and no other systemic cause for the difference between measured and predicted deflections. The EBITD results along with the initial cracking pattern are shown in Figure 38. The crack patterns in the test slab and the adjacent slabs after loading with the HVS is shown in Figures 39. Unlike Sections 535FD and 537FD, no cracks were observed on Section 538FD.

Table 5 Estimated Effective Built-In Temperature Difference (EBITD) for Section 538FD at Three Locations

Location on Slab		EBITD at Slab Location for Thermocouple Location, Extrapolated and Measured, ºF (ºC)					
		Thermocouple at Box		Thermocouple in Shade		Thermocouple at K-Rail	
		Extrapolated	Measured	Extrapolated	Measured	Extrapolated	Measured
Left Corner (JDMD4)	No Box	-26.9 (-14.9)	-25.8 (-14.3)	-26.0 (-14.4)	-22.4 (-12.4)	-24.2 (-13.4)	-26.9 (-14.9)
	With Box	-	-	-	-	-	-
Right Corner (JDMD2)	No Box	-33.7 (-18.7)	-32.7 (-18.2)	-32.7 (-18.2)	-29.3 (-16.3)	-31.0 (-17.2)	-33.7 (-18.7)
	With Box	-	-	-	-	-	-
Midslab (JDMD3)	No Box	> -9.0 (> -5.0)	> -9.0 (> -5.0)	> -9.0 (> -5.0)	> -9.0 (> -5.0)	> -9.0 (> -5.0)	> -9.0 (> -5.0)
	With Box	-	-	-	-	-	-

Data was collected only without a temperature control box using thermocouple data measured at various locations.

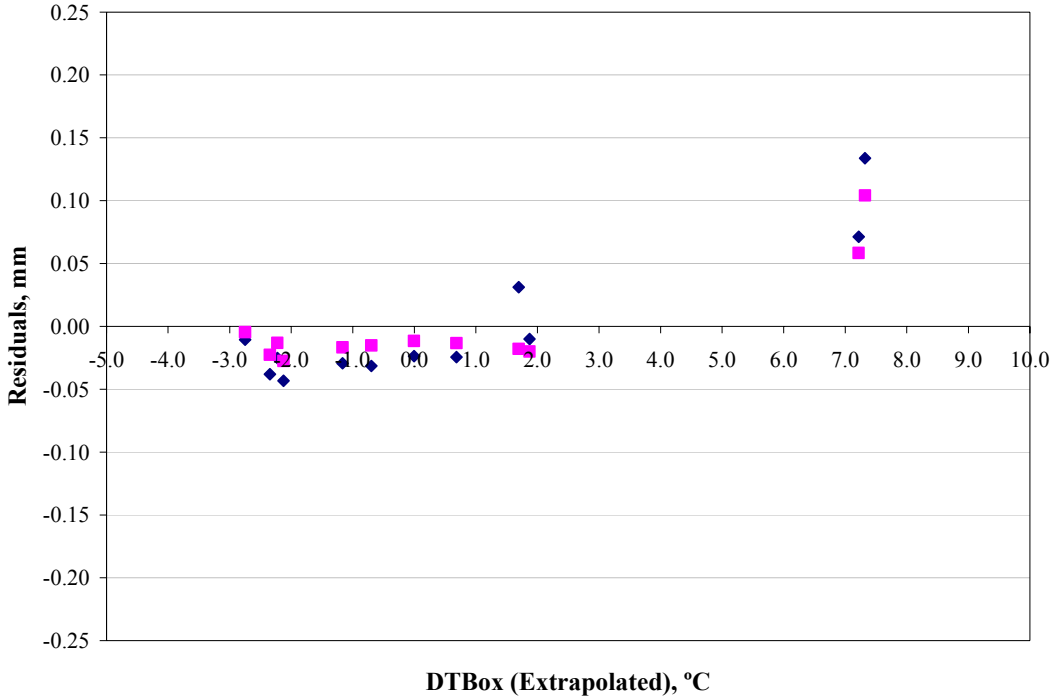

Figure 35. Residuals (difference in measured deflections and predicted deflections) as a function of extrapolated temperature difference (box) for JDMD2 and JDMD4 measured without the temperature control box for Section 538FD.

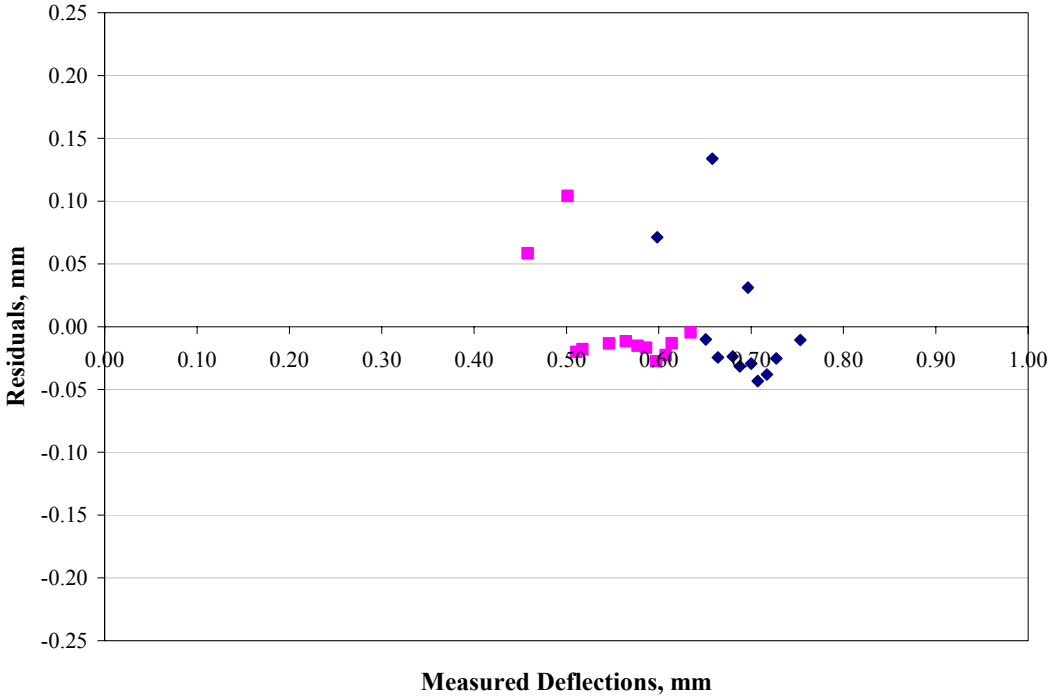

Figure 36. Residuals (difference in measured deflections and predicted deflections) as a function of measured deflections for JDMD2 and JDMD4 measured without the temperature control box for Section 538FD.

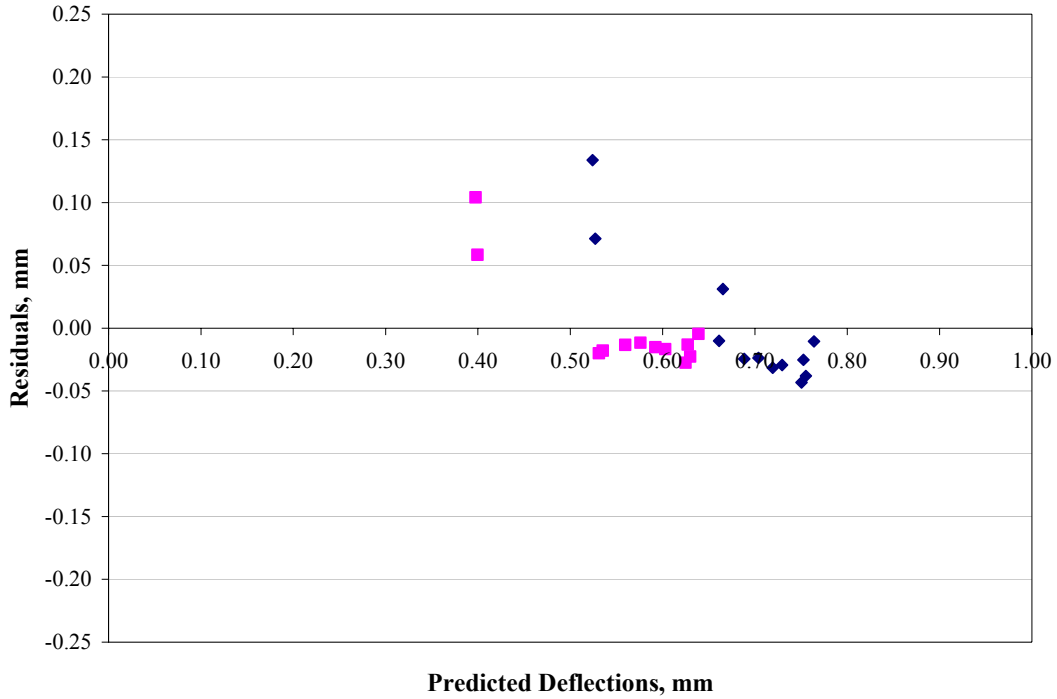

Figure 37. Residuals (difference in measured deflections and predicted deflections) as a function of predicted deflections for JDMD2 and JDMD4 measured without the temperature control box for Section 538FD.

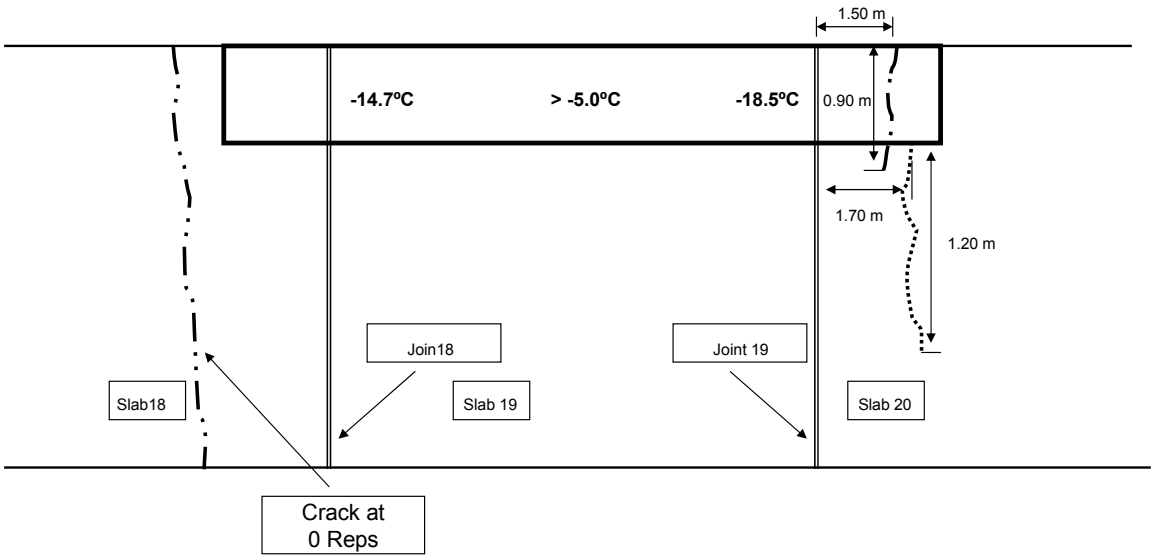

Figure 38. Crack pattern in slab (538FD) prior to load application and estimated effective built-in temperature difference at three locations in the test slab.

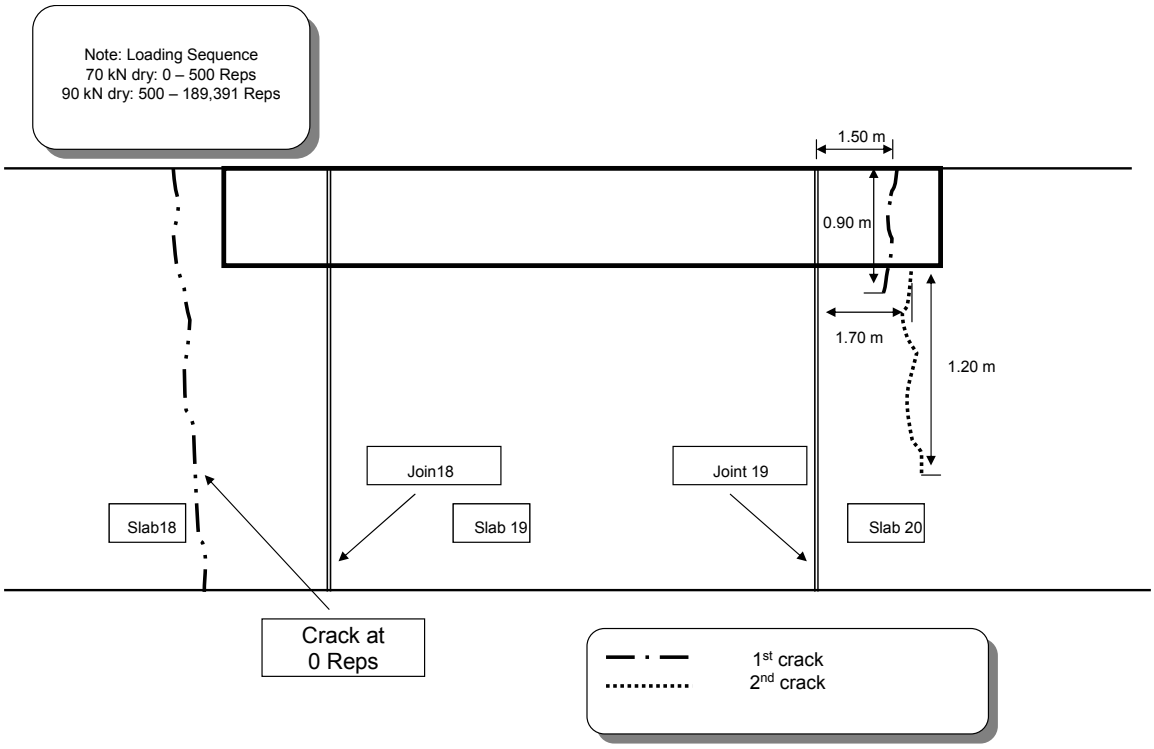

Figure 39. Crack pattern in slab (538FD) after fatigue damage load application.(*2*)

2.5 Section 539FD

The layout of Section 539FD and the locations of the sensors are shown in Figure 40.(*2*) The deflections measured by the JDMDs over the 24-hour cycle without the temperature control box are shown in Figure 41. The deflections measured by the MDDs over the same 24-hour cycle are shown in Figure 42. The corresponding temperature differences are shown in Figures 43 and 44. The MDD deflections of the treated base are high and are of the order of the slab deflections suggesting a bonded or contact condition between the slab and the treated base. The slab deflections under the 9,000-lb. (40-kN) load measured with the temperature control box in place are shown in Figure 45 for Section 539FD. The deflections measured by the MDDs over the same 24-hour cycle are shown in Figure 46. The corresponding temperature differences are shown in Figures 47 and 48.

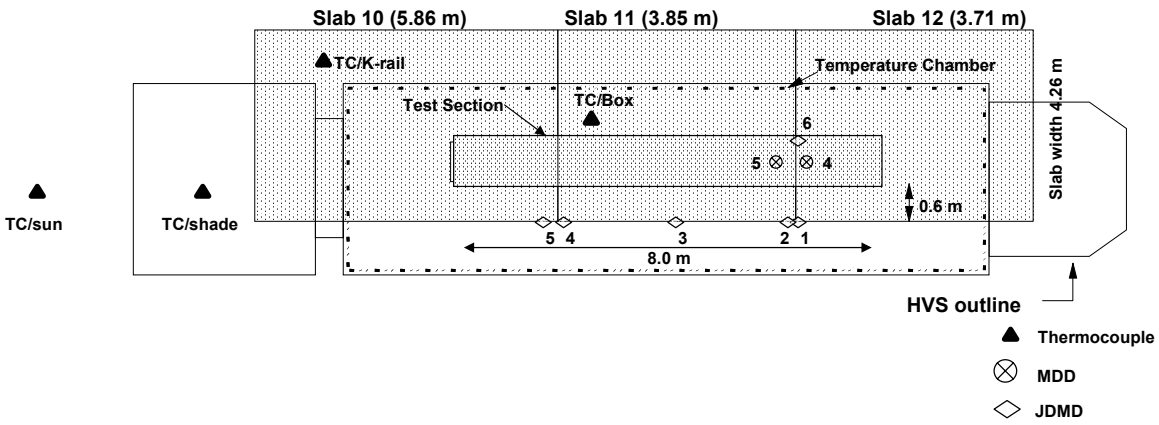

Figure 40. Instrumentation layout of Section 539FD.(*2*)

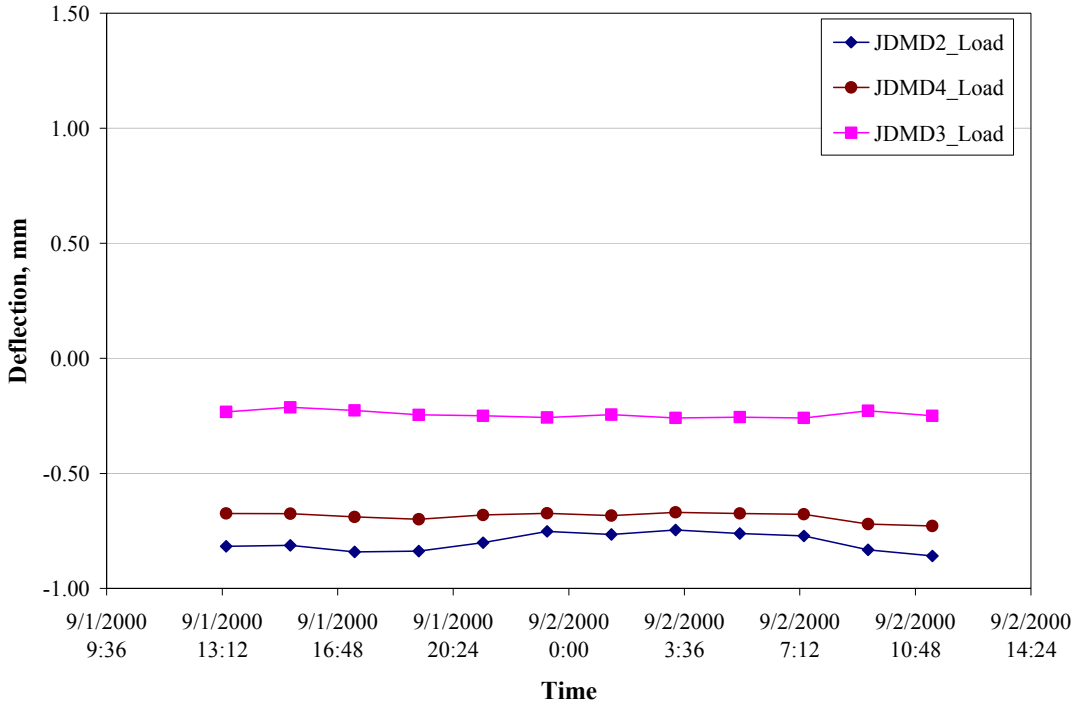

Figure 41. Corner (JDMD2 and JDMD4) and edge (JDMD3) deflections for Section 539FD without temperature control box.

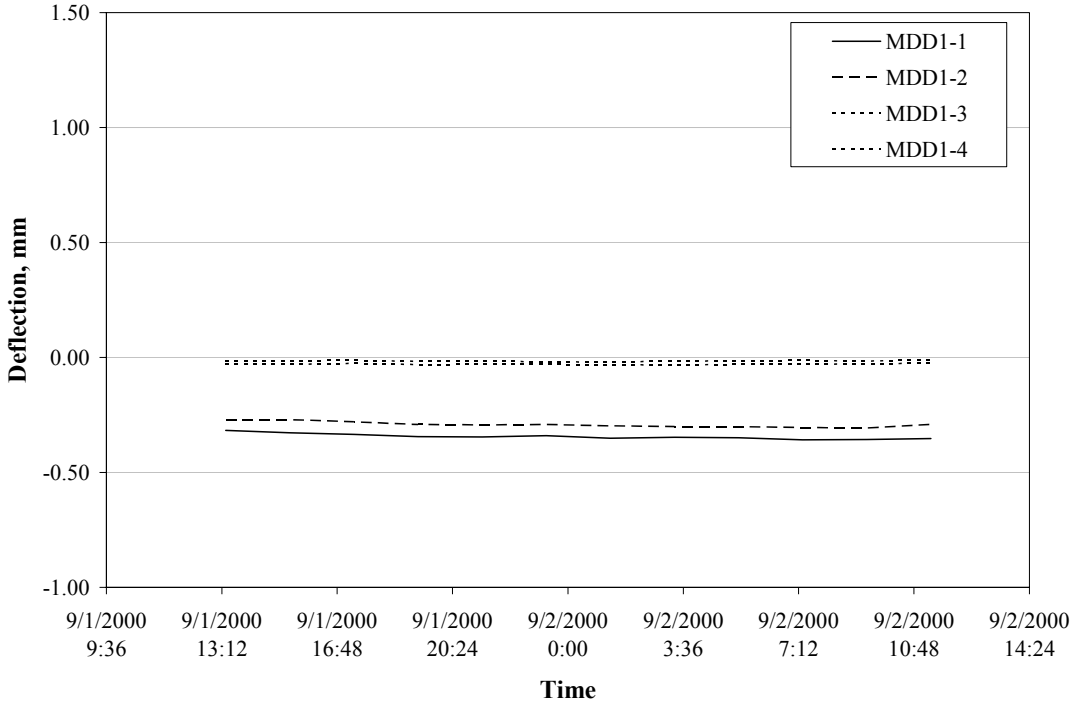

Figure 42. MDD deflections for Section 539FD measured over a loaded 24-hour cycle without temperature control box.

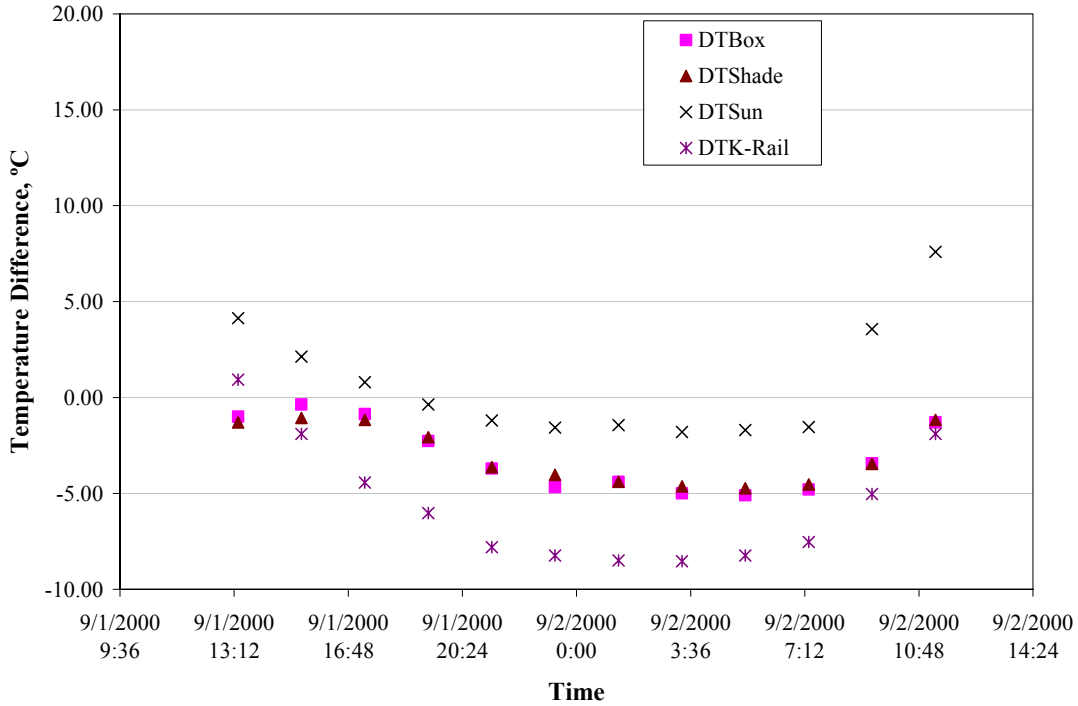

Figure 43. 24-hour temperature difference between the top sensor and the bottom sensor for Section 539FD measured using thermocouple assemblies at various locations (without temperature control box).

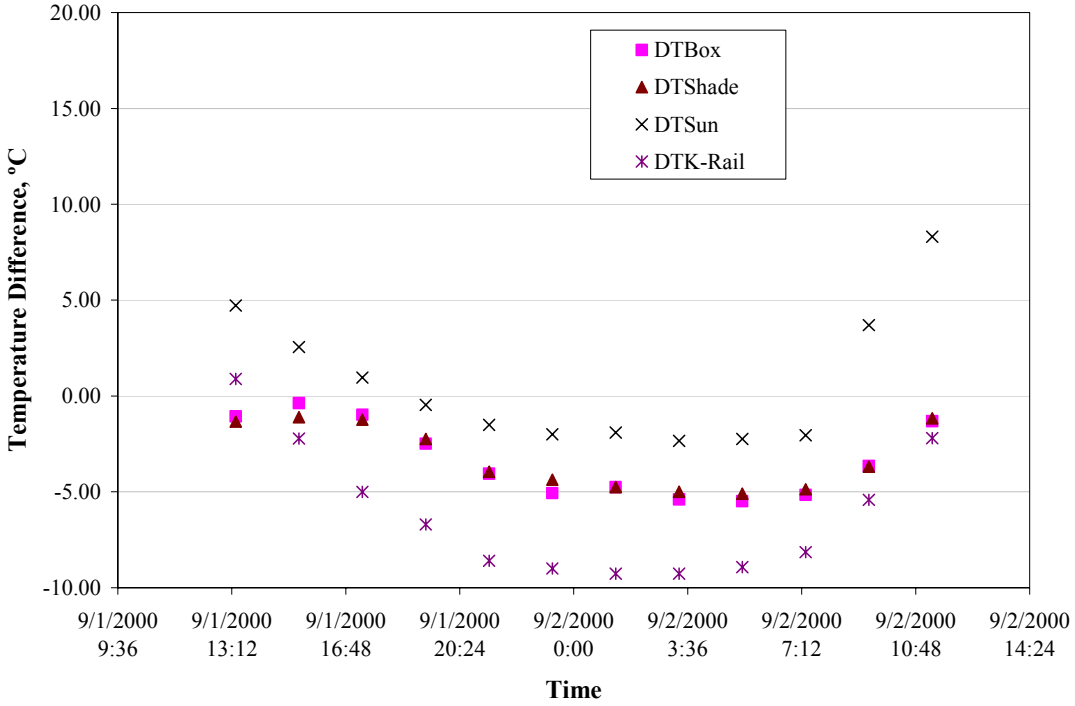

Figure 44. 24-hour temperature difference between the top of the slab and the bottom of the slab estimated using extrapolation and data collected using thermocouple assemblies at various locations (without temperature control box) for Section 539FD.

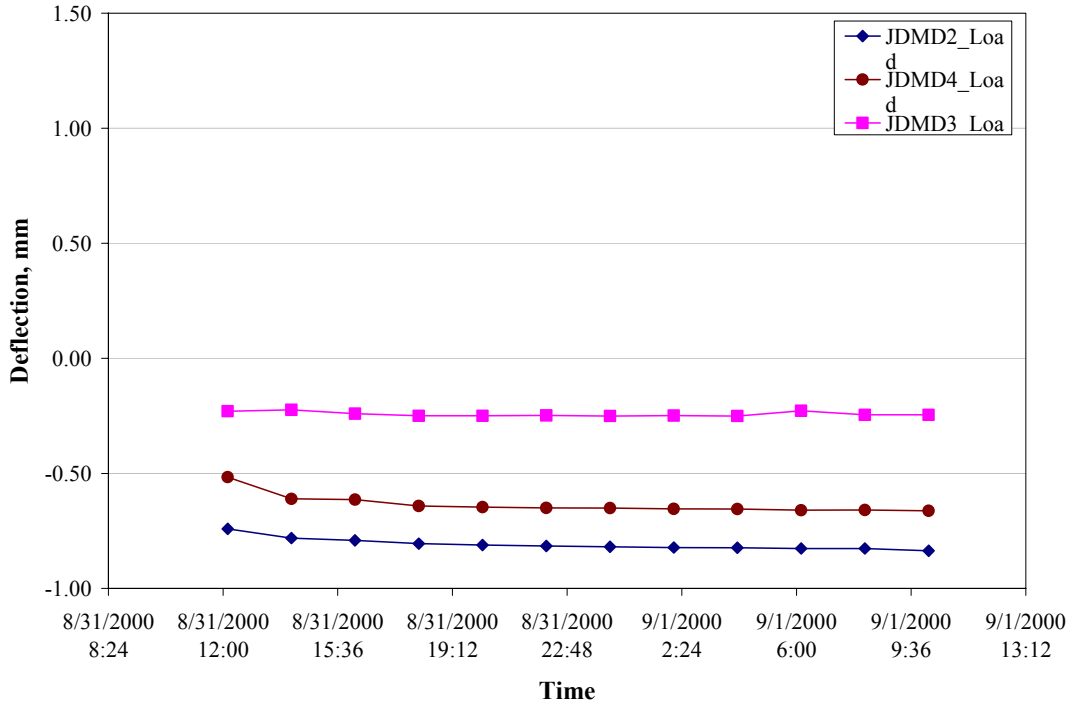

Figure 45. Corner (JDMD2 and JDMD4) and edge (JDMD3) deflections for Section 539FD with temperature control box.

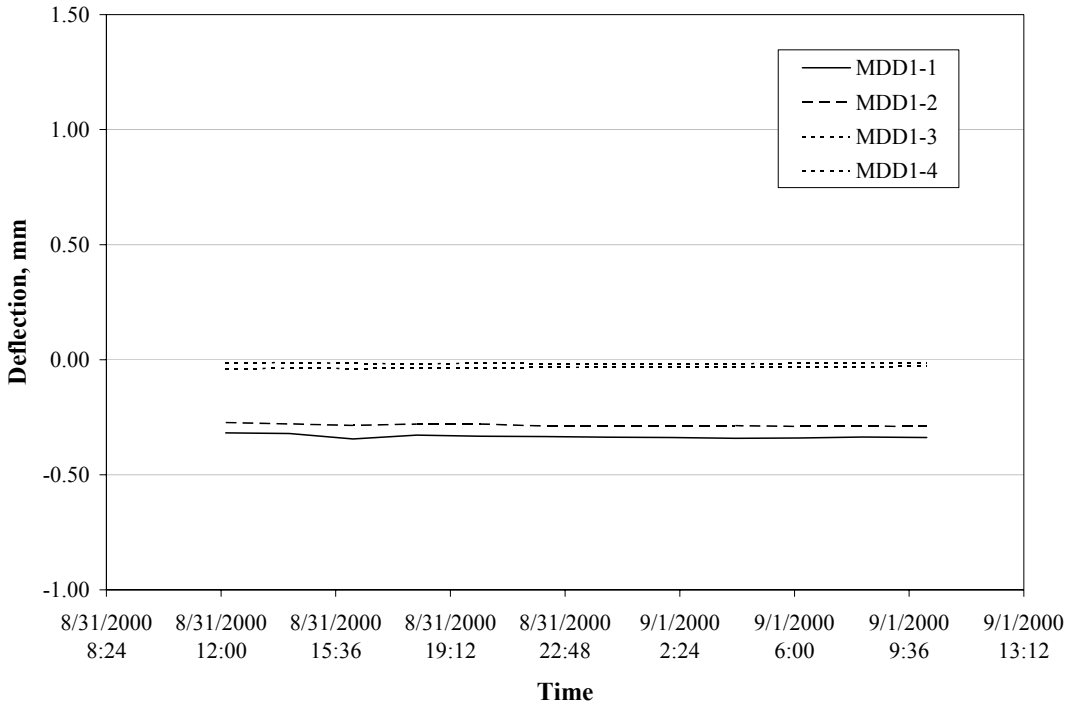

Figure 46. MDD deflections for Section 539FD measured over a loaded 24-hour cycle with temperature control box.

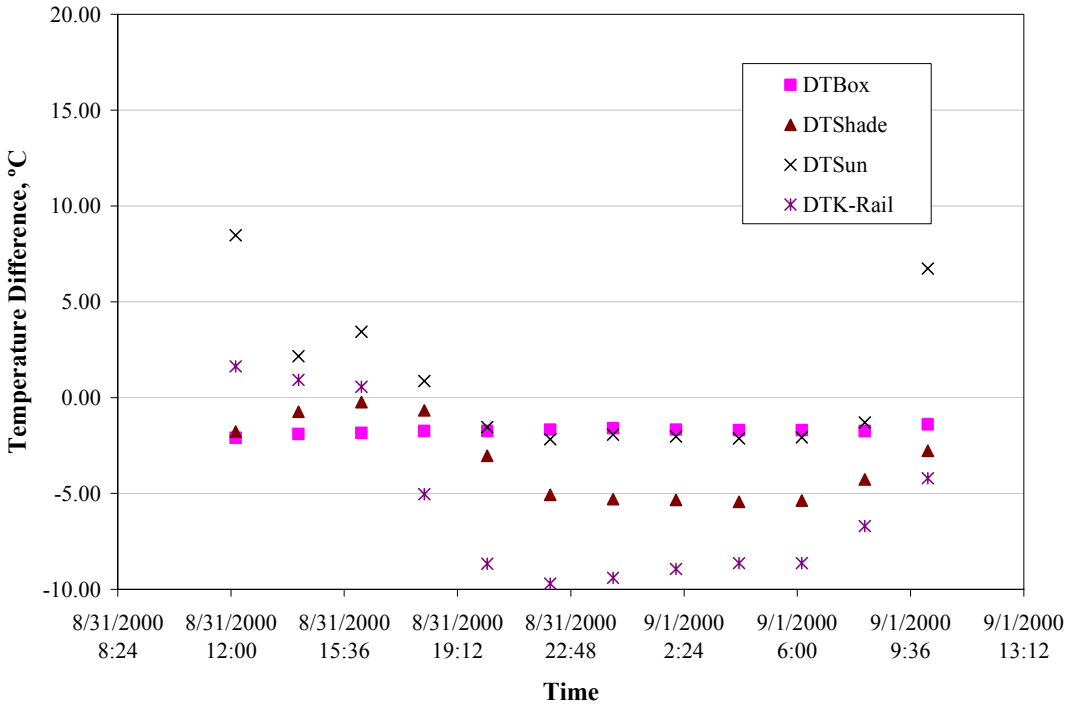

Figure 47. 24-hour temperature difference between the top sensor and the bottom sensor measured for Section 539FD using thermocouple assemblies at various locations (with temperature control box).

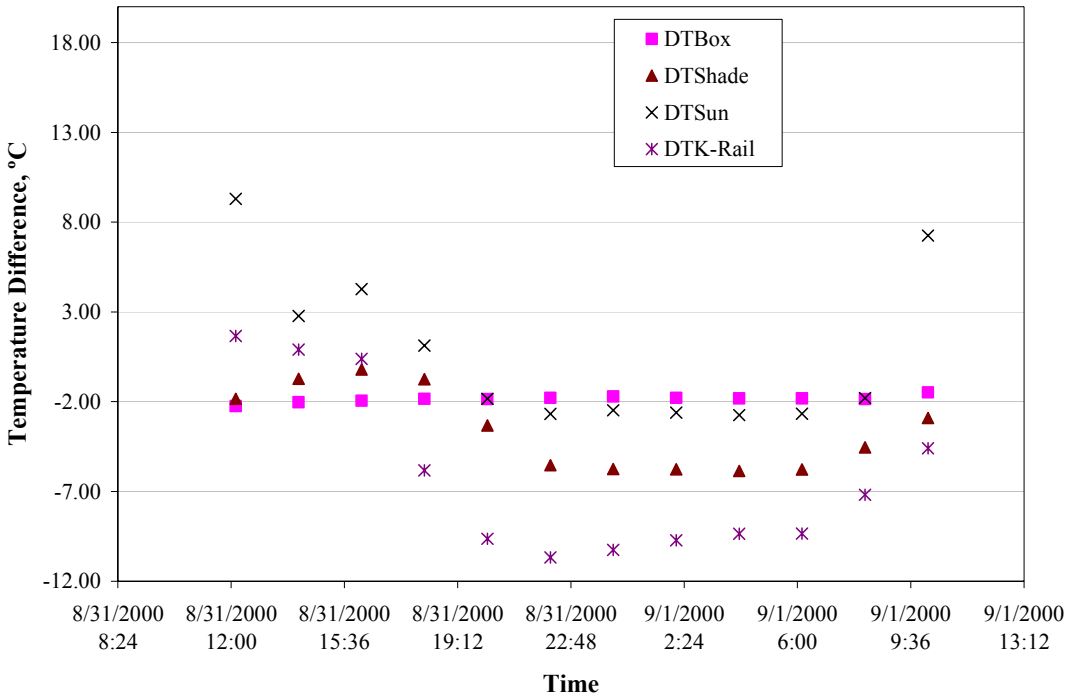

Figure 48. 24-hour temperature difference between the top of the slab and the bottom of the slab estimated using extrapolation and data collected using thermocouple assemblies at various locations (with temperature control box) for Section 539FD.

The results of the analysis, the estimated EBITDs at three slab locations, are shown in Table 6. Figures 49 through 51 show the residuals (difference between measured deflections and predicted deflections) as a function of various factors. The EBITD results along with the initial cracking pattern are shown in Figure 52. The crack patterns in the test slab and the adjacent slabs after loading with the HVS are shown in Figures 53. The failure of the slab occurred due to a midslab transverse crack.

Table 6 Estimated Effective Built-In Temperature Difference (EBITD) for Section 538FD at Three Locations

Location on Slab		EBITD at Slab Location for Thermocouple Location, Extrapolated and Measured, ºF (ºC)					
		Thermocouple at Box		Thermocouple in Shade		Thermocouple at K-Rail	
		Extrapolated	Measured	Extrapolated	Measured	Extrapolated	Measured
Left Corner (JDMD4)	No Box	-20.2 (-11.2)	-20.4 (-11.3)	-17.1 (-9.5)	-17.6 (-9.8)	-12.3 (-6.8)	-13.4 (-7.4)
	With Box	-19.8 (-11.0)	-20.3 (-11.3)	-20.0 (-11.1)	-20.4 (-11.3)	-14.7 (-8.2)	-15.7 (-8.7)
Right Corner (JDMD2)	No Box	-25.4 (-14.1)	-25.7 (-14.3)	-22.4 (-12.4)	-22.8 (-12.7)	-18.0 (-10.0)	-19.0 (-10.6)
	With Box	-22.5 (-12.5)	-22.9 (-12.7)	-22.7 (-12.6)	-23.0 (-12.8)	-17.5 (-9.7)	-18.5 (-10.3)
Midslab (JDMD3)	No Box	-12.5 (-6.9)	-12.7 (-7.1)	-8.7 (-4.8)	-9.2 (-5.1)	> -9.0 (> -5.0)	> -9.0 (> -5.0)
	With Box	-9.4 (-5.2)	-10.0 (-5.6)	-9.8 (-5.4)	-10.2 (-5.7)	> -9.0 (> -5.0)	> -9.0 (> -5.0)

Data was collected with and without a temperature control box and using thermocouple data measured at various locations.

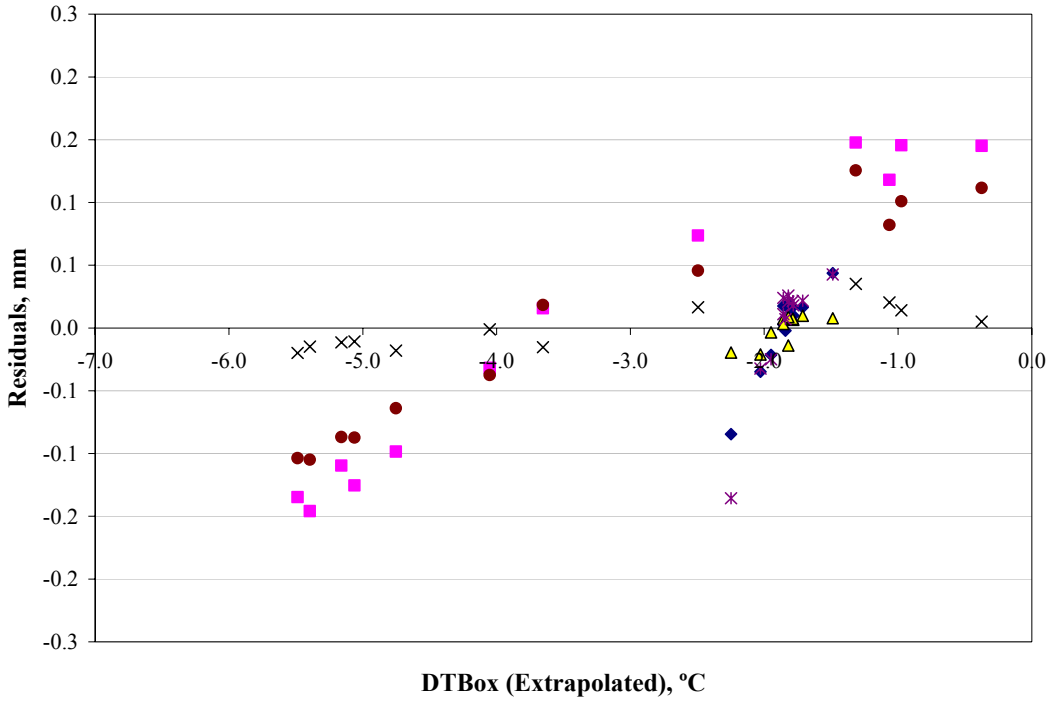

Figure 49. Residuals (difference in measured deflections and predicted deflections) as a function of extrapolated temperature difference (box) for JDMD2, JDMD3, and JDMD4 measured with and without the temperature control box for Section 539FD.

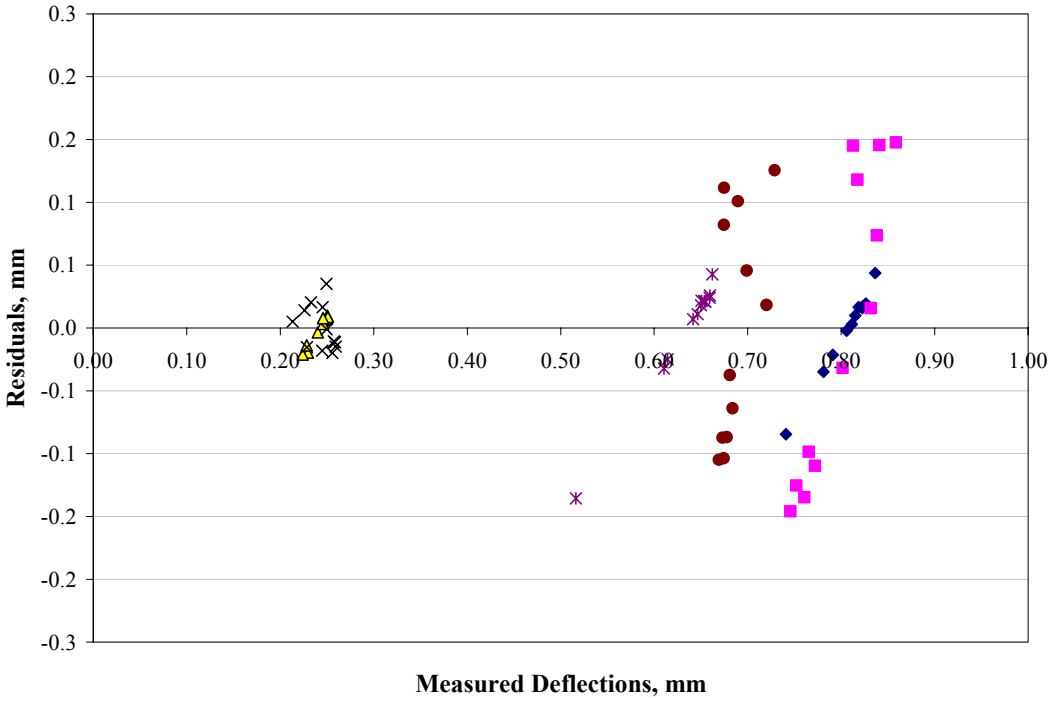

Figure 50. Residuals (difference in measured deflections and predicted deflections) as a function of measured deflections for JDMD2, JDMD3, and JDMD4 measured with and without the temperature control box for Section 539FD.

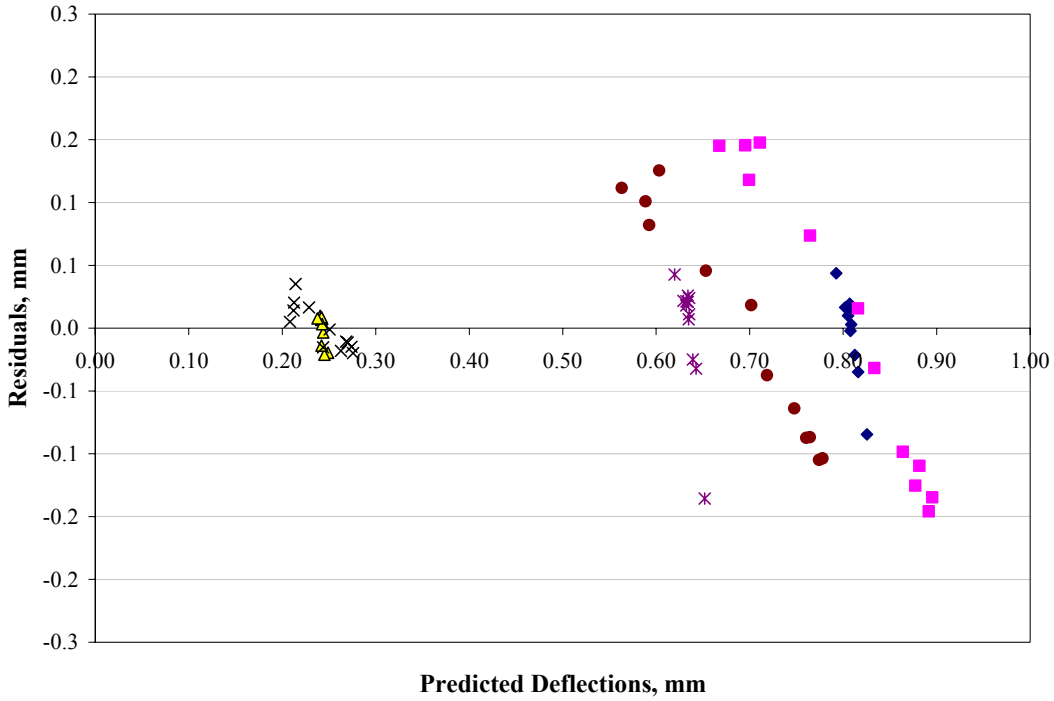

Figure 51. Residuals (difference in measured deflections and predicted deflections) as a function of predicted deflections for JDMD2, JDMD3, and JDMD4 measured with and without the temperature control box for Section 539FD.

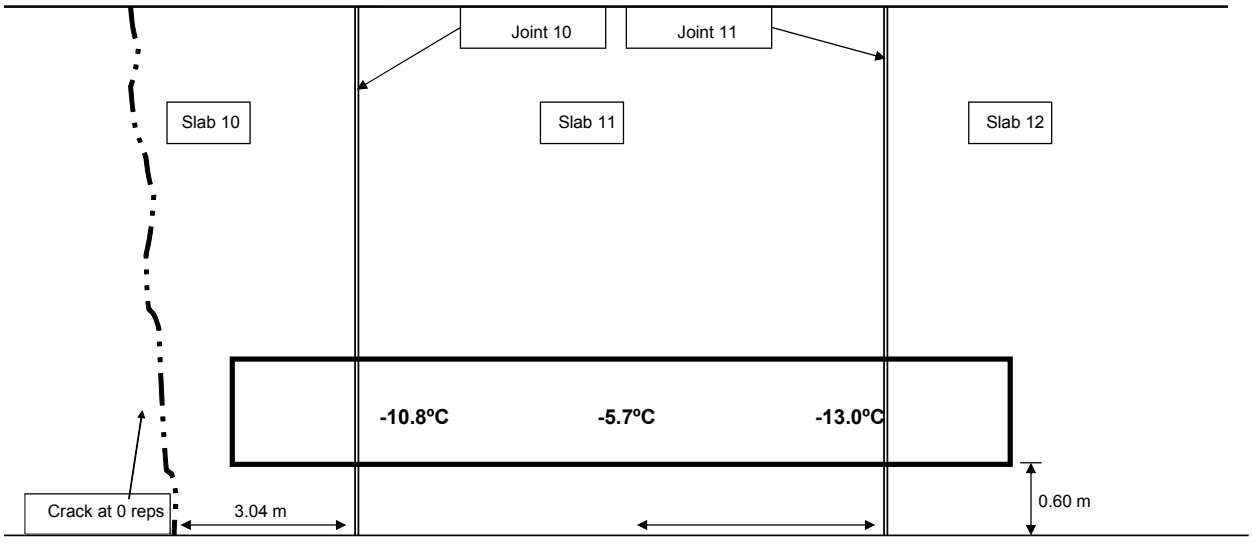

Figure 52. Crack pattern in slab (Section 539FD) prior to load application and estimated effective built-in temperature difference at three locations in the test slab.

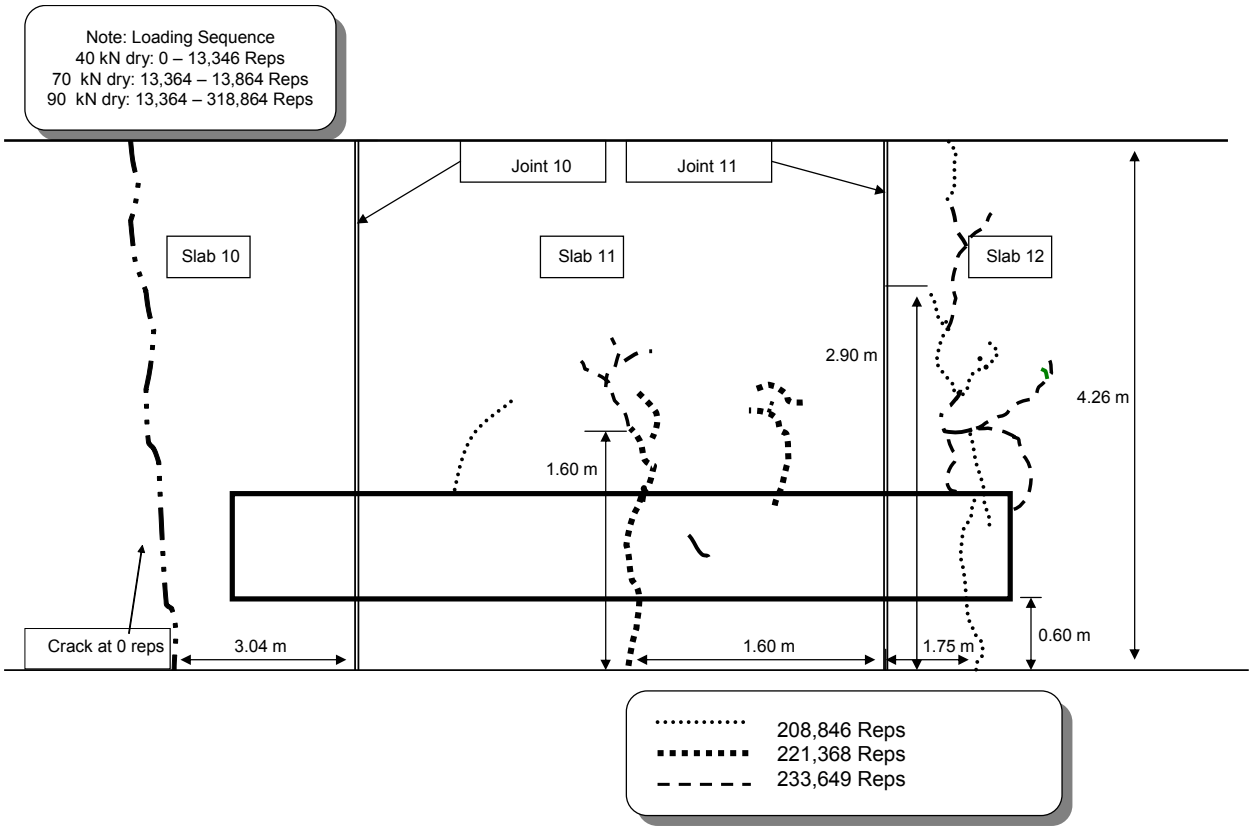

Figure 53. Crack pattern in slab (Section 539FD) after fatigue damage load application.(*2*)

2.6 Section 540FD

The layout of Section 540FD and the location of the sensors are shown in Figure 54.(*2*) The deflections measured by the JDMDs over the 24-hour cycle without the temperature control box are shown in Figure 55. The deflections measured by the MDDs over the same 24-hour cycle are shown in Figure 56. The corresponding temperature differences are shown in Figures 57 and 58. As with Section 539FD, the MDD deflections of the treated base are high and are of the order of the slab deflections suggesting a contact condition between the slab and the treated base. The MDD deflections suggest some amount of contact of the slab/base with the subbase at the location of the MDD. The deflections under the 9,000-lb. (40-kN) load measured with the temperature control box in place are shown in Figure 59. The deflections measured by the

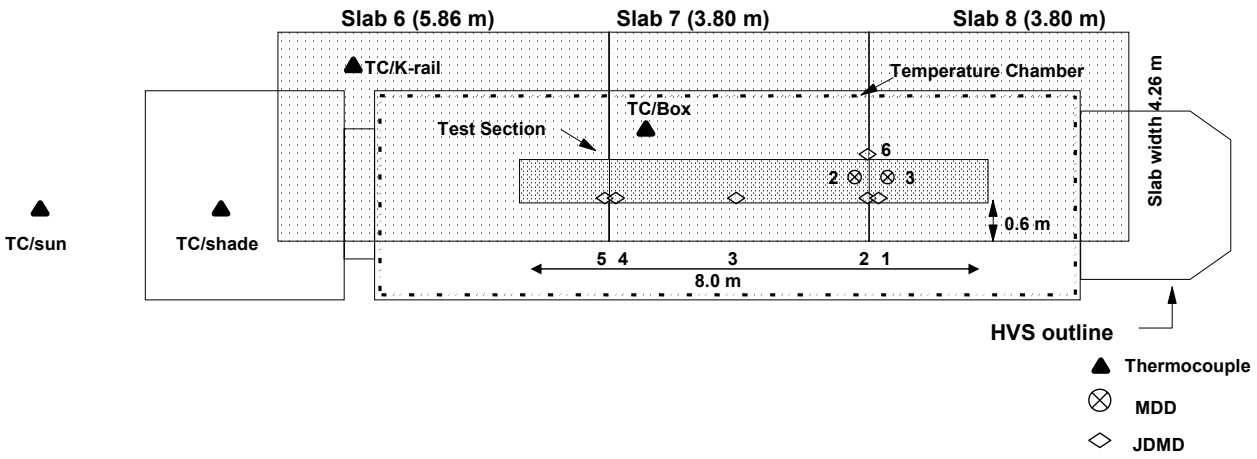

Figure 54. Instrumentation layout of Section 540FD.(*2*)

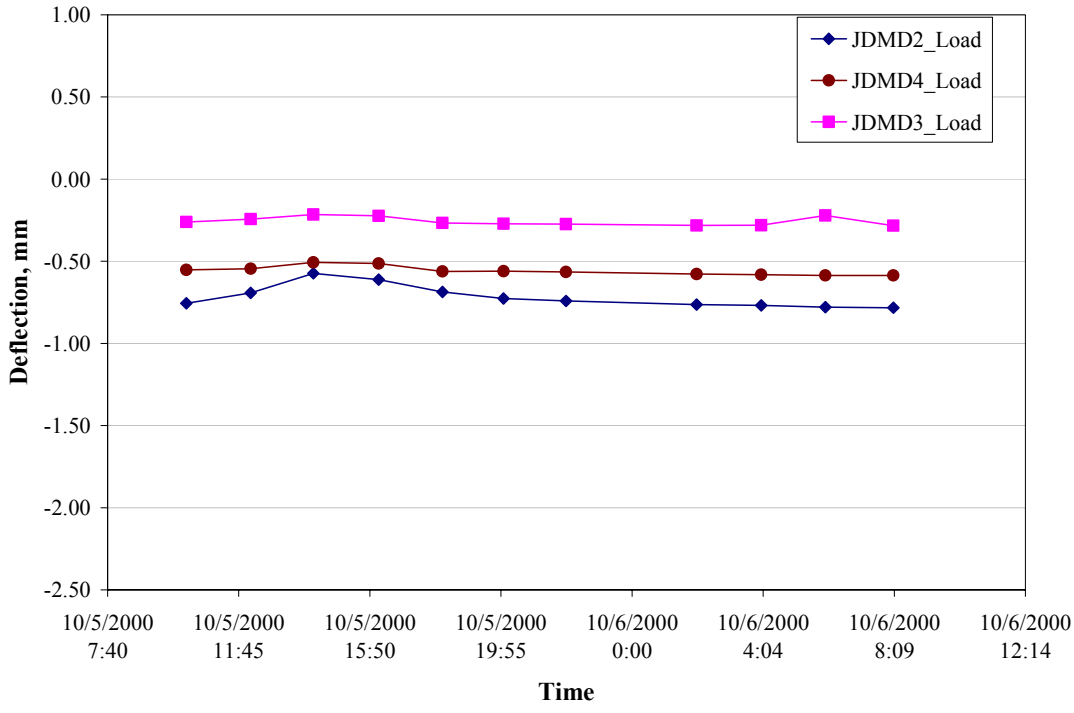

Figure 55. Corner (JDMD2 and JDMD4) and edge (JDMD3) deflections for Section 540FD without temperature control box.

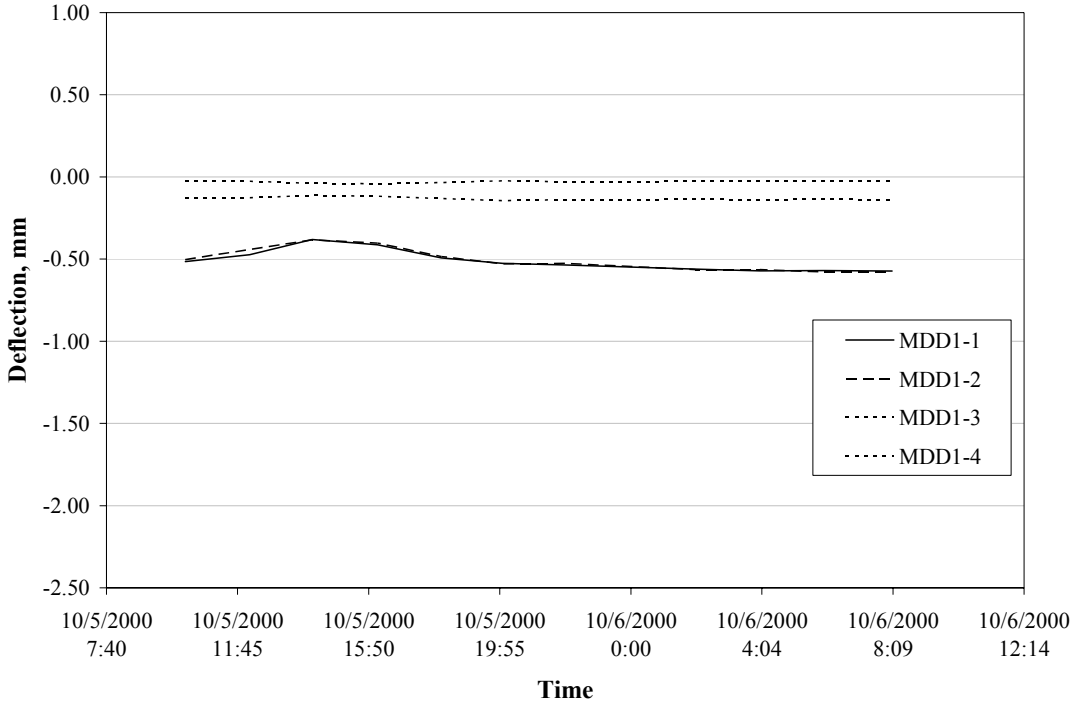

Figure 56. MDD deflections for Section 540FD measured over a loaded 24-hour cycle without temperature control box.

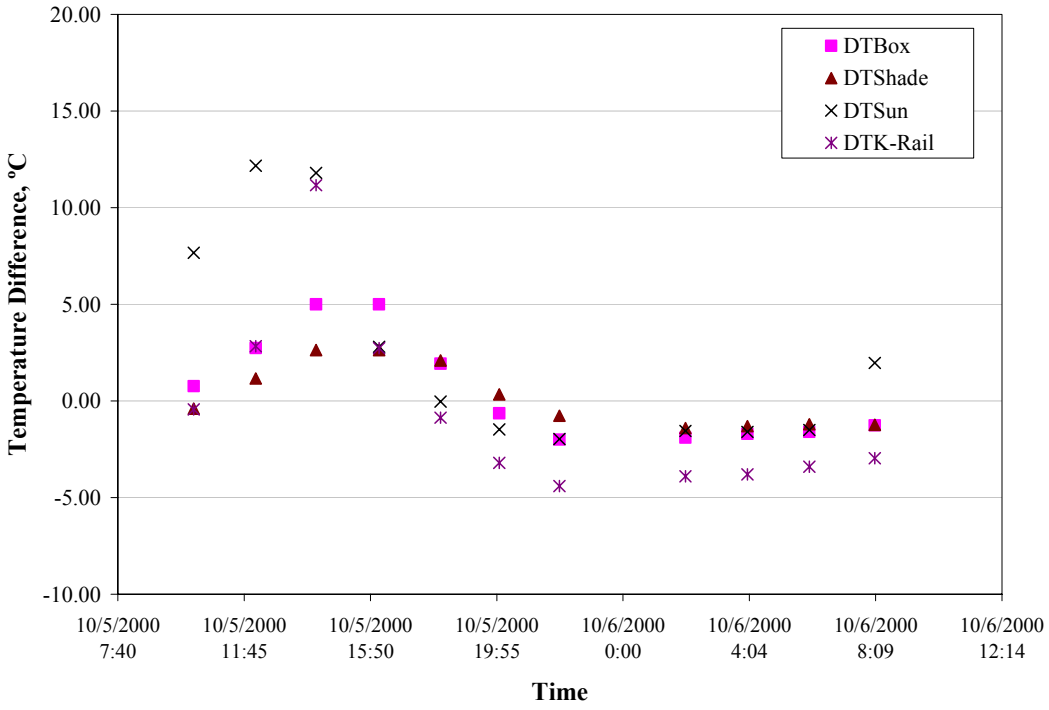

Figure 57. 24-hour temperature difference between the top sensor and the bottom sensor for Section 540FD measured using thermocouple assemblies at various locations (without temperature control box).

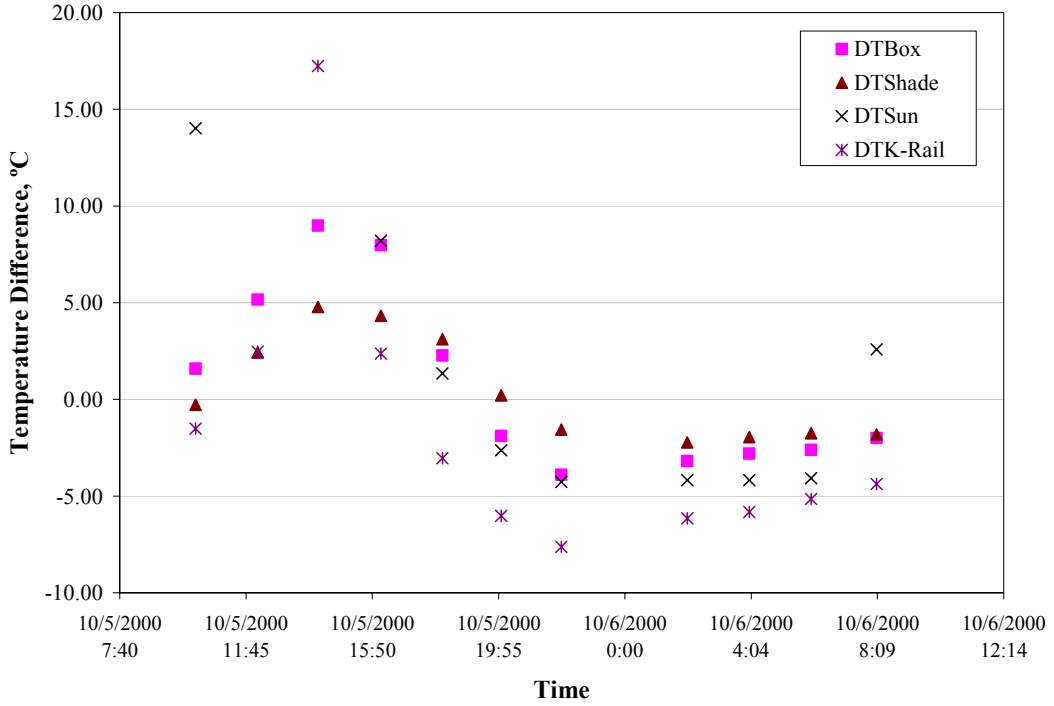

Figure 58. 24-hour temperature difference between the top of the slab and the bottom of the slab estimated using extrapolation and data collected using thermocouple assemblies at various locations (without temperature control box) for Section 540FD.

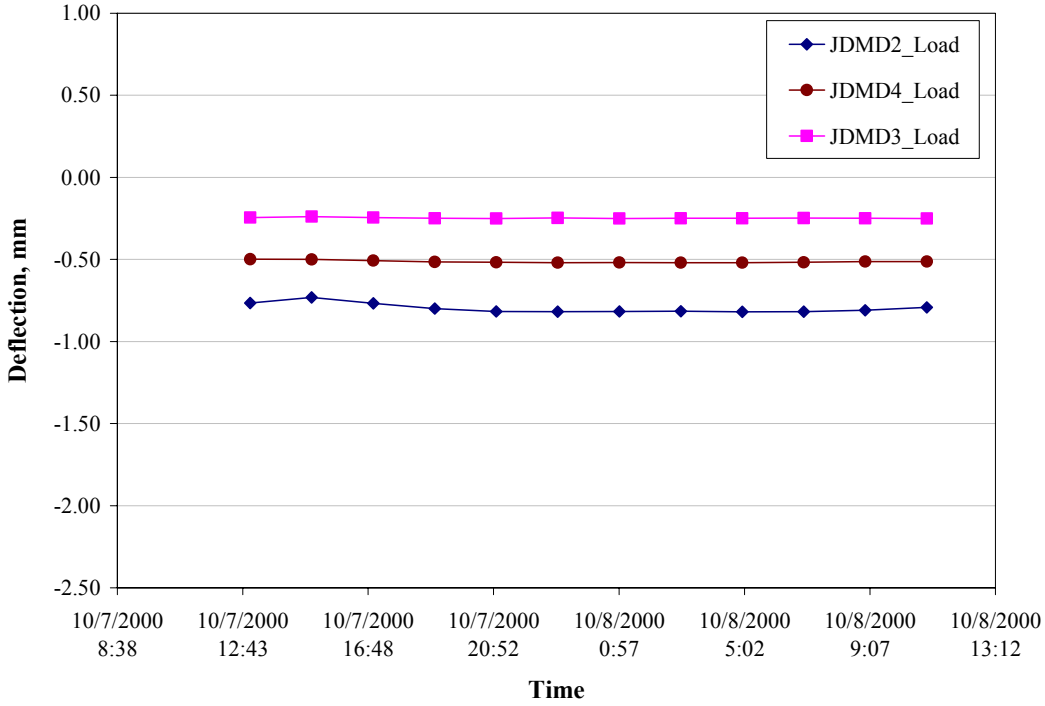

Figure 59. Corner (JDMD2 and JDMD4) and edge (JDMD3) deflections for Section 540FD with temperature control box.

MDDs over the same 24-hour cycle are shown in Figure 60. The corresponding temperature differences are shown in Figures 61 and 62.

The results of the analysis, the estimated EBITDs at three slab locations, are shown in Table 7. Figures 63 through 65 show the residuals (difference between measured deflections and predicted deflections) as a function of various factors. The EBITD results along with the initial cracking pattern are shown in Figure 66. The crack patterns in the test slab and the adjacent slabs after loading with the HVS are shown in Figure 67. As with Sections 535FD and 537FD, the corner break in the concrete slab corresponded to the side of the slab with the highest EBITD.

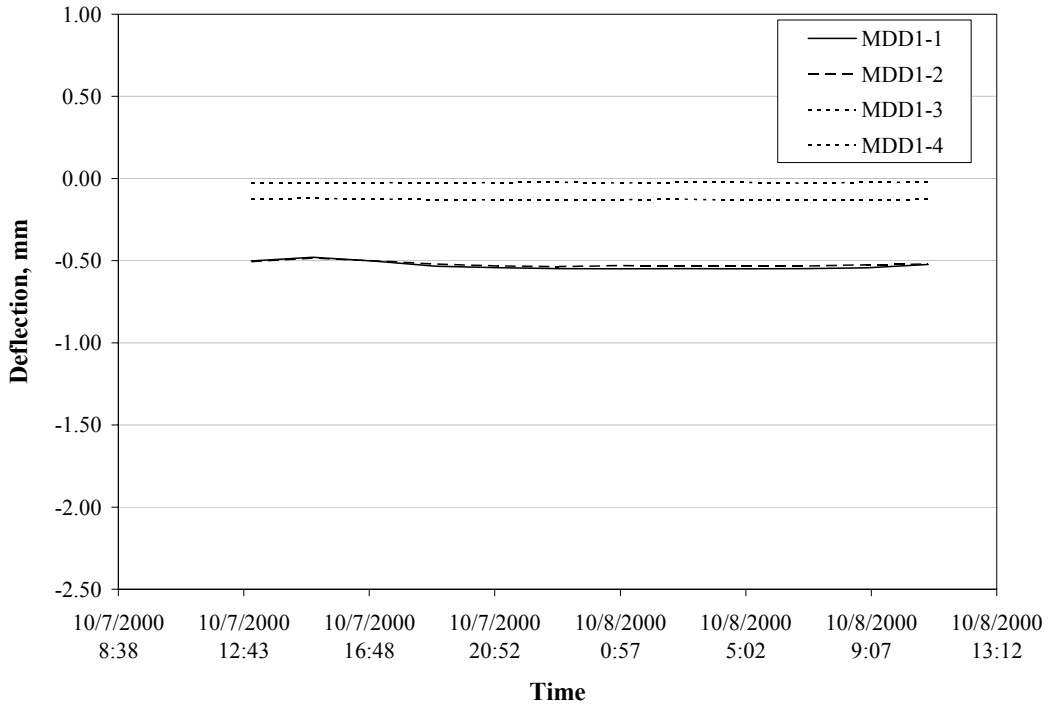

Figure 60. MDD deflections for Section 540FD measured over a loaded 24-hour cycle with temperature control box.

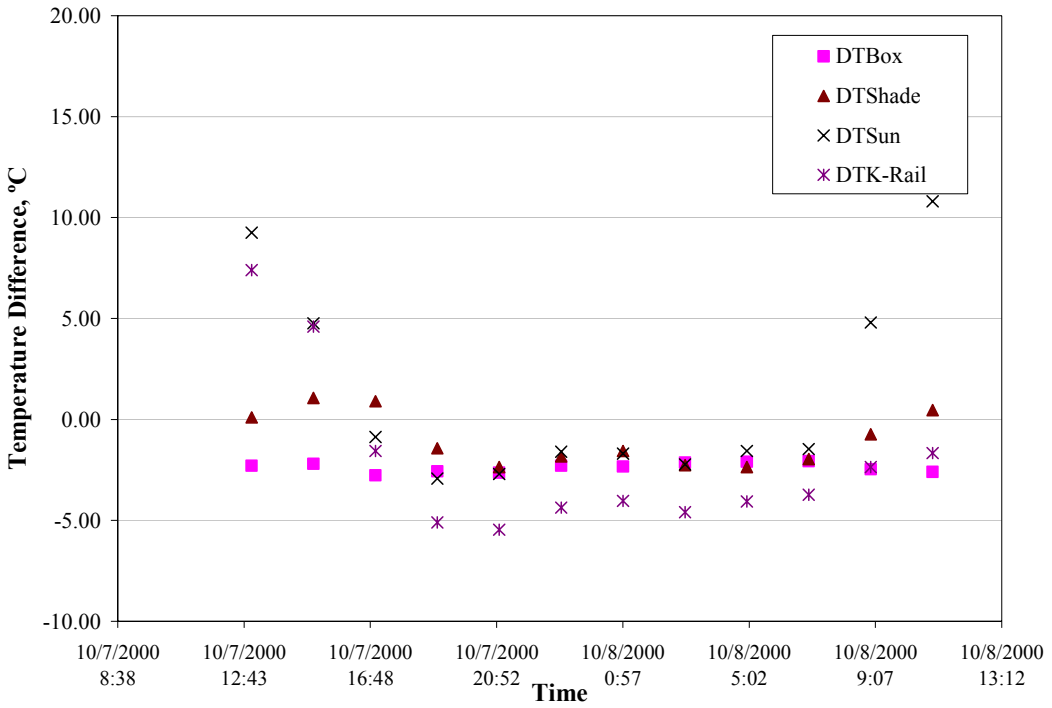

Figure 61. 24-hour temperature difference between the top sensor and the bottom sensor measured for Section 540FD using thermocouple assemblies at various locations (with temperature control box).

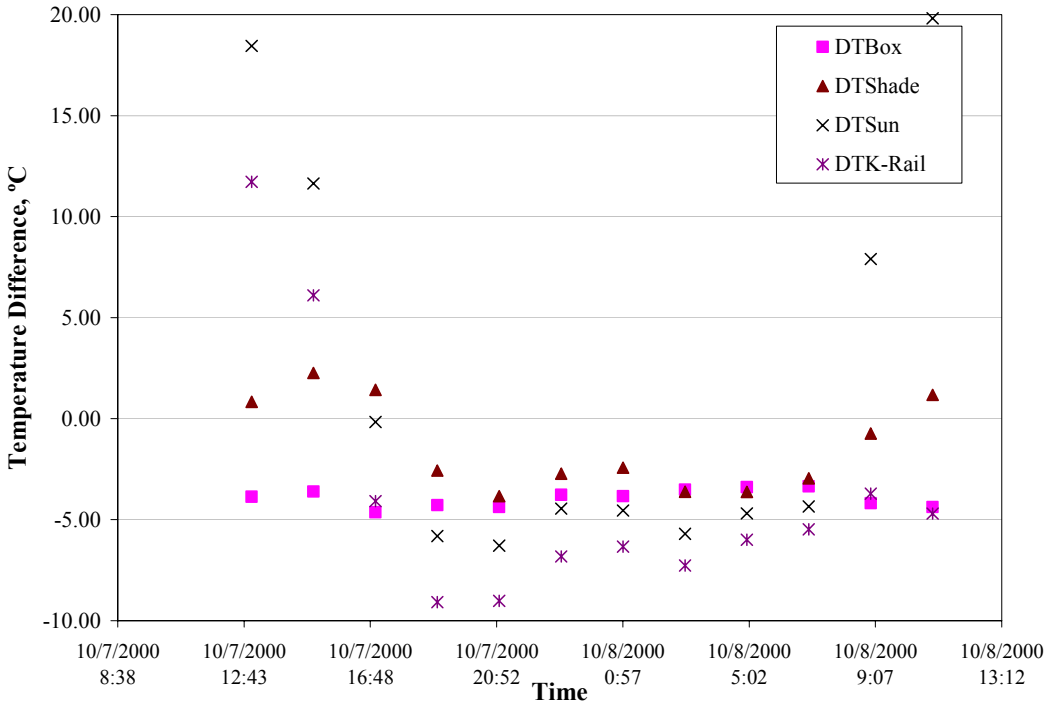

Figure 62. 24-hour temperature difference between the top of the slab and the bottom of the slab estimated using extrapolation and data collected using thermocouple assemblies at various locations (with temperature control box) for Section 540FD.

Table 7 Estimated Effective Built-In Temperature Difference (EBITD) for Section 540FD at Three Locations

Location on Slab		EBITD at Slab Location for Thermocouple Location, Extrapolated and Measured, ºF (ºC)					
		Thermocouple at Box		Thermocouple in Shade		Thermocouple at K-Rail	
		Extrapolated	Measured	Extrapolated	Measured	Extrapolated	Measured
Left Corner (JDMD4)	No Box	-25.7 (-14.3)	-25.3 (-14.1)	-25.1 (-13.9)	-24.7 (-13.7)	-19.5 (-10.8)	-22.6 (-12.6)
	With Box	-14.8 (-8.2)	-17.6 (-9.8)	-19.4 (-10.8)	-20.1 (-11.2)	-13.1 (-7.3)	-17.5 (-9.7)
Right Corner (JDMD2)	No Box	-31.9 (-17.7)	-31.2 (-17.3)	-31.0 (-17.2)	-30.5 (-16.9)	-26.2 (-14.6)	-29.1 (-16.2)
	With Box	-27.1 (-15.1)	-30.0 (-16.7)	-31.8 (-17.7)	-32.4 (-18.0)	-27.7 (-15.4)	-30.7 (-17.1)
Midslab (JDMD3)	No Box	-20.0 (-11.1)	-20.7 (-11.5)	-20.5 (-11.4)	-20.4 (-11.3)	-13.6 (-7.6)	-17.4 (-9.7)
	With Box	-11.9 (-6.6)	-14.8 (-8.2)	-16.2 (-9.0)	-17.1 (-9.5)	-9.1 (-5.1)	-13.8 (-7.7)

Data was collected with and without a temperature control box and using thermocouple data measured at various locations.

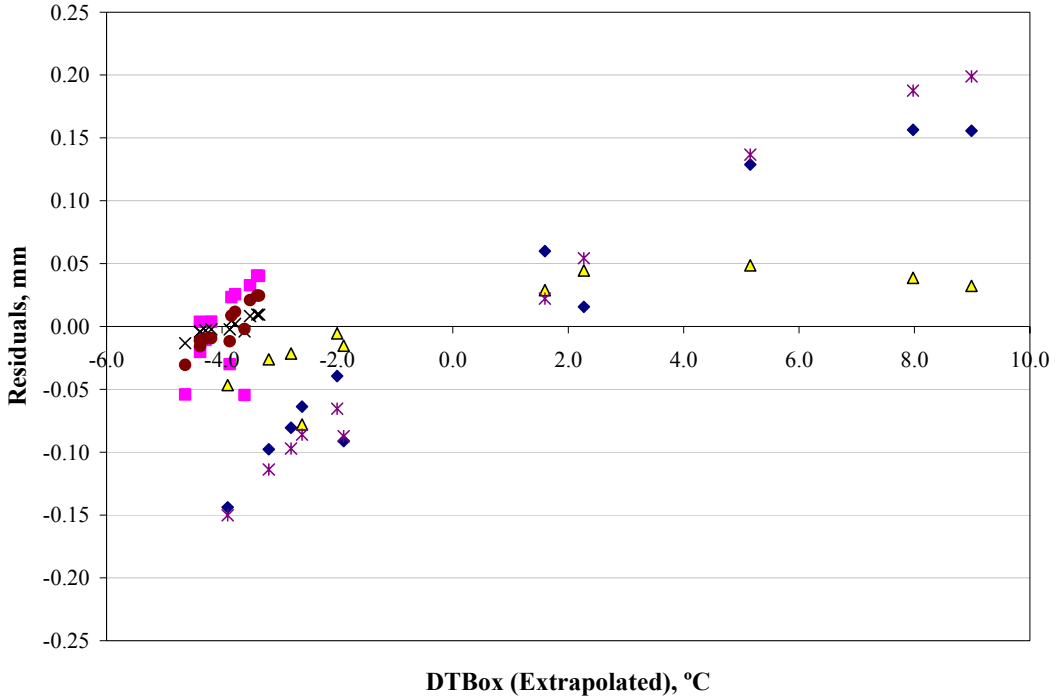

Figure 63. Residuals (difference in measured deflections and predicted deflections) as a function of extrapolated temperature difference (box) for JDMD2, JDMD3, and JDMD4 measured with and without the temperature control box for Section 540FD.

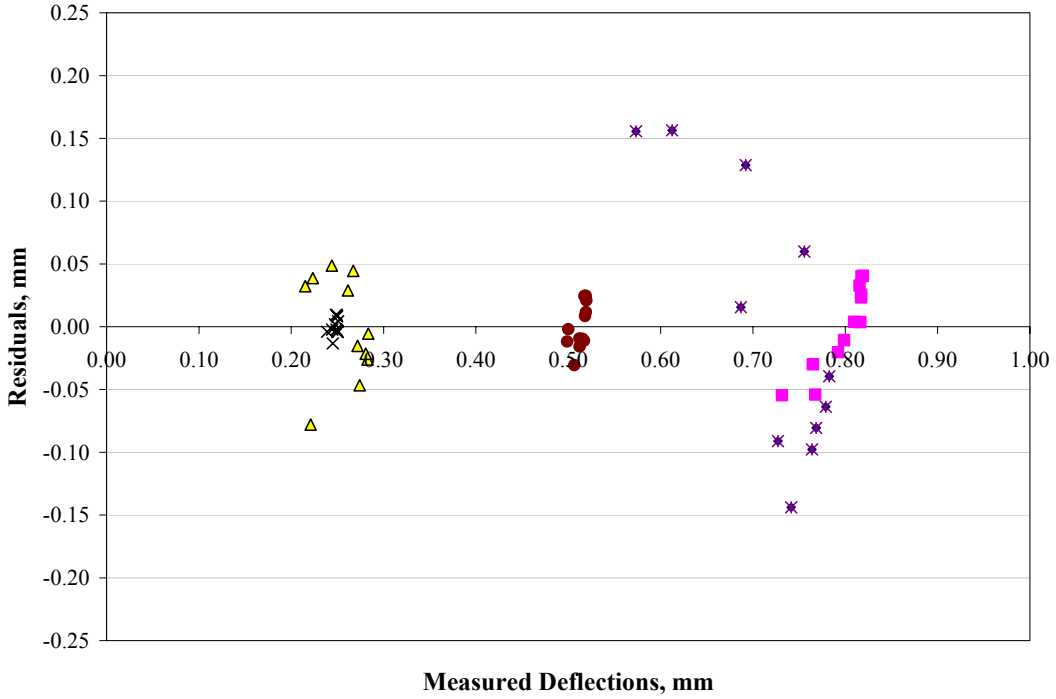

Figure 64. Residuals (difference in measured deflections and predicted deflections) as a function of measured deflections for JDMD2, JDMD3, and JDMD4 measured with and without the temperature control box for Section 540FD.

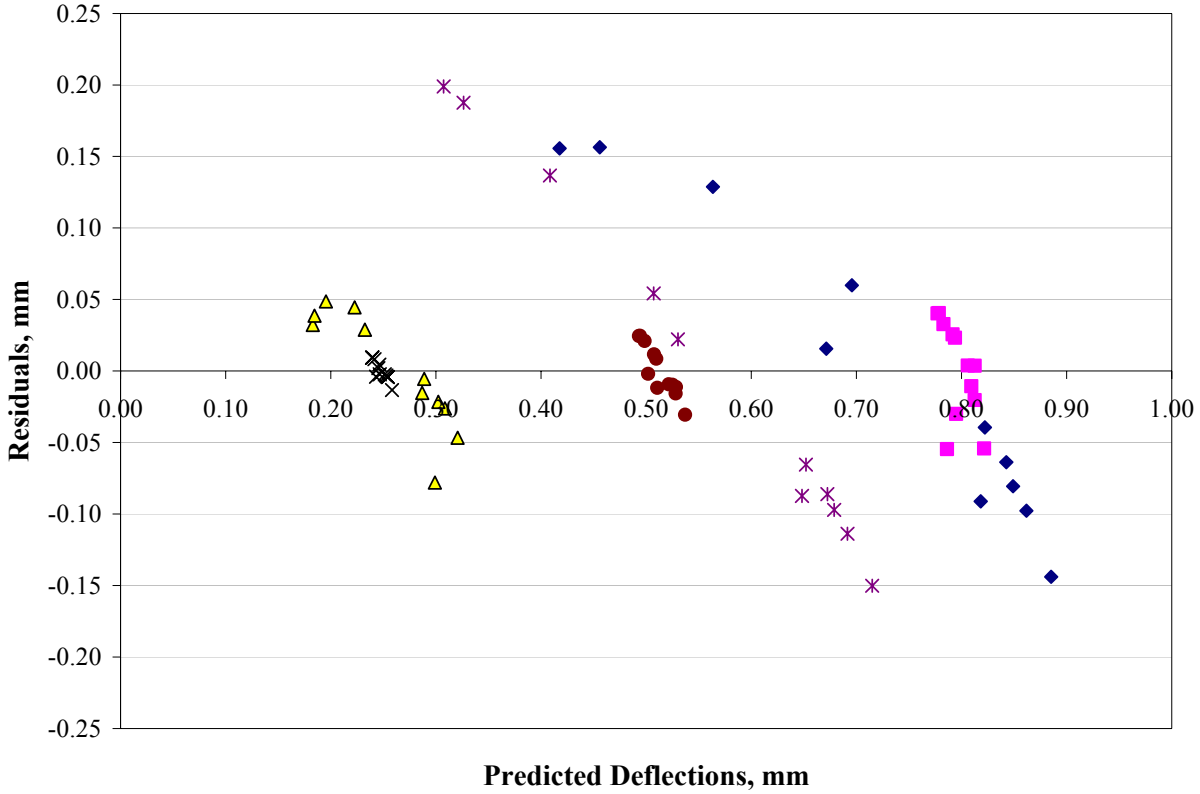

Figure 65. Residuals (difference in measured deflections and predicted deflections) as a function of predicted deflections for JDMD2, JDMD3, and JDMD4 measured with and without the temperature control box for Section 541FD.

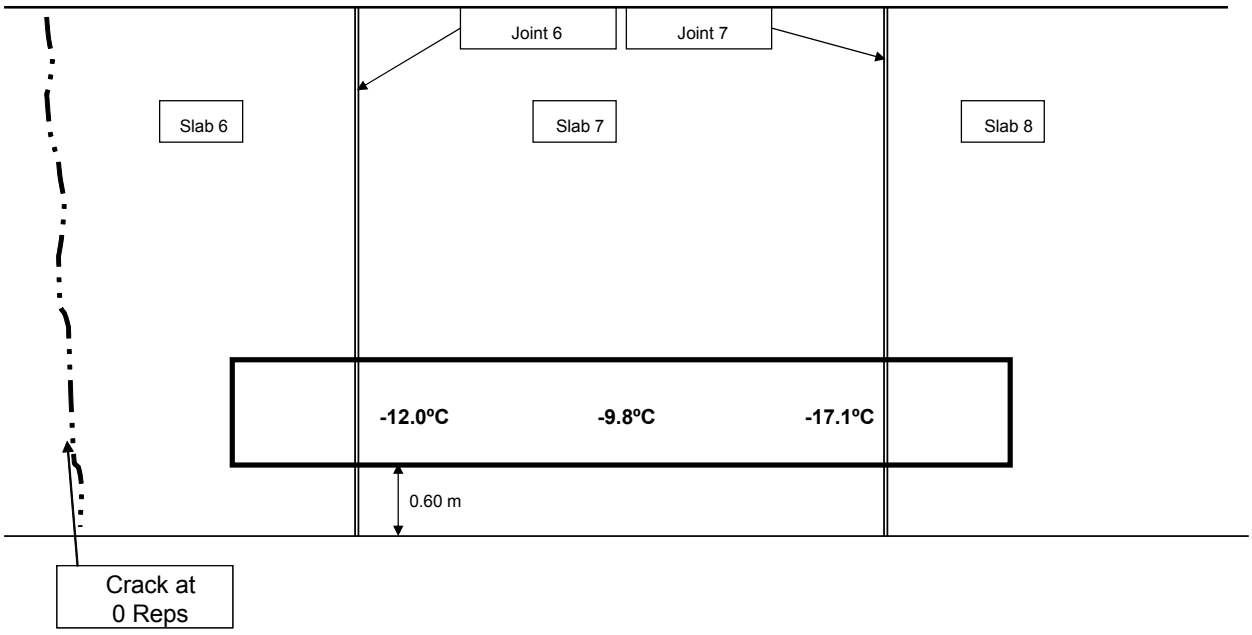

Figure 66. Crack pattern in slab (Section 540FD) prior to load application and estimated effective built-in temperature difference at three locations in the test slab.

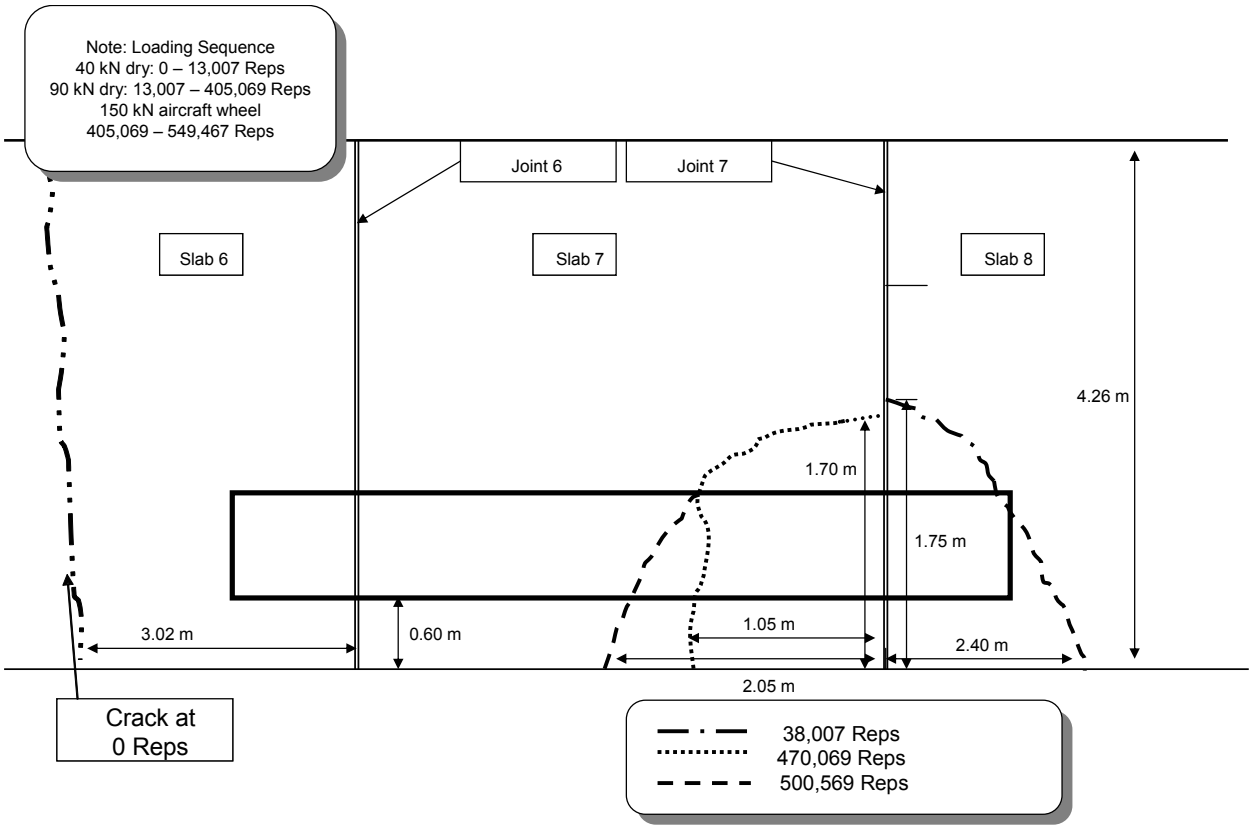

Figure 67. Crack pattern in slab (Section 540FD) after fatigue damage load application(*2*).

2.7 Section 541FD

The layout of the section and the locations of the sensors are shown in Figure 68.(*2*). The deflections measured by the JDMDs over the 24-hour cycle without the temperature control box are shown in Figure 69. No MDD data were collected for Section 541FD. The corresponding temperature differences are shown in Figures 70 and 71. 24-hour loaded deflection data with the temperature control box were not collected for Section 541FD.

The results of the analysis, the estimated EBITDs at three slab locations, are shown in Table 8. Figures 72 through 74 show the residuals (difference between measured deflections and predicted deflections) as a function of various factors. The EBITD results along with the initial cracking pattern are shown in Figure 75. As shown in Figure 76, Section 541FD did not have any cracks after HVS load application.

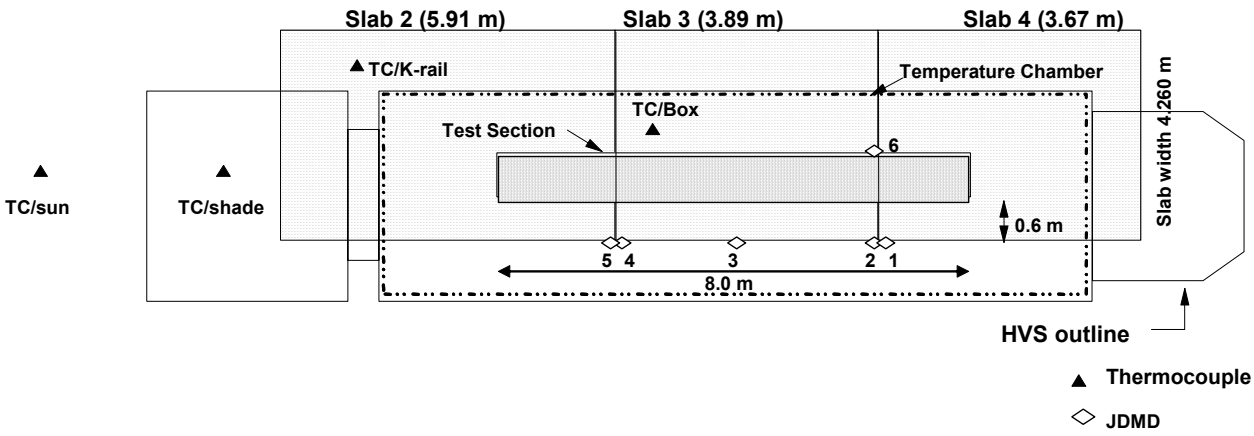

Figure 68. Instrumentation layout of Section 541FD.(*2*)

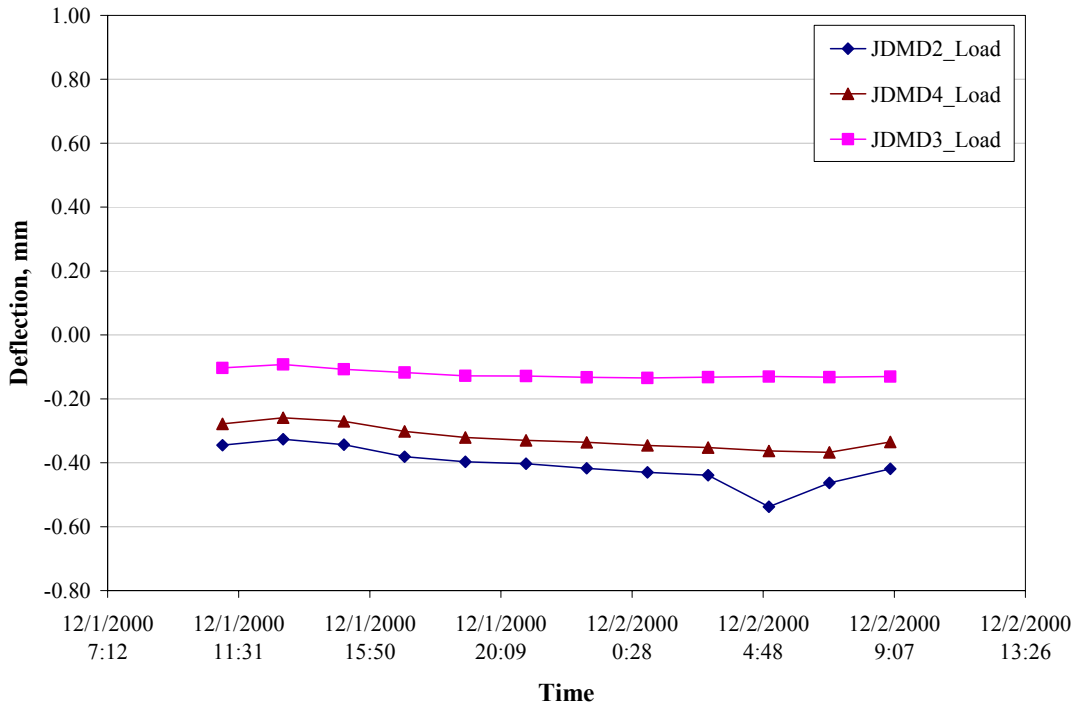

Figure 69. Corner (JDMD2 and JDMD4) and edge (JDMD3) deflections for Section 541FD without temperature control box.

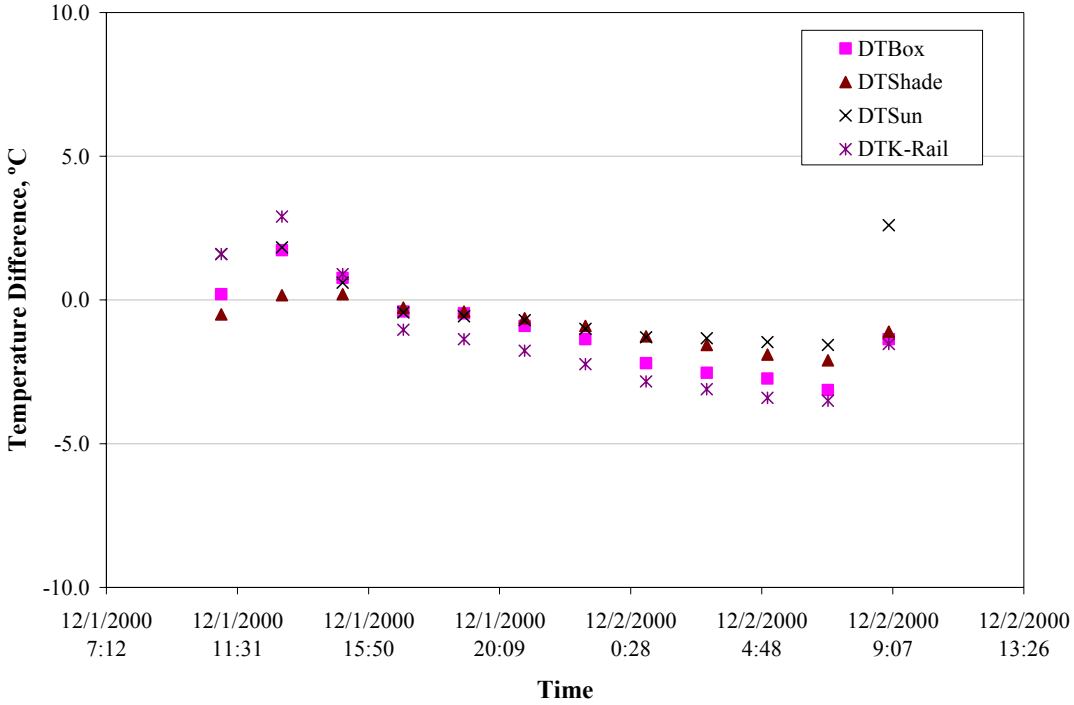

Figure 70. 24-hour temperature difference between the top sensor and the bottom sensor measured using thermocouple assemblies at various locations (without temperature control box) for Section 541FD.

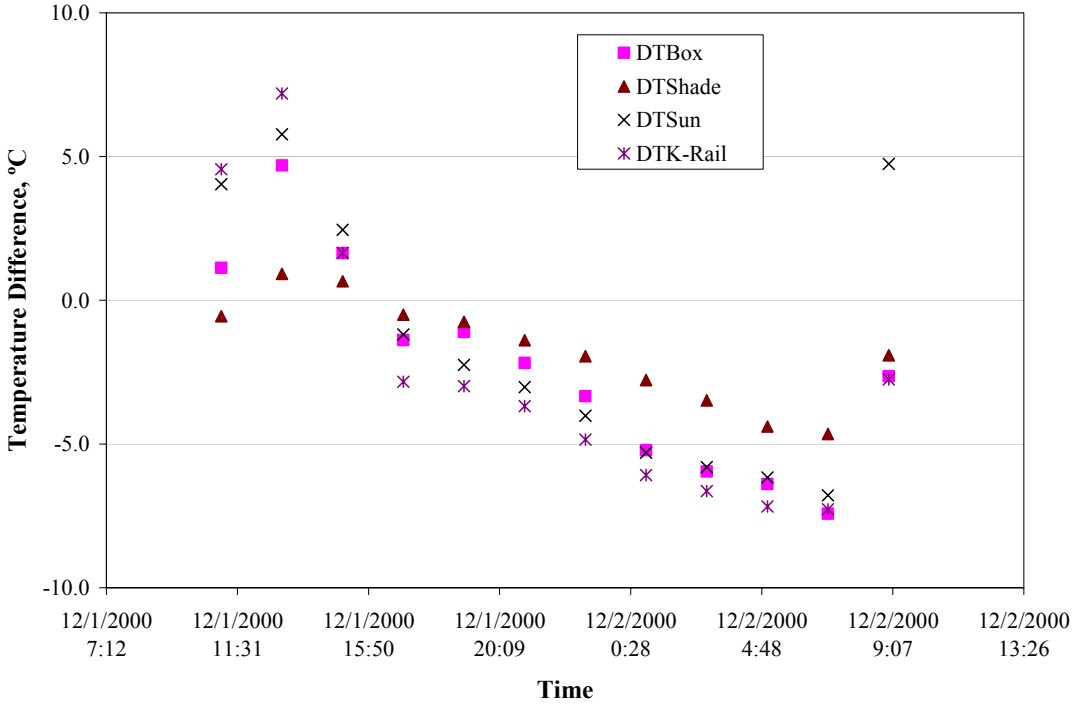

Figure 71. 24-hour temperature difference between the top of the slab and the bottom of the slab estimated using extrapolation and data collected using thermocouple assemblies at various locations (without temperature control box) for Section 541FD.

Table 8 Estimated Effective Built-In Temperature Difference (EBITD) for Section 541FD at Three Locations

Location on Slab		EBITD at Slab Location for Thermocouple Location, Extrapolated and Measured, ºF (ºC)					
		Thermocouple at Box		Thermocouple in Shade		Thermocouple at K-Rail	
		Extrapolated	Measured	Extrapolated	Measured	Extrapolated	Measured
Left Corner (JDMD4)	No Box	> -9.0 (> -5.0)	-11.1 (-6.2)	-9.7 (-5.4)	-11.6 (-6.4)	> -9.0 (> -5.0)	-10.3 (-5.7)
	With Box	-	-	-	-	-	-
Right Corner (JDMD2)	No Box	-13.3 (-7.4)	-16.2 (-9.0)	-14.9 (-8.3)	-16.5 (-9.2)	-12.0 (-6.7)	-15.6 (-8.7)
	With Box	-	-	-	-	-	-
Midslab (JDMD3)	No Box	> -9.0 (> -5.0)	> -9.0 (> -5.0)	> -9.0 (> -5.0)	> -9.0 (> -5.0)	> -9.0 (> -5.0)	> -9.0 (> -5.0)
	With Box	-	-	-	-	-	-

Data was collected only without a temperature control box and using thermocouple data measured at various locations.

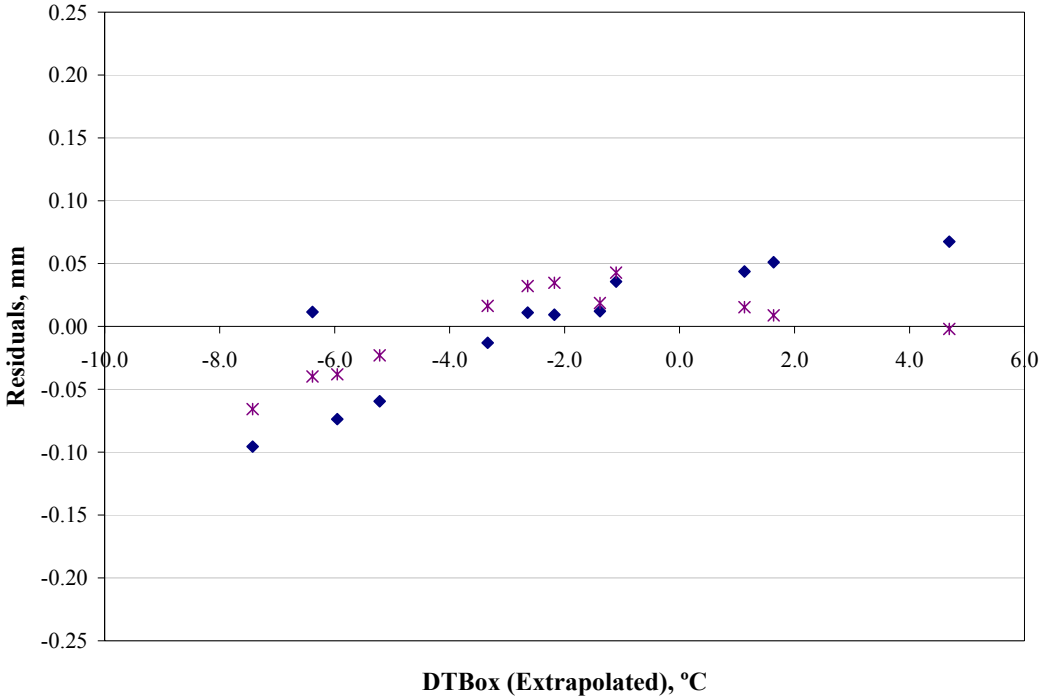

Figure 72. Residuals (difference in measured deflections and predicted deflections) as a function of extrapolated temperature difference (box) for JDMD2 and JDMD4 measured with and without the temperature control box for Section 541FD.

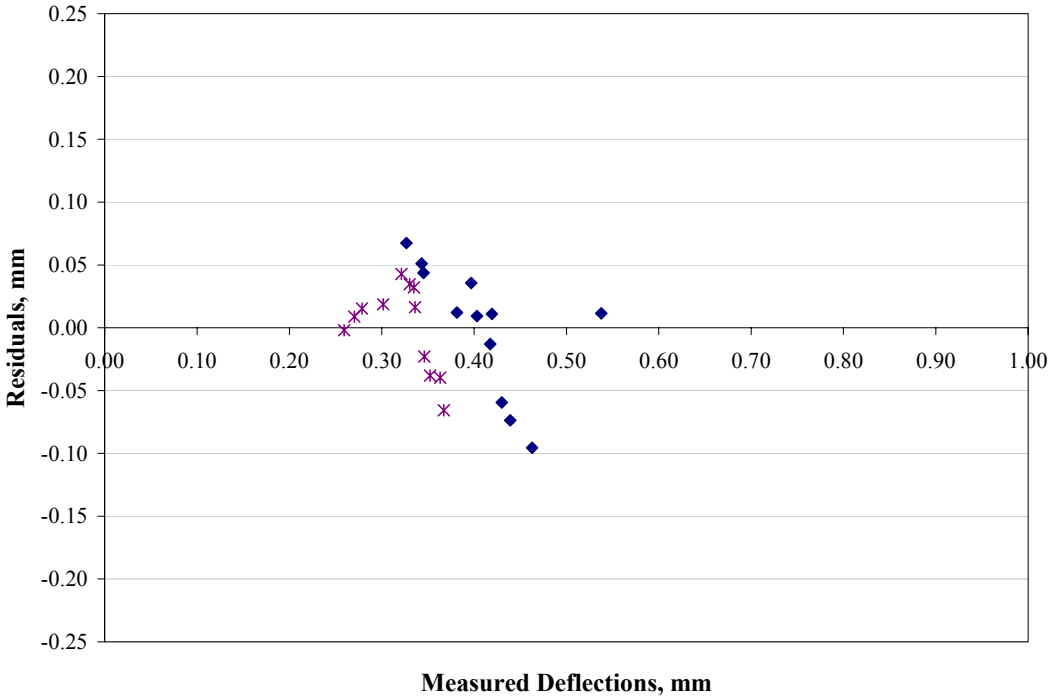

Figure 73. Residuals (difference in measured deflections and predicted deflections) as a function of measured deflections for JDMD2 and JDMD4 measured with and without the temperature control box for Section 541FD.

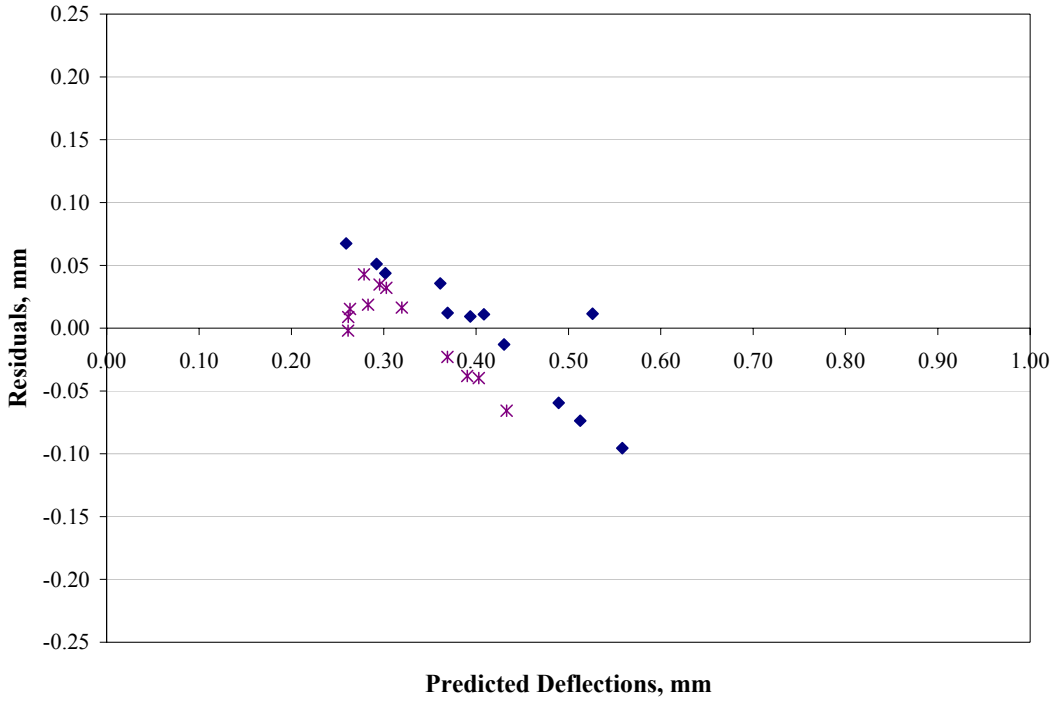

Figure 74. Residuals (difference in measured deflections and predicted deflections) as a function of predicted deflections for JDMD2 and JDMD4 measured with and without the temperature control box for Section 541FD.

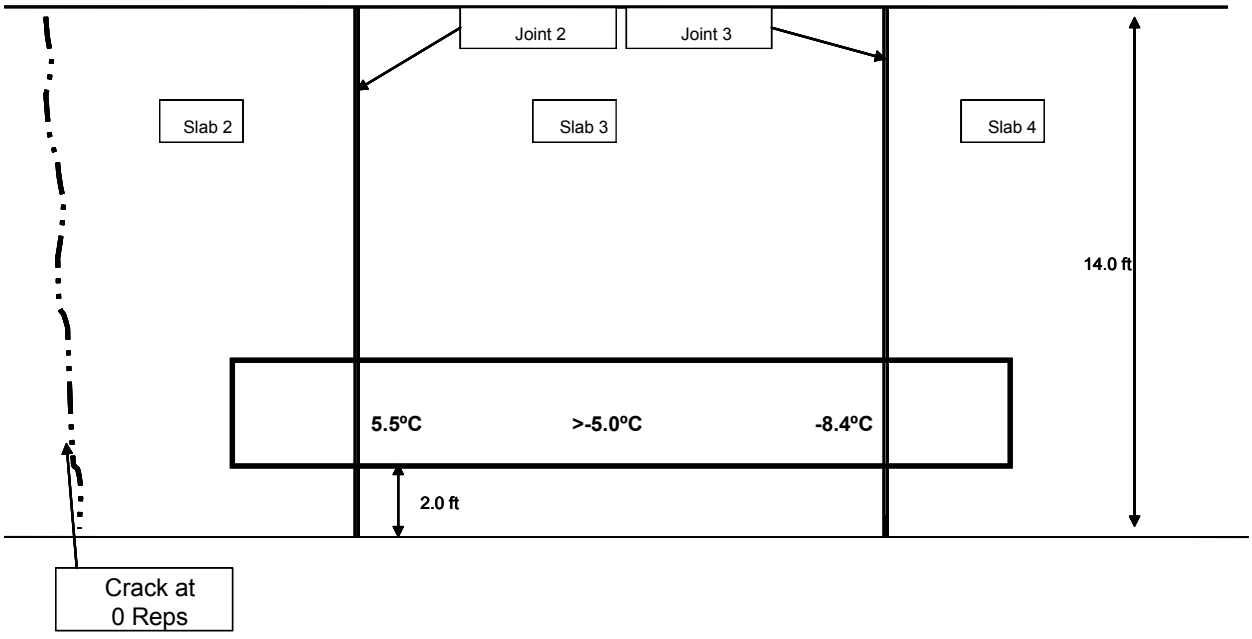

Figure 75. Crack pattern in slab (Section 541FD) prior to load application and estimated effective built-in temperature difference at three locations in the test slab.

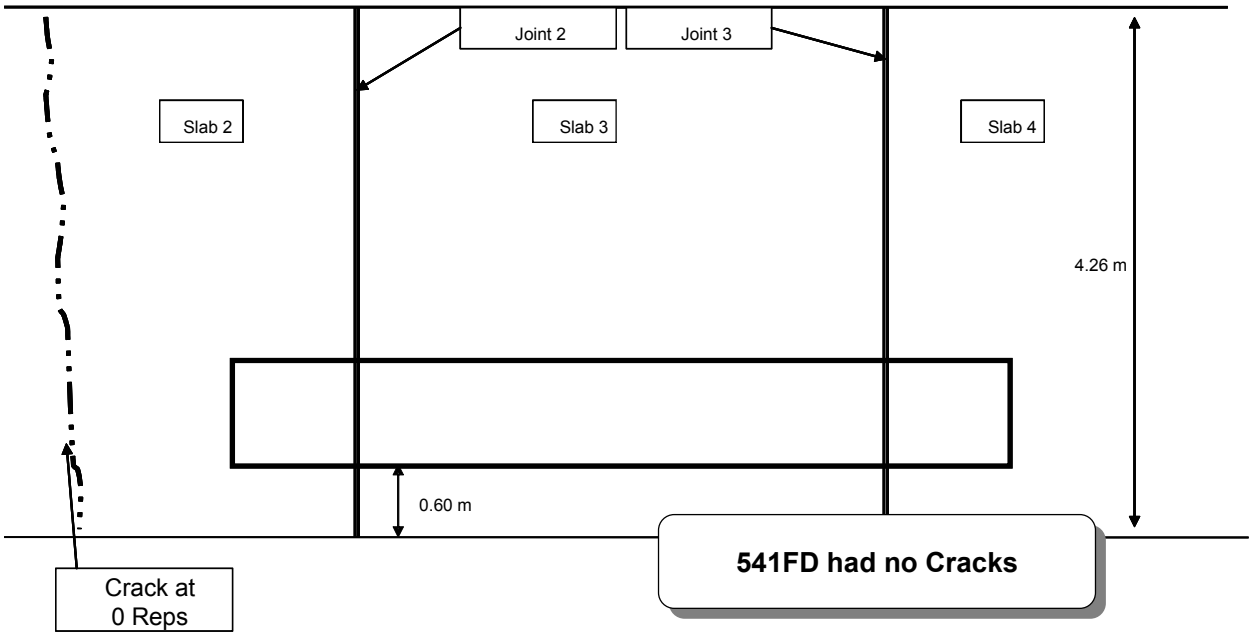

Figure 76. Crack pattern in slab (Section 541FD) after fatigue damage load application.(*2*)

2.8 Summary of 9,000-lb. (40-kN) Loaded JDMD Analysis

The EBITD analysis results for all test sections are summarized in Table 9. The average EBITD is based on two independent calculations of EBITD: with and without the temperature control box. Only the box and shade results were used for calculation of the average EBITD. As seen in Table 9, the EBITD varied considerably among sections and from one corner of the slab to the other. The highest EBITD occurred on Section 535FD [59.9ºF (15.5ºC)], which had the least amount of restraint on the slab (no dowels or tied concrete shoulders). The widened lane sections with dowels at the transverse joints (539FD to 541FD) had smaller calculated EBITD.

On all sections, the corners of the slab had a higher EBITD compared with the mid-slab edge. For Section 535FD, the estimated EBITDs were -59.9, -37.7, and -39.2ºF (-15.5, -20.9, and -21.8ºC) for the left corner, midslab edge, and right corner, respectively. The EBITD along the slab longitudinal edge was asymmetric, as shown in Figure 1c. Although the EBITD appeared high in Section 535FD, the concrete slabs satisfied many conditions relevant to high

Table 9 Summary of Estimated Effective Built-In Temperature Difference for North Tangent Sections at JDMD Locations

Section ID	Effective Built-In Temperature Difference at Location for Given Condition, °F (°C)								
	Left Corner			Midslab			Right Corner		
	No Temperature Control Box	With Temperature Control Box	Average	No Temperature Control Box	With Temperature Control Box	Average	No Temperature Control Box	With Temperature Control Box	Average
535FD[a]	-56.9 (-31.6)	-63.0 (-35.0)	-59.9 (-33.3)	-35.8 (-19.9)	-39.6 (-22.0)	-37.7 (-20.9)	-38.5 (-21.4)	-40.0 (-22.2)	-39.2 (-21.8)
537FD[b]	> -9.0 (> -5.0)	> -9.0 (> -5.0)	> -9.0 (> -5.0)	> -9.0 (> -5.0)	> -9.0 (> -5.0)	> -9.0 (> -5.0)	-16.6 (-9.2)	-22.7 (-12.6)	-19.6 (-10.9)
538FD[b]	-26.5 (-14.7)	-	-26.5 (-14.7)	> -9.0 (> -5.0)	-	> -9.0 (> -5.0)	-33.3 (-18.5)	-	-33.3 (-18.5)
539FD[c]	-18.9 (-10.5)	-20.2 (-11.2)	-19.5 (-10.8)	-10.8 (-6.0)	-9.9 (-5.5)	-10.3 (-5.7)	-24.1 (-13.4)	-22.9 (-12.7)	-23.4 (-13.0)
540FD[c]	-25.2 (-14.0)	-18.0 (-10.0)	-21.6 (-12.0)	-20.3 (-11.3)	-14.9 (-8.3)	-17.7 (-9.8)	-31.1 (-17.3)	-30.2 (-16.8)	-30.8 (-17.1)
541FD[c]	-9.9 (-5.5)	-	-9.9 (-5.5)	> -9.0 (> -5.0)	-	> -9.0 (> -5.0)	-15.2 (-8.4)	-	-15.2 (-8.4)

a. No dowels, AC shoulder
b. Dowels, tied PCC shoulder
c. Dowels, widened lane, AC shoulder (analysis corresponding to wheelpath position, i.e., 2 ft. (0.61 m) from slab/shoulder joint).

EBITD including fast-setting high-early-strength concrete, desert conditions, daytime construction, and low restraint (no dowels and AC shoulders). The results were consistent with those observed by Byrum who studied curvatures of jointed concrete pavement slabs.(*21*) Byrum observed equivalent linear temperature gradients ranging from -8.0ºF/in. to +10ºF/in. (-1.7ºC/cm to +2.2ºC/cm) or TELTDs of -64 to +80ºF for 8-in. slabs (-35.6 to 44.4ºC for 200-mm slabs). The results are further supported by the fact that all the long slabs [18 or 19 ft. (5.49 or 5.79 m) at the test site had cracked prior to any load application.(*22*)

2.9 MDD Deflection Analysis

The analysis described in the previous section was also performed for interior vertical surface deflections measured by the MDDs. The MDD locations and the results for the analysis sections are summarized in Table 10. The results of the JDMD analysis and the MDD analysis in Tables 9 and 10 suggest a slight reduction in EBITD going from the slab edges towards the interior of the slab.

Table 10 Summary of Estimated Effective Built-In Temperature Difference for North Tangent Sections at MDD Locations

Section	MDD Location	No Temperature Control Box	With Temperature Control Box	Average
535FD	Midslab, 1.0 ft. (.30 m) from shoulder	-34.0 (-18.9)	-37.1 (-20.6)	-35.5 (-19.7)
537FD	Right corner, 1.0 ft. (.30 m) from shoulder, 1.0 ft. (.30 m) from transverse joint	> -9.0 (> -5.0)	> -9.0 (> -5.0)	> -9.0 (> -5.0)
538FD	No MDD	-	-	-
539FD	Right corner, 1.0 ft. (.30 m) from lane edge (3.0 ft. from shoulder), 1.0 ft. (.30 m) from transverse joint	-12.4 (-6.9)	-12.2 (-6.8)	-12.3 (-6.8)
540FD	Right corner, 1.0 ft. (.30 m) from lane edge [3.0 ft. (.91 m) from shoulder), 1.0 ft. (.30 m) from transverse joint	-31.5 (-17.5)	-27.9 (-15.5)	-29.7 (-16.5)
541FD	No MDD	-	-	-

3.0 ANALYSIS OF 4,500–18,000 LB. (20-80 KN) INCREMENTALLY LOADED CORNER AND MIDSLAB EDGE DEFLECTIONS

As part of the 24-hour loading analysis of the North Tangent sections, each test slab was subject to incremental rolling dual-wheel HVS loads ranging from 4,500 to 18,000 lb. (20-80 kN) in increments of 2,250 lb. (10 kN). These incremental loads were typically applied within 5 minutes of each other and the entire set of incremental loading for a given section was completed within an hour. Deflections resulting from the rolling HVS load were collected during testing using JDMDs as in the case of the 4,500-lb. (20-kN) 24-hour load tests. The vertical temperature profile data in the slab were also collected using the embedded thermocouples. Since all the data for each section were collected within an hour, there was no significant difference in thermocouple readings between different load increments.

3.1 Data Analysis Procedure

The 4,500–18,000 lb. (20–80 kN) incremental loaded corner and midslab edge deflection analysis was performed to verify results of the JDMD analysis of 4,500-lb. (20-kN) loaded corner and midslab edge deflections performed previously and the values of the EBITD obtained from that analysis. The average estimated EBITD was added to the temperature difference measured by the embedded thermocouples to obtain the TELTD in the slab. Using known layer properties and slab geometry, ISLAB2000 was used to calculate the slab deflections corresponding to each load increment. These calculations were performed for both corners and the midslab edge of the test slabs.

The deflections measured by the JDMDs over the incremental load cycle are shown in Figure 77. The deflections measured by the MDDs during the same cycle are shown in Figure 78. The temperature differences during this analysis are not plotted because there was no

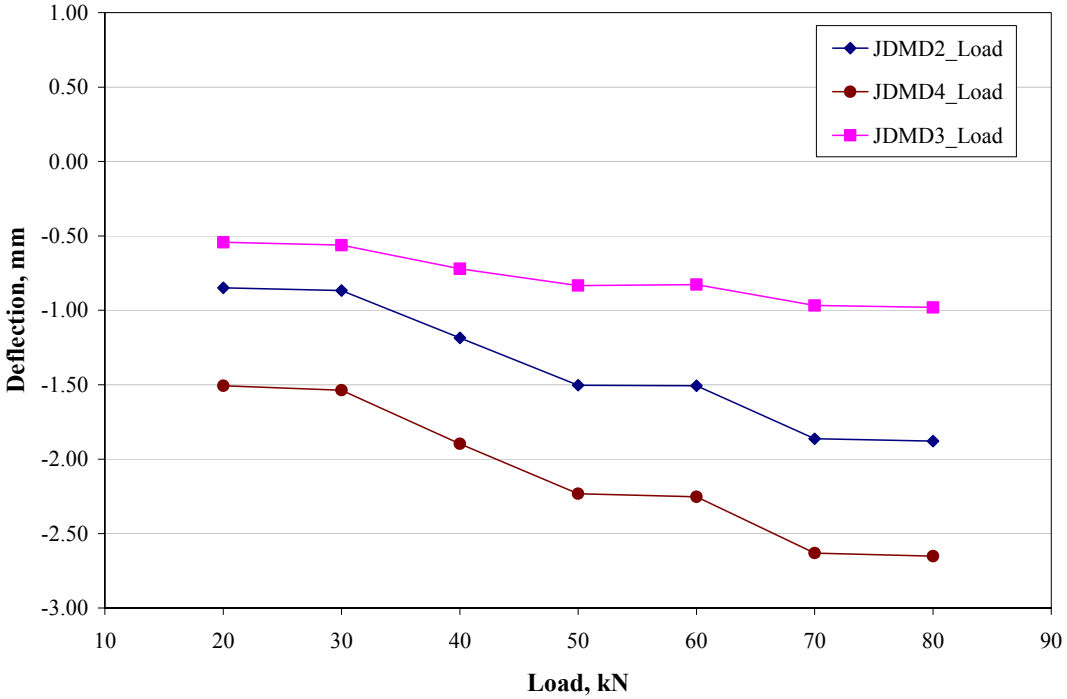

Figure 77. Corner (JDMD2 and JDMD4) and edge (JDMD3) deflections for Section 535FD under the influence of 4,500–18,000 lb. (20–80 kN) incremental loads with no significant difference in slab temperatures.

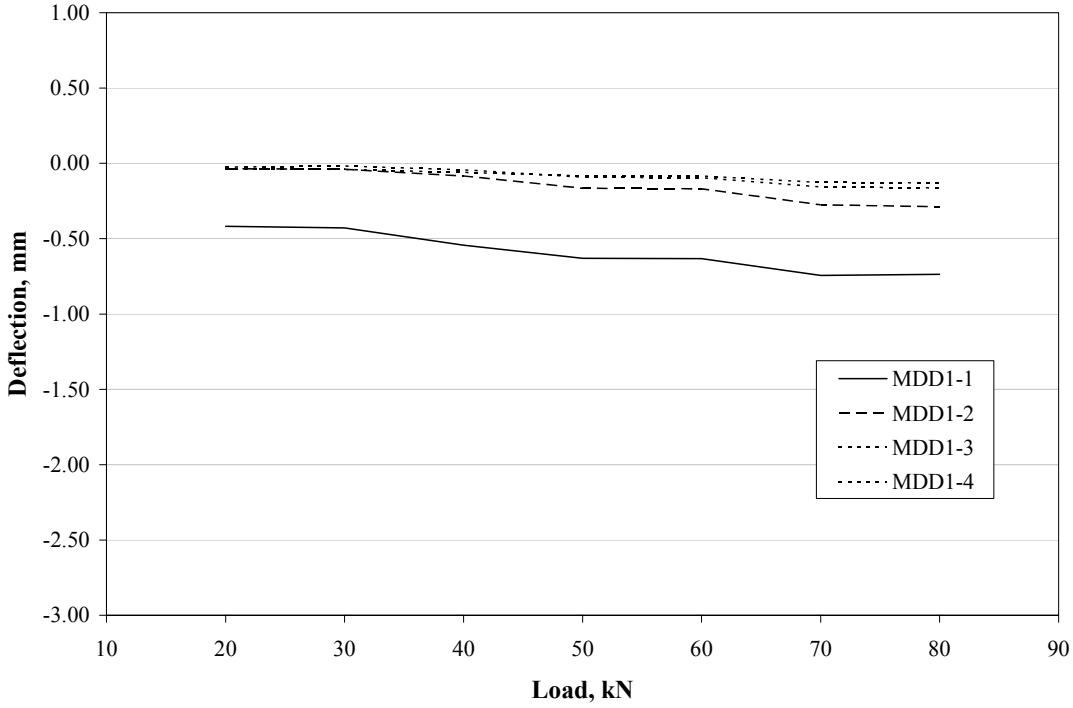

Figure 78. MDD deflections for Section 535FD under the influence of 4,500–18,000 lb. (20–80 kN) incremental loads with no significant difference in slab temperatures.

significant change in thermocouple temperatures within the hour that the data was collected. The results of the analysis are shown in Figures 79 and 80. Figure 79 shows a plot of deflections (both measured and predicted using the EBITD and ISLAB2000) versus load. Figure 80 shows a plot of predicted deflections versus measured deflections. The measured JDMD and MDD deflections and the results of the analysis for Sections 537FD through 541FD are shown in Figures 81 through 98.

3.2 Summary of Incremental Load JDMD Analysis

The results of the incremental load analysis show good agreement between the deflections predicted using calculated EBITD and ISLAB2000 and the measured deflections at the test locations for Sections 535FD, 540FD, and 541FD, as shown in Figures 80, 90, and 98. The agreement between the predicted and measured deflections at test locations on Sections 537FD, 538FD, and 539FD are poor, particularly at higher load levels (Figures 84, 87, and 94). For Section 537FD, the trend in Figure 83 suggests that this may be due to an incorrect assumption regarding at least one parameter (modulus, thickness, etc.) used in the analysis. The incorrect assumption of this parameter interacts with the load to produce the difference between measured and predicted deflections.

For Sections 538FD and 539FD, the measured deflections do not increase with the load at low load levels as seen in Figure 85 and figure 91 as would be expected. This could be a result of the HVS load not being set correctly. The HVS load level is set manually and read through a dial gage and this may be a source of the discrepancies for 538FD and 539FD.

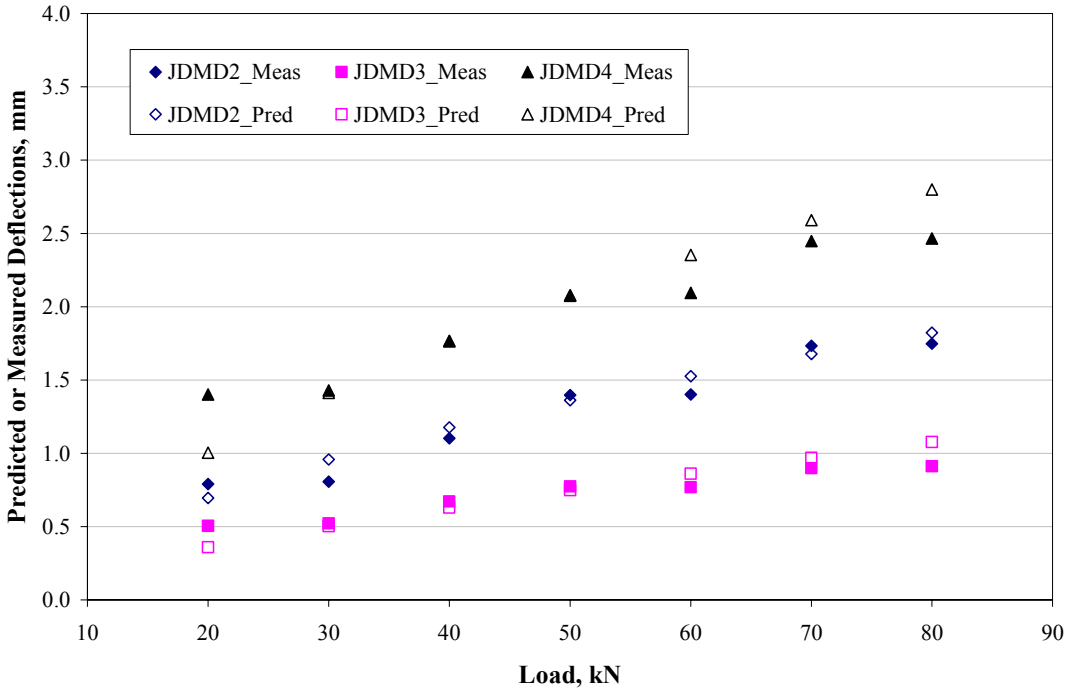

Figure 79. Comparisons of predicted and measured corner (JDMD2 and JDMD4) and edge (JDMD3) deflections for Section 535FD under the influence of 4,500–18,000 lb. (20–80 kN) incremental loads.

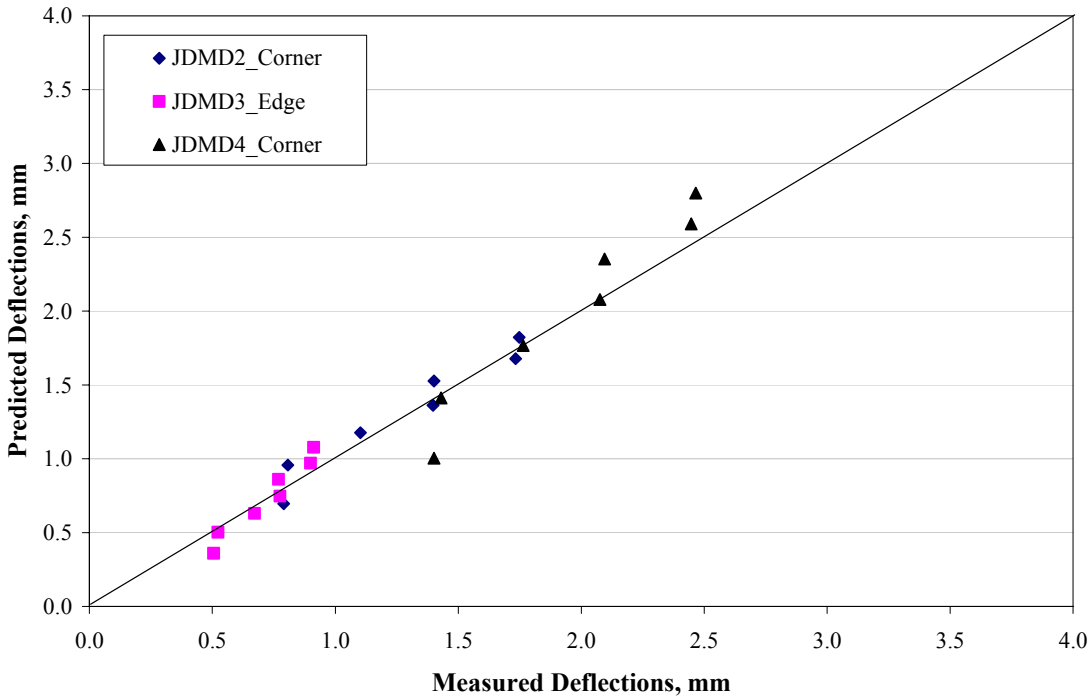

Figure 80. Predicted versus measured corner (JDMD2 and JDMD4) and edge (JDMD3) deflections for Section 535FD under the influence of 4,500–18,000 lb. (20-80 kN) incremental loads.

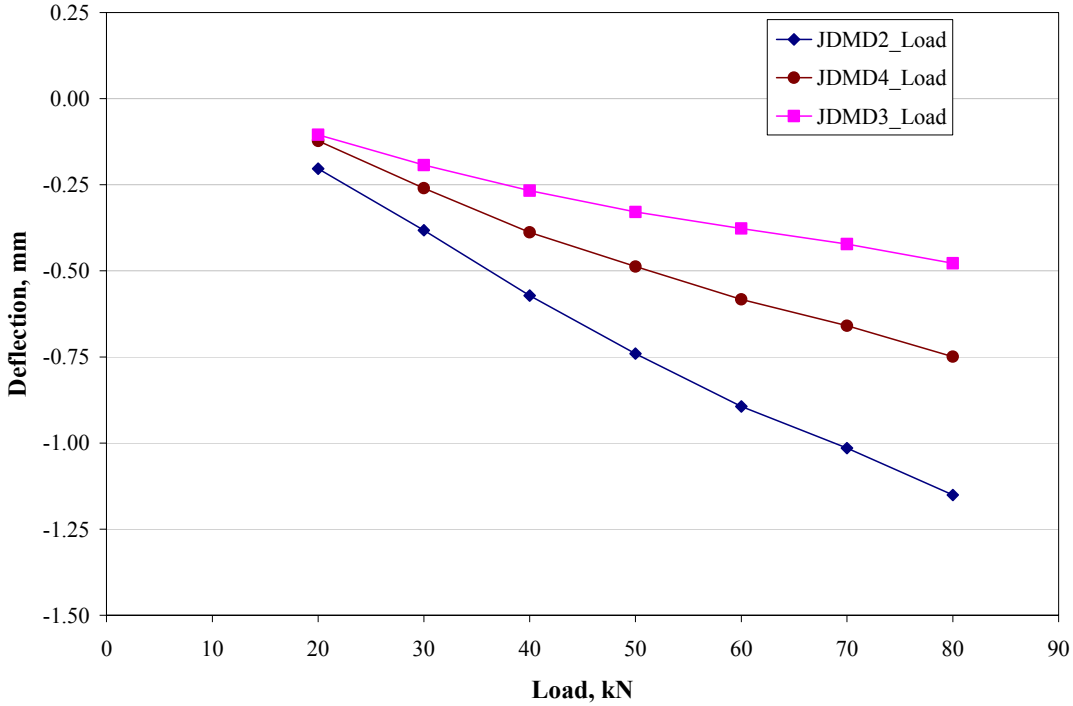

Figure 81. Corner (JDMD2 and JDMD4) and edge (JDMD3) deflections for Section 537FD under the influence of 4,500–18,000 lb. (20–80 kN) incremental loads with no significant difference in slab temperatures.

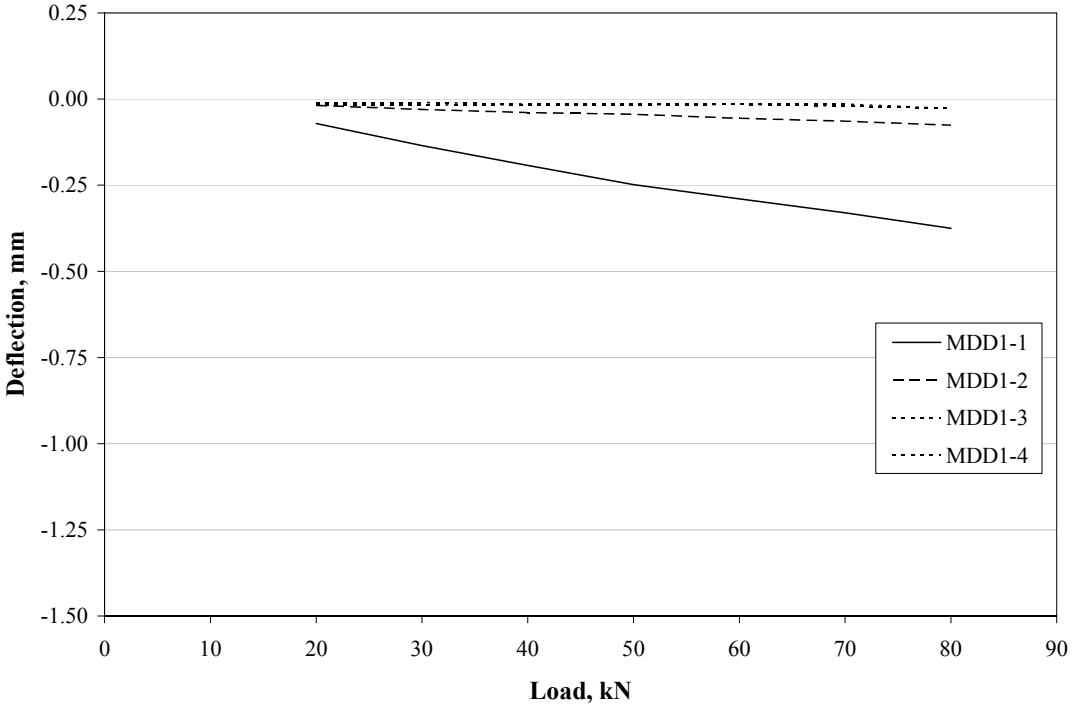

Figure 82. MDD deflections for Section 537FD under the influence of 4,500–18,000 lb. (20-80 kN) incremental loads with no significant difference in slab temperatures.

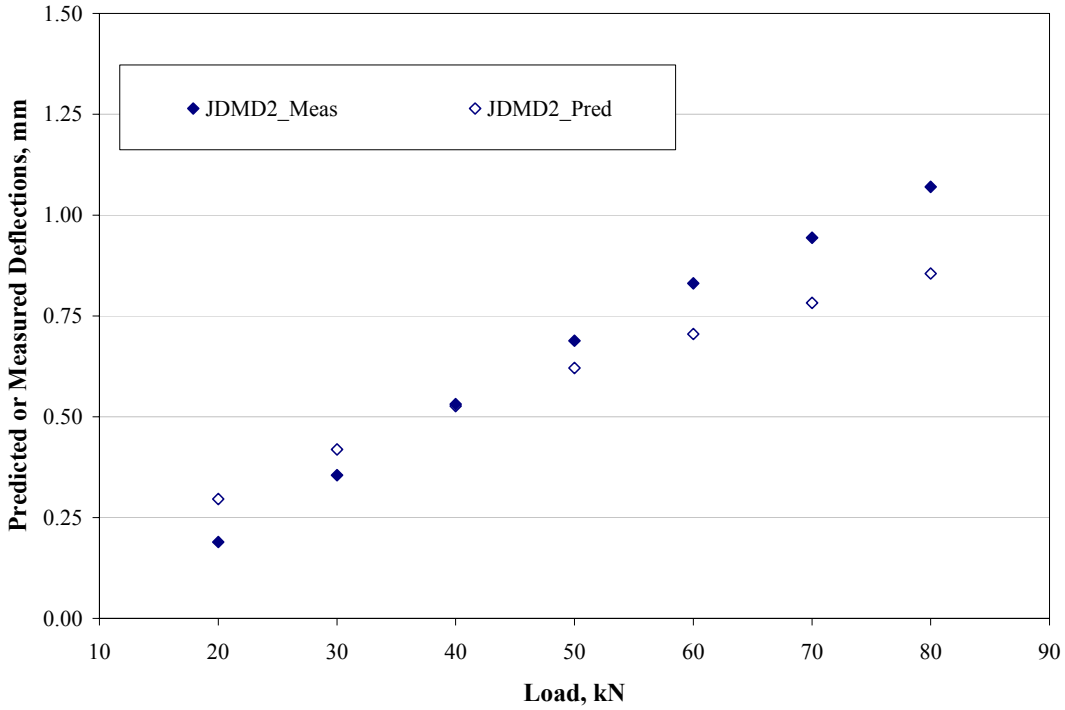

Figure 83. Comparisons of predicted and measured corner (JDMD2) deflections for Section 537FD under the influence of 4,500–18,000 lb. (20-80 kN) incremental loads.

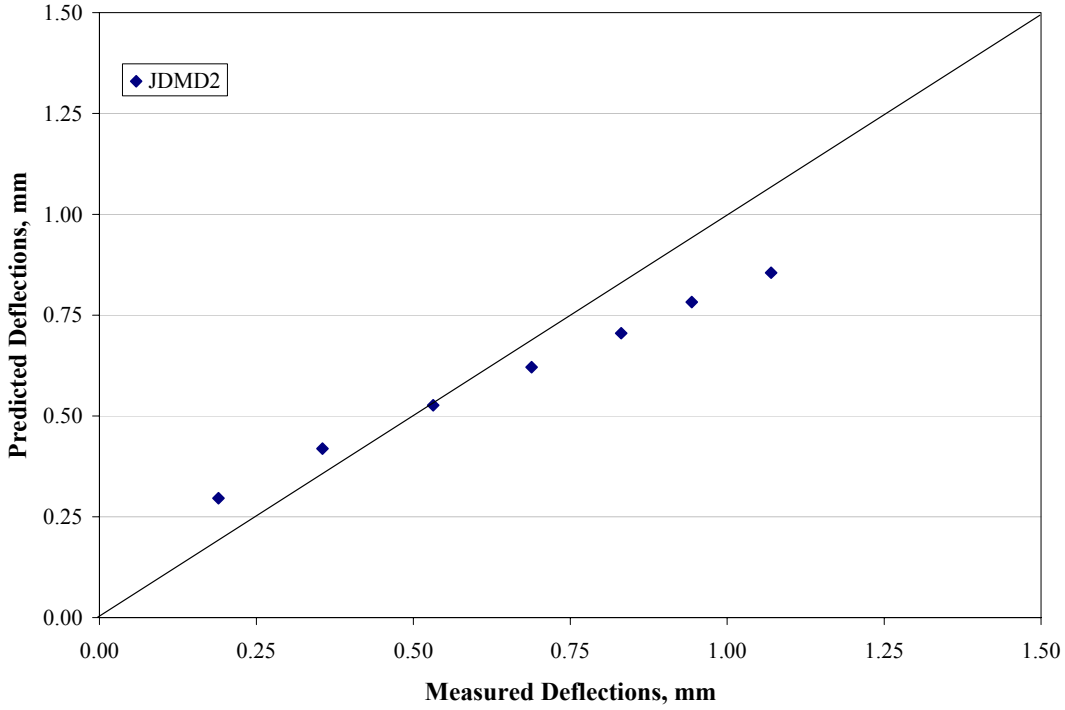

Figure 84. Predicted versus measured corner (JDMD2) deflections for Section 537FD under the influence of 4,500–18,000 lb. (20-80 kN) incremental loads.

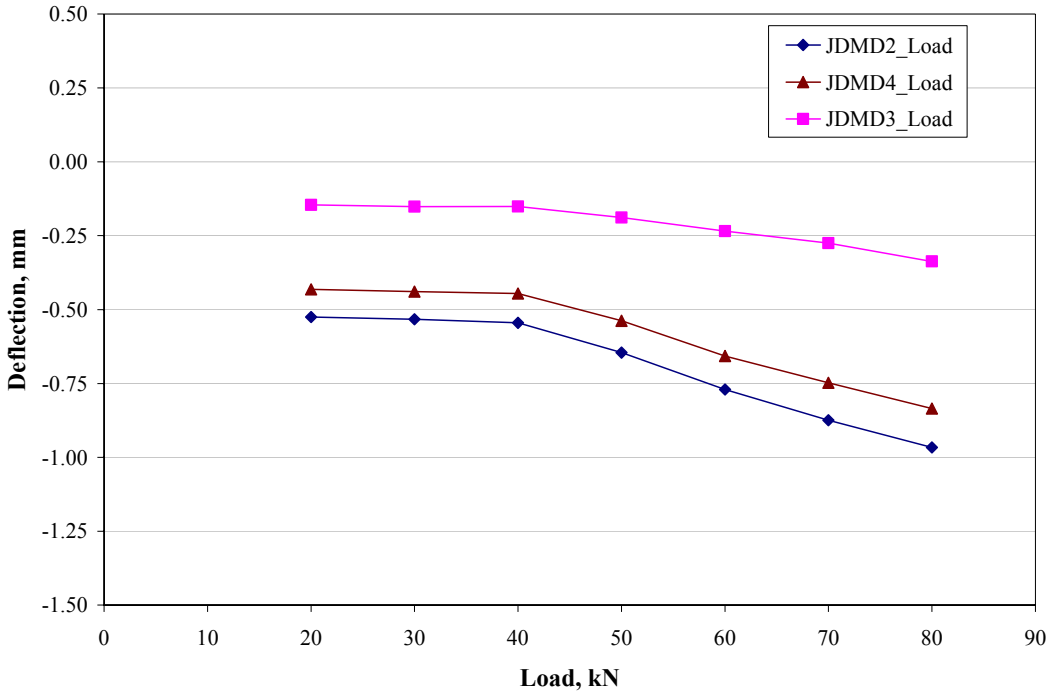

Figure 85. Corner (JDMD2 and JDMD4) and edge (JDMD3) deflections for Section 538FD under the influence of 4,500–18,000 lb. (20-80 kN) incremental loads with no significant difference in slab temperatures.

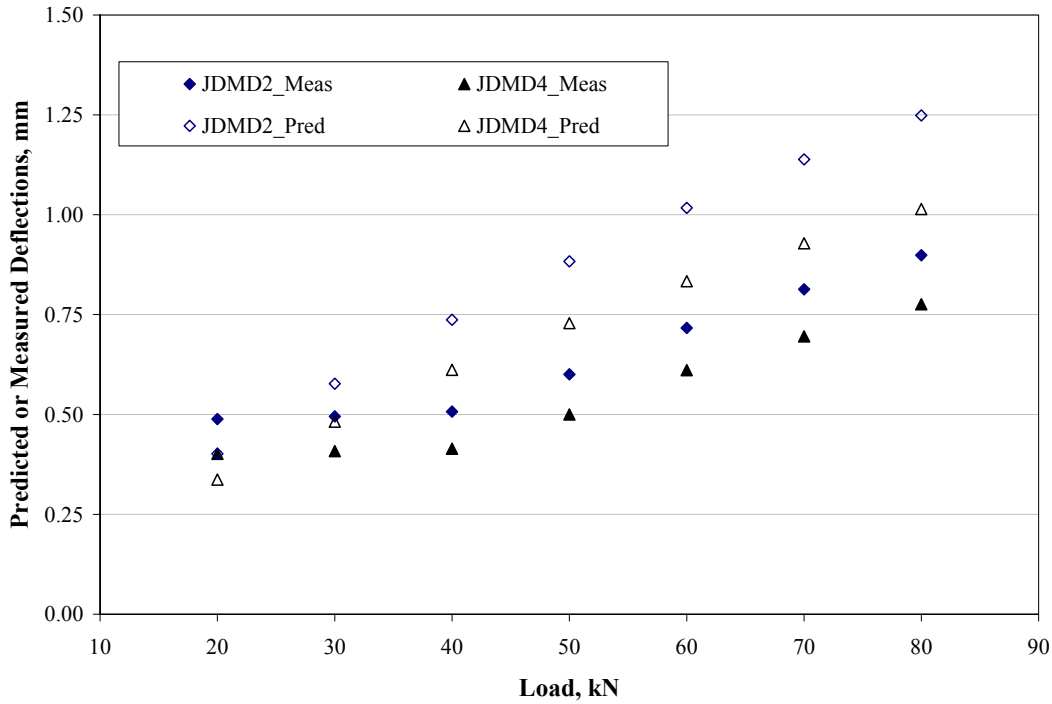

Figure 86. Comparisons of predicted and measured corner (JDMD2 and JDMD4) deflections for Section 538FD under the influence of 4,500–18,000 lb. (20-80 kN) incremental loads.

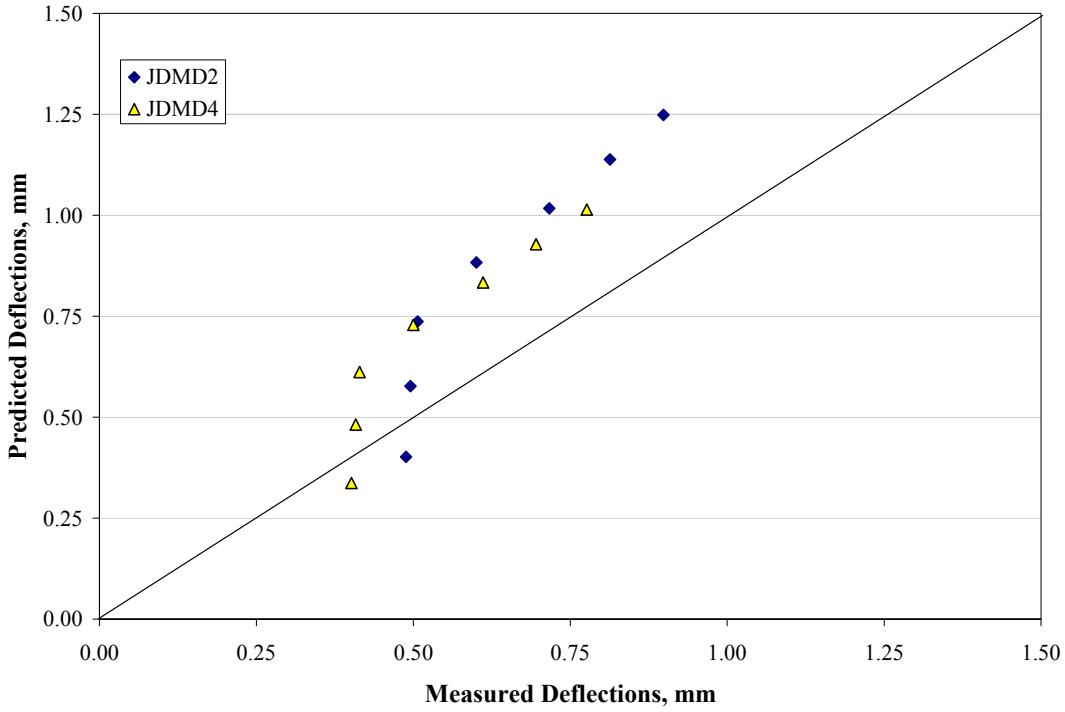

Figure 87. Predicted versus measured corner (JDMD2 and JDMD4) deflections for Section 538FD under the influence of 4,500–18,000 lb. (20–80 kN) incremental loads.

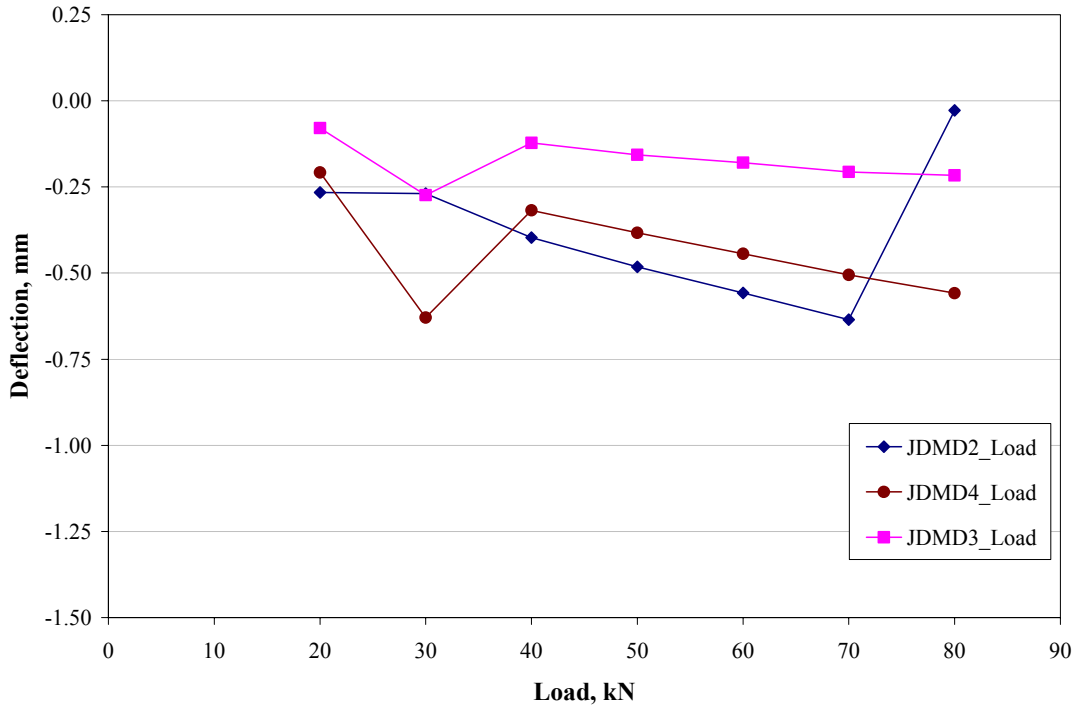

Figure 88. Corner (JDMD2 and JDMD4) and edge (JDMD3) deflections for Section 541FD under the influence of 4,500–18,000 lb. (20-80 kN) incremental loads with no significant difference in slab temperatures.

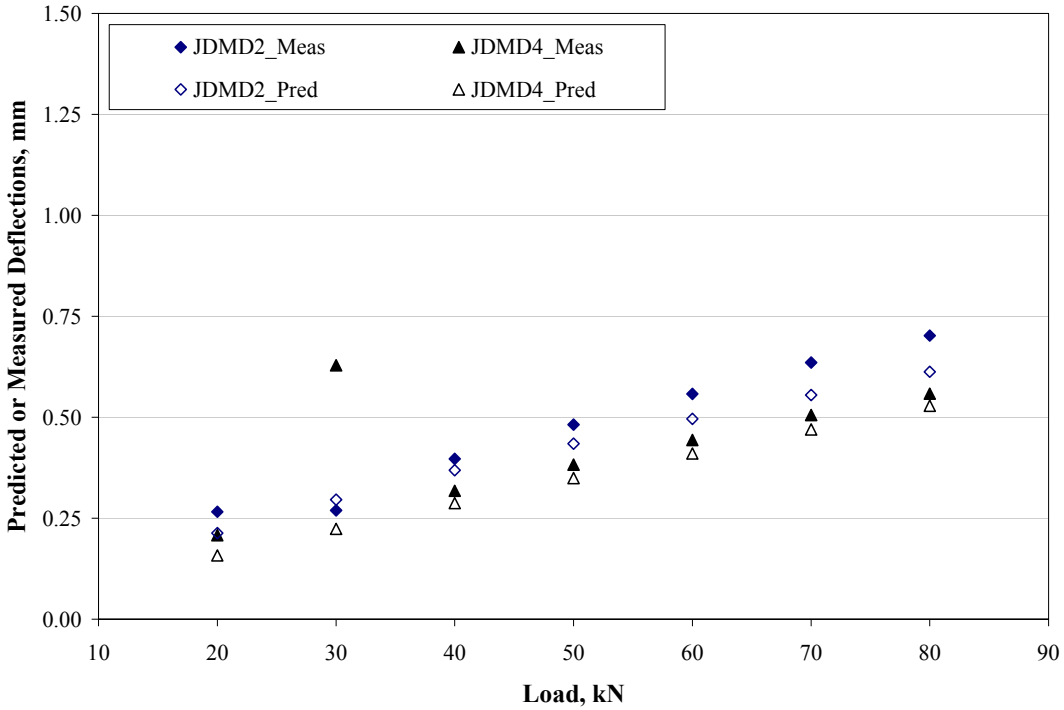

Figure 89. Comparisons of predicted and measured corner (JDMD2 and JDMD4) deflections for Section 541FD under the influence of 4,500–18,000 lb. (20-80 kN) incremental loads.

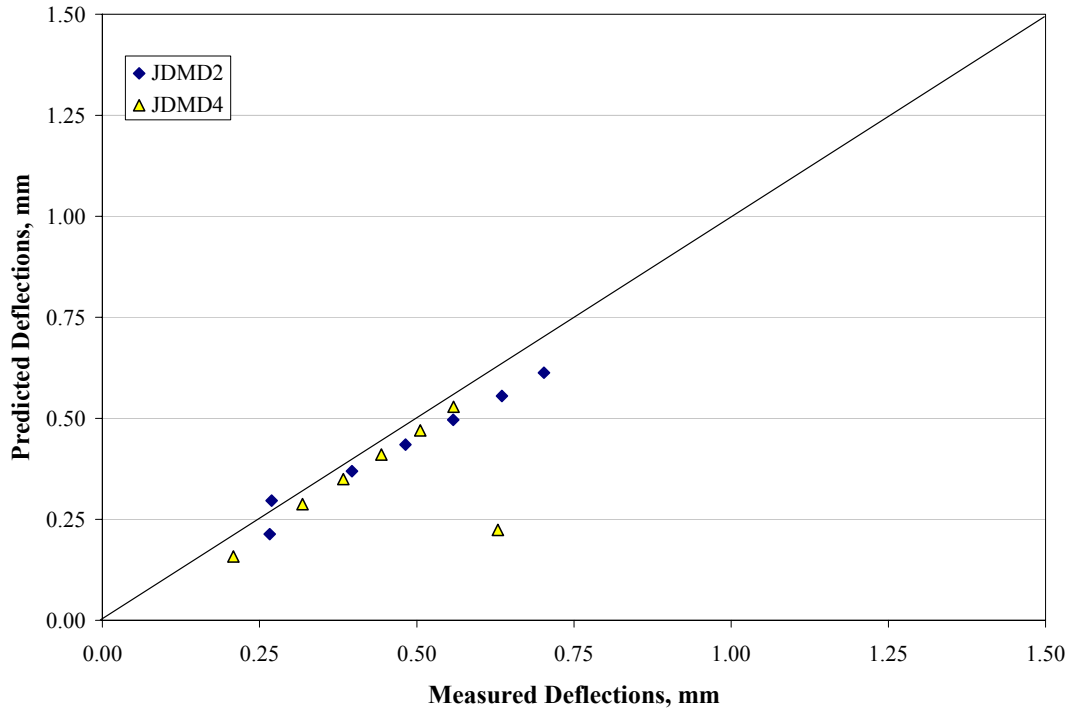

Figure 90. Predicted versus measured corner (JDMD2 and JDMD4) deflections for Section 541FD under the influence of 4,500–18,000 lb. (20–80 kN) incremental loads.

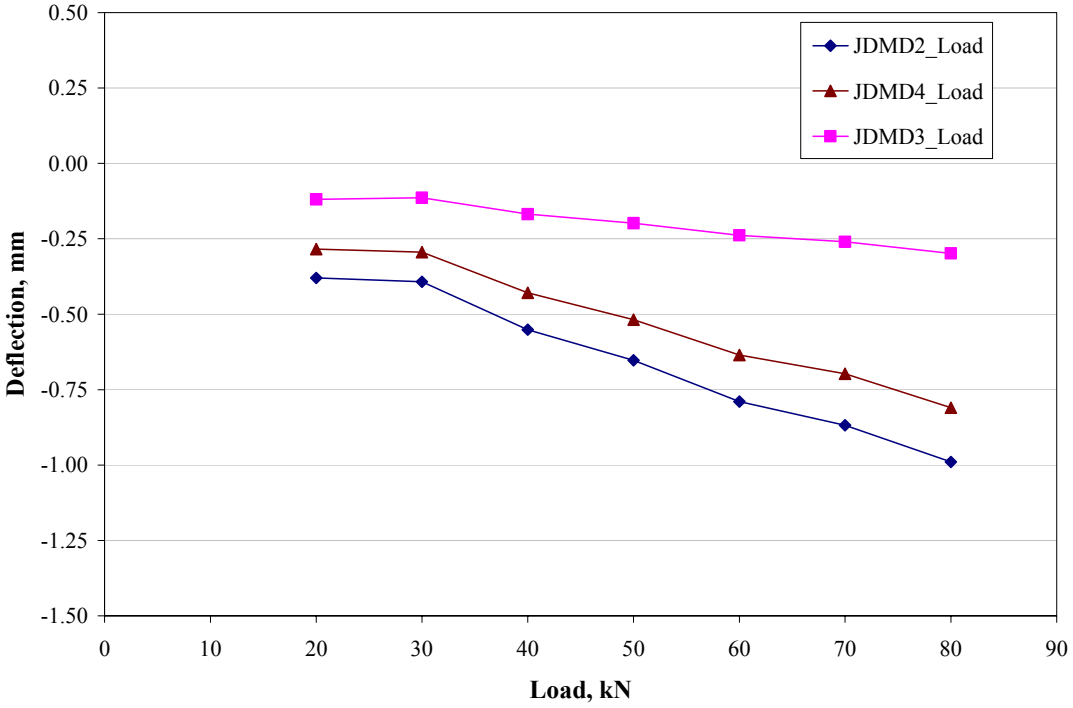

Figure 91. Corner (JDMD2 and JDMD4) and edge (JDMD3) deflections for Section 539FD under the influence of 4,500–18,000 lb. (20–80 kN) incremental loads with no significant difference in slab temperatures.

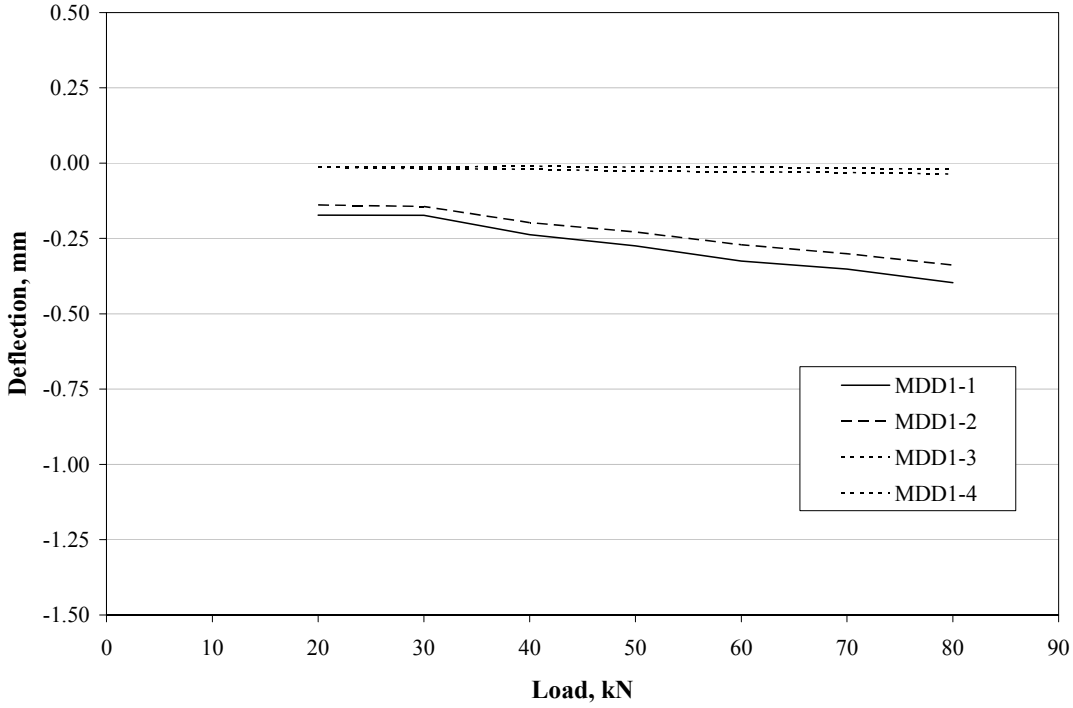

Figure 92. MDD deflections for Section 539FD under the influence of 4,500–18,000 lb. (20–80 kN) incremental loads with no significant difference in slab temperatures.

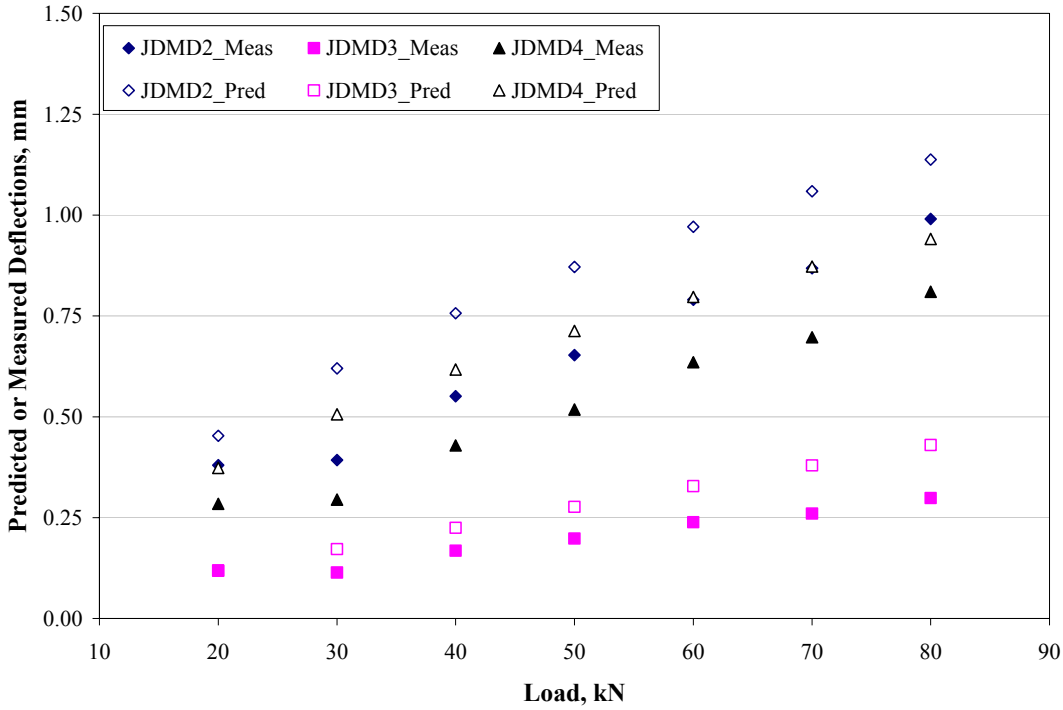

Figure 93. Comparisons of predicted and measured corner (JDMD2 and JDMD4) and edge (JDMD3) deflections for Section 539FD under the influence of 4,500–18,000 lb. (20–80 kN) incremental loads.

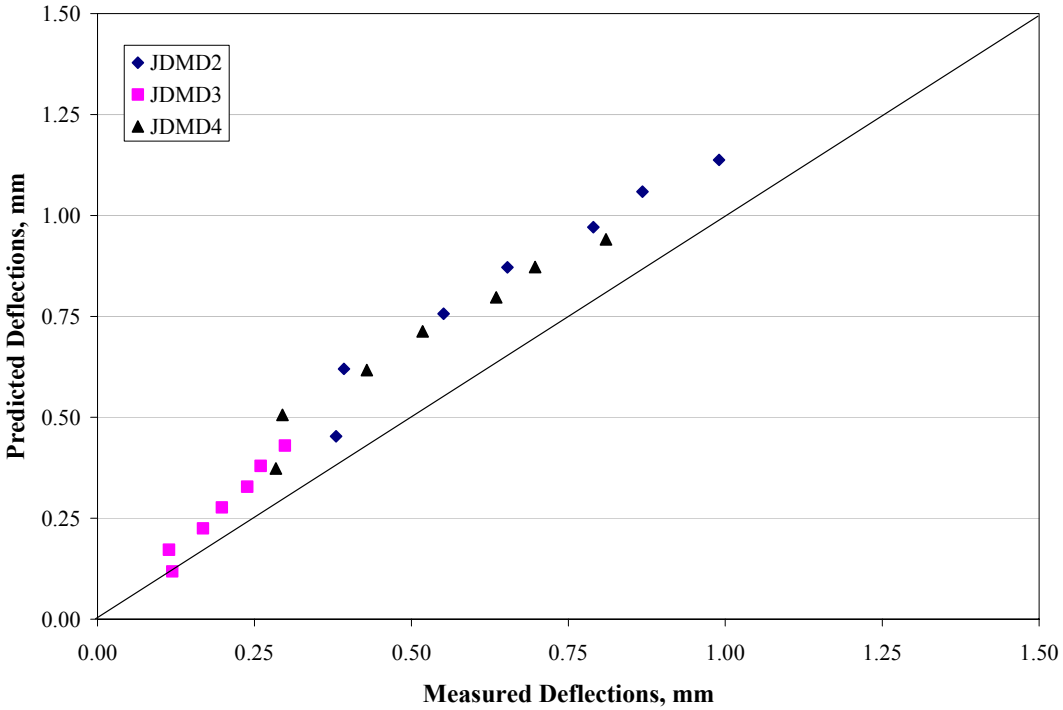

Figure 94. Predicted versus measured corner (JDMD2 and JDMD4) and edge (JDMD3) deflections for Section 539FD under the influence of 4,500–18,000 lb. (20–80 kN) incremental loads.

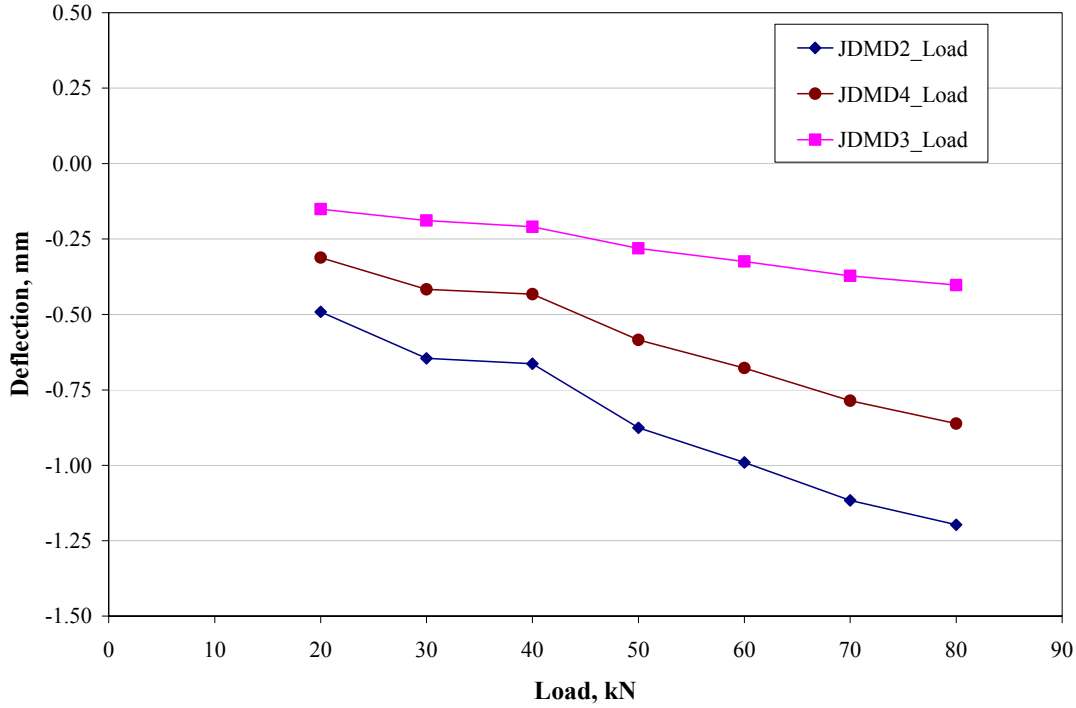

Figure 95. Corner (JDMD2 and JDMD4) and edge (JDMD3) deflections for Section 540FD under the influence of 4,500–18,000 lb. (20–80 kN) incremental loads with no significant difference in slab temperatures.

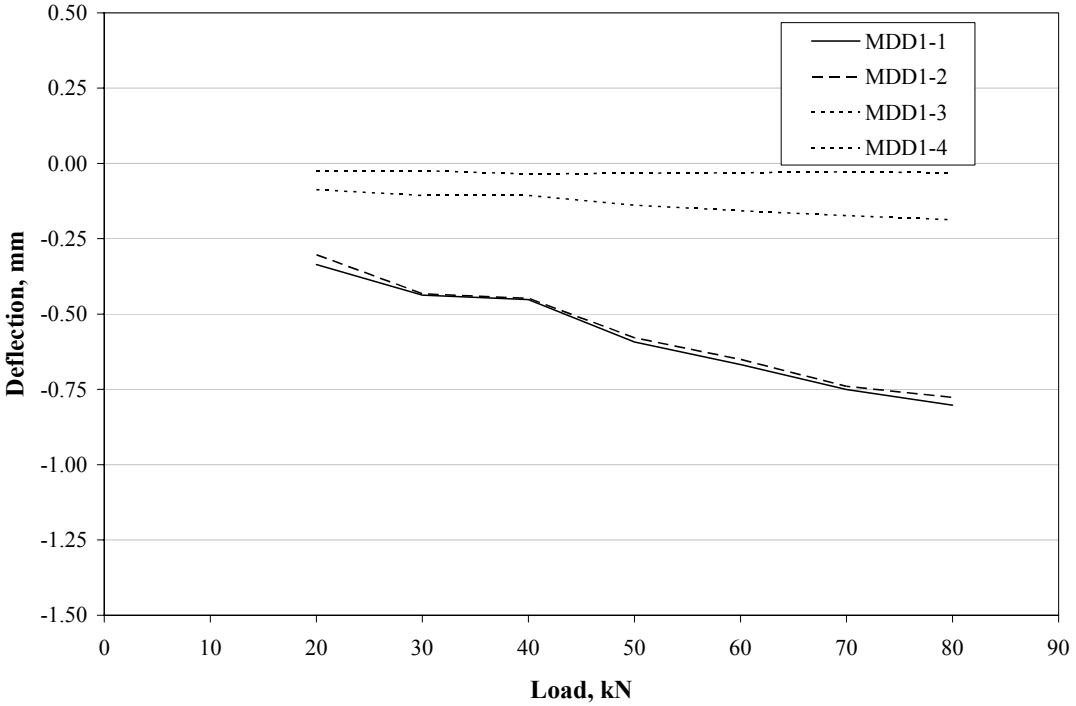

Figure 96. MDD deflections for Section 540FD under the influence of 4,500–18,000 lb. (20–80 kN) incremental loads with no significant difference in slab temperatures.

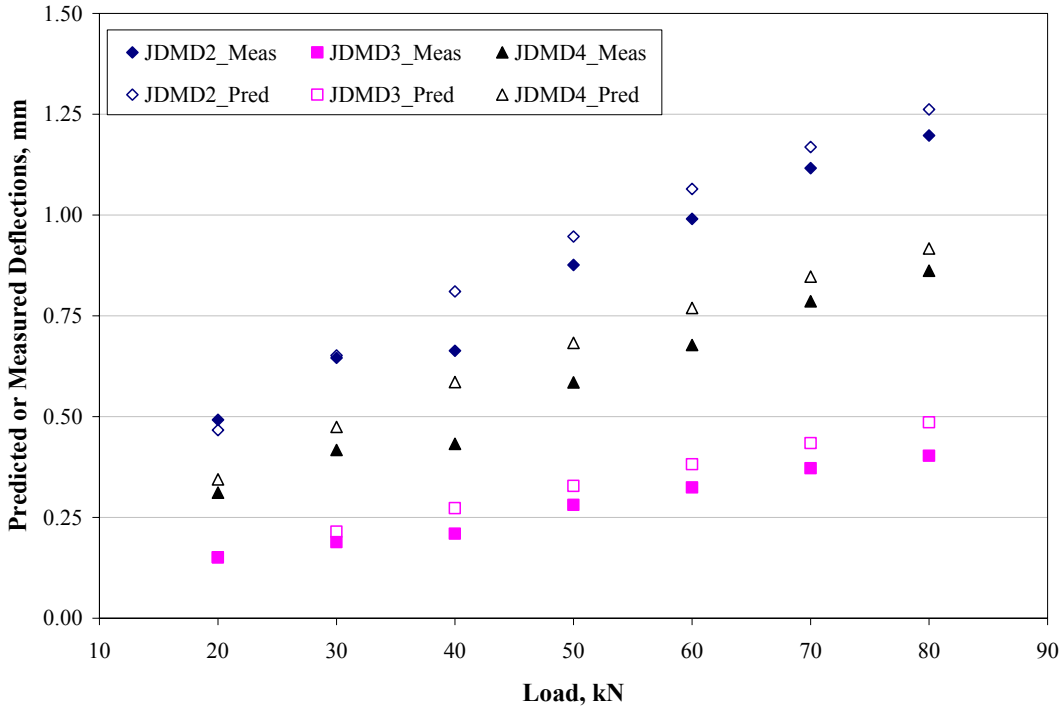

Figure 97. Comparisons of predicted and measured corner (JDMD2 and JDMD4) and edge (JDMD3) deflections for Section 540FD under the influence of 4,500–18,000 lb. (20–80 kN) incremental loads.

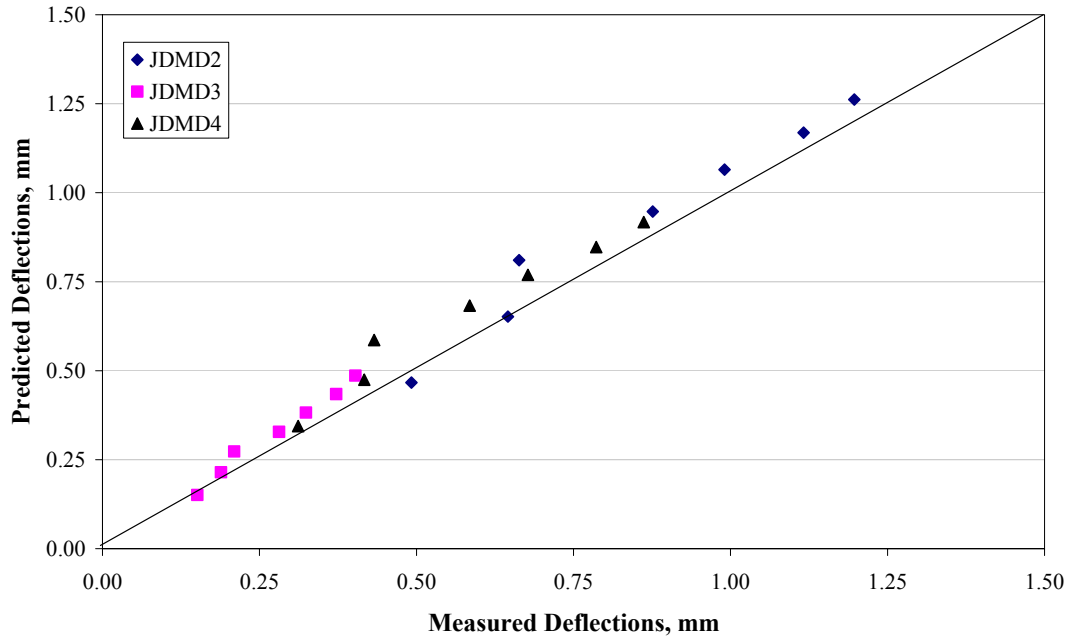

Figure 98. Predicted versus measured corner (JDMD2 and JDMD4) and edge (JDMD3) deflections for Section 540FD under the influence of 4,500–18,000 lb. (20-80 kN) incremental loads.

4.0 24-HOUR UNLOADED CORNER AND MIDSLAB EDGE DEFLECTIONS

Deflections resulting from daily temperature fluctuations were collected on the North Tangent test sections using JDMDs and MDDs without HVS loading. Corresponding vertical temperature profile data in the slab were collected using thermocouples embedded in the slab. The deflection and temperature data were collected approximately every two hours over the 24-hour cycle. The deflection results for Section 535FD are shown in Figures 99 through 101. The deflections in Figures 99 through 101 are presented relative to the first data point and not relative to the flat slab condition. The first data point may have significant curvature due to curling and therefore the plotted data is not a representation of the amount of curling in the slab.

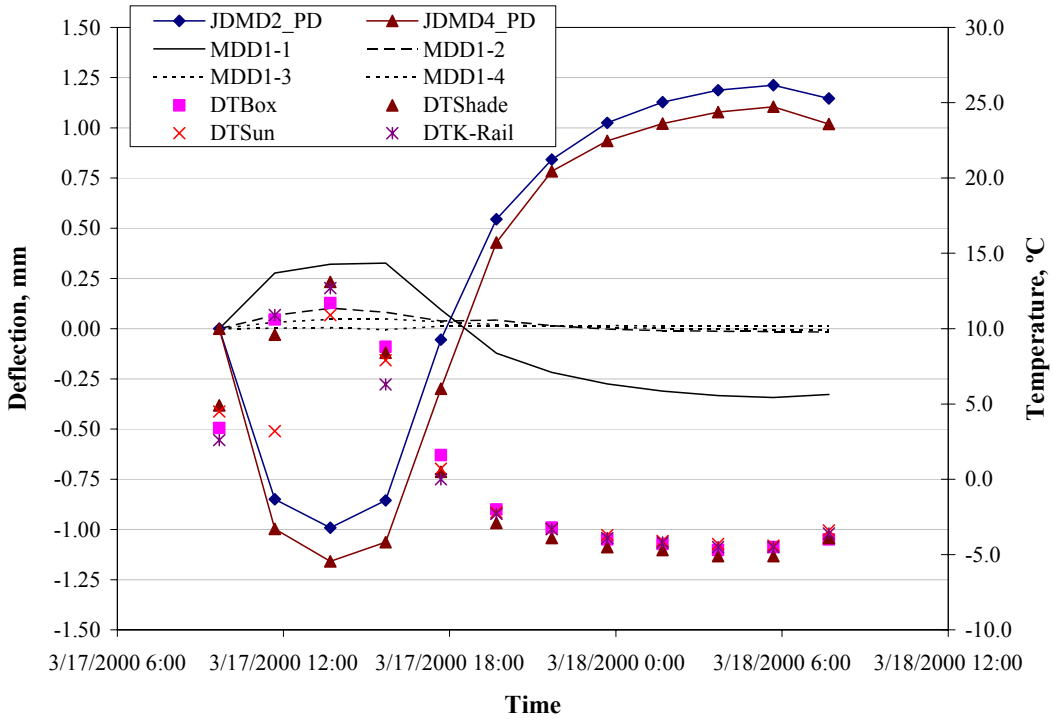

Figure 99. 24-hour unloaded slab (Section 535FD) deflections without HVS and without temperature control box plotted with temperature difference between the top sensor and the bottom sensor measured using thermocouple assemblies at various locations.

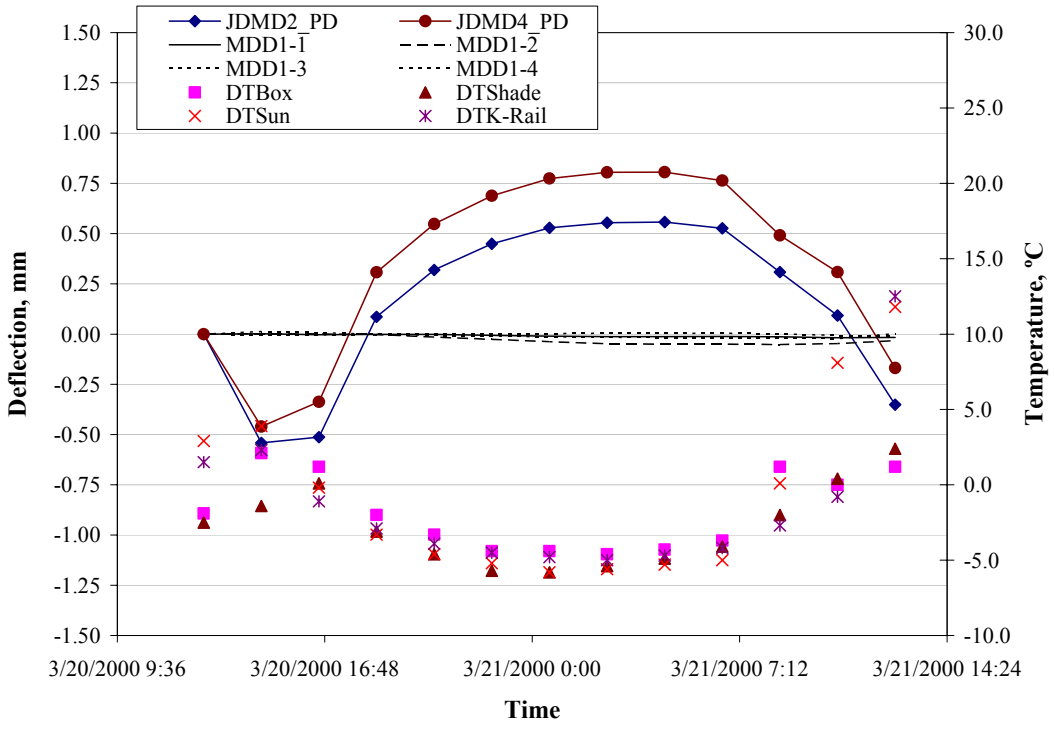

Figure 100. 24-hour unloaded slab (Section 535FD) deflections with HVS but without temperature control box.

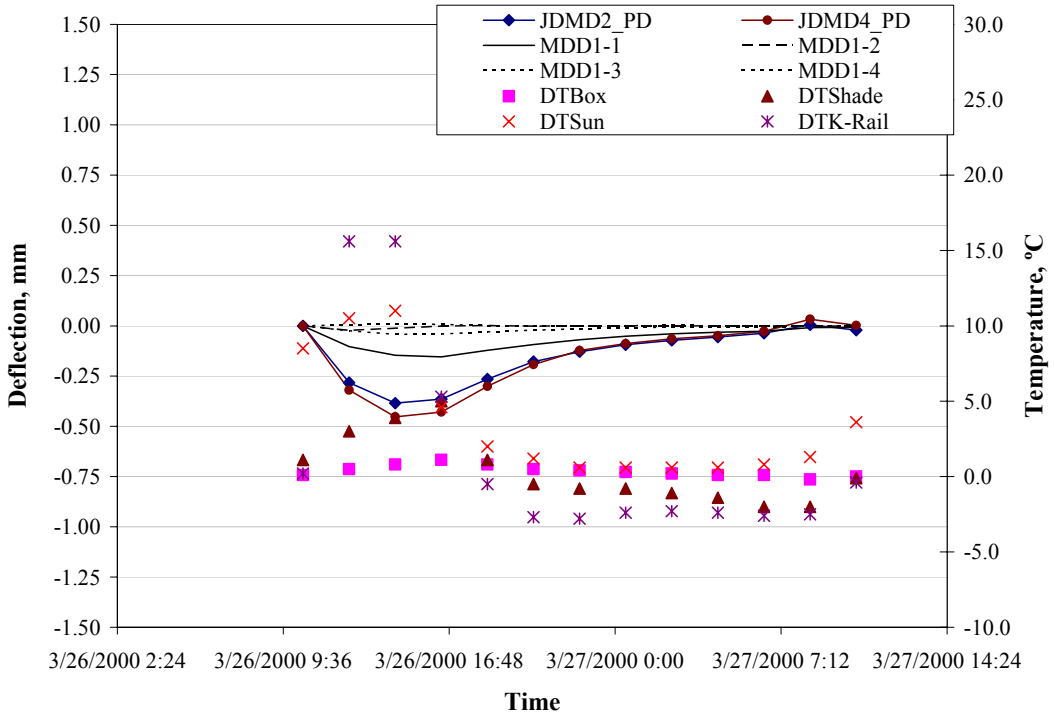

Figure 101. 24-hour unloaded slab (Section 535FD) deflections with HVS and with temperature control box.

Figure 99 shows the deflections with no HVS and no temperature control box. Figure 99 also shows the corresponding temperature difference between the top sensor and the bottom sensor of a thermocouple assembly measured at 4 different locations (box, shade, k-rail, and sun). The deflection at the three slab locations moved downward as the temperature difference increased, while the corner and edges moved upward as the temperature difference decreased. Corner deflections (JDMD2 and JDMD4) had similar deflection magnitude while the edge deflection (JDMD3) was smaller for the same change in temperature difference.

Figure 100 shows the deflections with the HVS but without the temperature control box. Figure 101 show the deflections with the HVS and with the temperature control box. The thermocouples in the slab under the temperature control box show very little change over the 24-hour period. However, the thermocouples in the shade and directly exposed to the sunlight showed greater variation of temperature difference over the 24-hour period. Even though the part of the slab corresponding to the JDMD locations was completely covered by the temperature control box, the JDMDs were affected by the temperature cycling of the exposed portion of the slab. The magnitude of corner and edge deformations was much less than the condition when no temperature box and HVS were present on the test section (Figure 99).

5.0 24-HOUR UNLOADED SLAB DEFLECTION ANALYSIS

The use of unloaded slab deflections to estimate EBITD using a finite element program requires a reference point for the analysis. The reference point has to be one for which the exact position of the slab (and the temperature difference across the slab) is known relative to the flat slab condition. The reference point could also be the JDMD reading corresponding to the flat slab condition. When collecting field data, it is not possible to easily identify a flat slab condition. The Palmdale data does not include such a reference point and therefore the raw deflections themselves could not be used to EBITD.

The range of the deflection data over the 24-hour cycle or the deflection relative to the first data point can also be used to estimate the EBITD instead of the absolute deflection measurement. This is illustrated in Figure 102, which shows the predicted relative slab corner deflections using EBITDs of 0ºF (0ºC), -18ºF (-10ºC), -45ºF (-25ºC), and -63ºF (-35ºC). By matching the ranges at different estimated values of EBITD to the measured range, an estimate of the EBITD can be obtained. However, this procedure can only be used when the EBITD magnitude is less than the range of the measured temperature difference (over the 24-hour cycle, typically around 25 to 35ºF (14 to 19ºC) for slabs exposed to ambient air/sunlight). When this is true, the slab comes in contact with the base at least once over the 24-hour cycle. If the EBITD is highly negative, then the slab corner never comes in contact with the base over the 24-hour cycle and the relative unloaded slab deflections cannot be used to estimate EBITD. This can be seen in Figure 102, where there is no significant difference between using -45ºF (-25ºC) EBITD, and -63ºF (-35ºC) EBITD (within field data margin of error) and either one of those could be the actual EBITD.

This is further illustrated in Figure 103, which shows the results of the analysis for JDMD4 (left corner deflection) for Section 535FD. The measured deflection range (difference

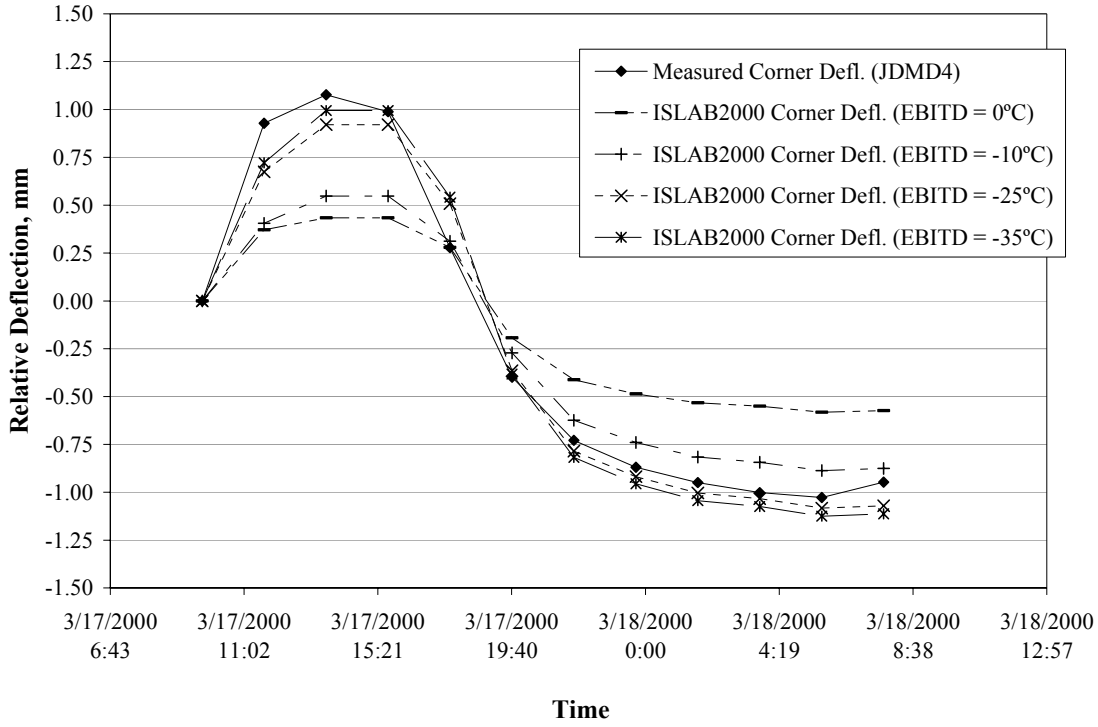

Figure 102. Predicted unloaded slab corner relative deflections assuming 0, -18, -45, and -63ºF (0, -10, -25, and -35ºC) effective built-in temperature difference and measured deflections (Section 535FD, JDMD4) under ambient conditions.

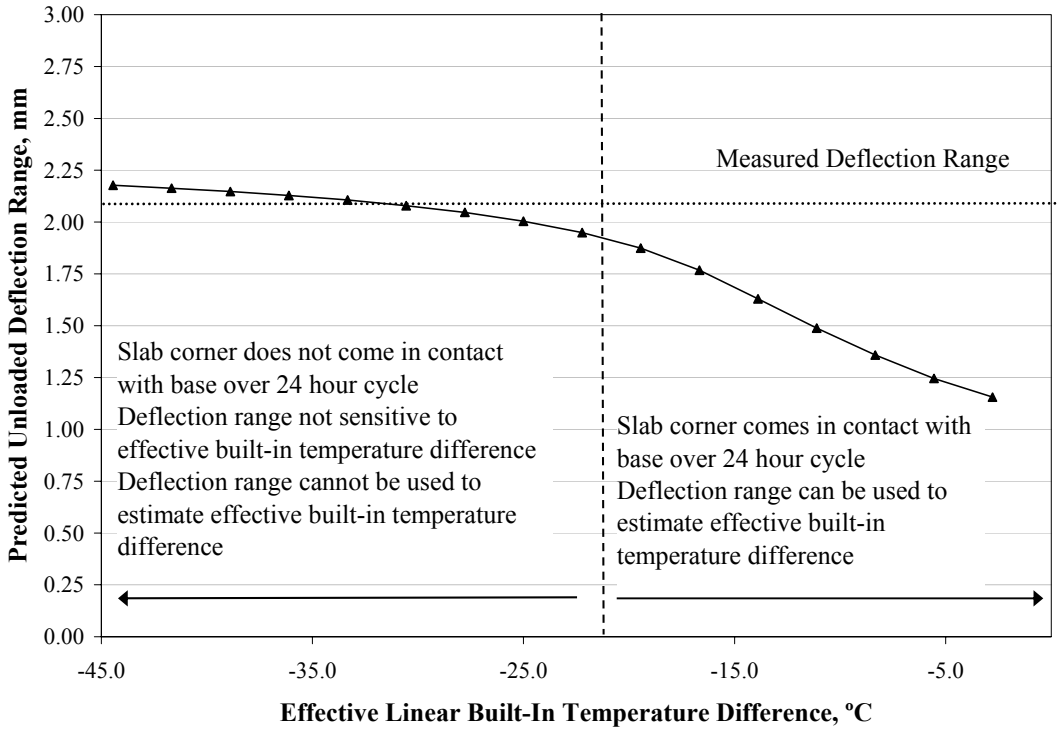

Figure 103. Predicted unloaded slab deflection range versus effective built-in temperature difference for JDMD4 (corner) of slab (Section 535FD).

between highest JDMD4 reading and lowest JDMD4 reading) is approximately 0.08 in. (2.03 mm). The predicted unloaded deflection range matches the measured unloaded deflection range at value of EBITD greater than 35ºF (19ºC). This is the flat part of the curve and EBITD cannot be confidently estimated because small measurement errors result in large changes in EBITD. In other words, if a slab never comes in contact with the base over a 24-hour unloaded cycle, a slab warped due to the EBITD will deflect approximately the same amount due to daily variations in temperature regardless of the extent of warping. It is important to note that Figures 102 and 103 are specific to the conditions for the analysis of JDMD4 of Section 535FD and do not present general plots applicable to all pavements under all conditions. Results will vary for other slab structures, support conditions, load transfer, and joint spacing, etc., and even different values of maximum temperature difference and minimum temperature difference for the same slab.

Many of the North Tangent sections have large EBITD (as evidenced by the analysis presented in Section 3) and therefore the unloaded slab deflections cannot be used to estimate EBITD for this site. In these cases, the unloaded slab deflections however do provide an estimate of the minimum amount of EBITD in the slab.

6.0 HWD ANALYSIS OF CORNER DEFLECTIONS

Heavy weight deflectometer (HWD) data was collected on the North Tangent sections at three different load levels (low, medium, and high) at the leave corner of the slab. The low load level was on the order of 9,000 to 10,000 lb. (40–44 kN), medium level on the order of 14,000 to 16,000 lb. (62–71 kN), and the high load level on the order of 19,000 to 21,000 lb. (85–93 kN). ISLAB2000 was used to calculate the estimated deflections (beneath the load plate) due to the HWD loads at the leave corner of the test slab for a range of EBITD values. Since no thermocouple data was available during the HWD data collection, the linear temperature difference in the slab was estimated based on air temperature, slab surface temperature, and time of day. The EBITD value corresponding to a match between the ISLAB2000 predicted deflection and the measured deflection is the estimated EBITD value. The results of this analysis are shown in Table 11.

Table 11 Estimated Effective Built-In Temperature Difference (right corner) from JDMD Analysis (Previous Section) and from HWD Analysis

	Effective Built-In Temperature Difference at Load, ºF (ºC)				
Section ID	**JDMD (Predicted)**	**HWD (Low Load)**	**HWD (Medium Load)**	**HWD (High Load)**	**HWD (Average)**
535FD	-39.2 (-21.8)	-40.9 (-22.7)	-40.3 (-22.4)	-41.1 (-22.8)	-40.8 (-22.7)
537FD	-19.6 (-10.9)	-17.0 (-9.4)	-17.8 (-9.9)	-18.5 (-10.3)	-17.7 (-9.8)
538FD	-33.3 (-18.5)	-31.2 (-17.3)	-32.0 (-17.8)	-33.0 (-18.3)	-32.1 (-17.8)
539FD	-23.4 (-13.0)	-28.8 (-16.0)	-28.7 (-15.9)	-30.3 (-16.8)	-28.6 (-15.9)
540FD	-30.8 (-17.1)	-22.4 (-12.4)	-23.6 (-13.1)	-24.4 (-13.6)	-23.5 (-13.1)
541FD	-15.3 (-8.5)	-38.0 (-21.1)	-38.3 (-21.3)	-40.8 (-22.7)	-39.4 (-21.9)

The results show good agreement between EBITD estimated using JDMD deflections and HWD deflections for Section 535FD, 537FD, and 538FD. The results of the widened lane Sections 539FD through 541FD have a greater amount of difference between the HWD estimate and the JDMD estimate. It should be noted that the HWD data was collected several years after the 24-hour 9,000 lb. (40 kN) loaded analysis and after fatigue testing of the slabs. The most significant difference was in Section 541FD where higher corner HWD deflections were observed likely due to more differential shrinkage and there were no failure cracks during HVS trafficking.

7.0 CONCLUSIONS

The cumulative effect of built-in temperature gradient, shrinkage, and creep for analysis purposes can be defined as an effective built-in temperature difference, (EBITD). The EBITD is a linear temperature difference between the top and bottom of a concrete slab that produces the same deflection response as the cumulative effects of non-linear built-in temperature gradient and non-linear shrinkage gradient reduced over time by creep. Factors affecting estimated EBITD include curing, climatic conditions during construction, material properties, structural properties, support conditions, and restraints (from adjacent slabs and base friction), many of which can vary from one slab location to another. This variation contributes to a large extent to differences in deflections between two corners of a slab and consequently differences in cracking patterns between two joints and or corners of the same slab (e.g. slabs with single corner breaks).

EBITD could not be accurately predicted if the slab (corner or edge location) came into contact with the base during the 24-hour loading cycle. If the slab had a large negative curvature and the analysis location (corner or edge) did not come in contact with the base over the 24-hour loading cycle, then the slab deflection was used to estimate the EBITD.

EBITD varied considerably among the sections analyzed. The Palmdale test slabs were constructed using fast-setting high-early-strength concrete under desert conditions and daytime construction. These conditions result in high EBITD values [-35 to -65ºF (-19.4 to -36.1ºC)] for sections with low restraint (e.g., Section 535FD with no dowels or tied concrete shoulders) and low to moderate EBITD values [0 to -35ºF (0 to -19.4ºC)] for sections with high restraint (e.g., 539FD to 541FD, widened lane sections with dowels at the transverse joints). These magnitudes of EBITD are in line with those observed by other researchers.(*5, 12, 21*).

The EBITD also varied from one corner of the slab to the other. On all sections, the corners of the slab had a higher EBITD compared with the mid-slab edge. The MDD analysis

showed a slight reduction in EBITD going from the slab edges to the interior of the slab. The excessive EBITD results in corner cracks at the side of the slab with the higher EBITD.

An analysis of deflections using incremental loading from 4,500 to 18,000 lb. (20-80 kN) and independent deflection measurements in the wheel path verified the magnitude of the EBITD calculated from the corner and edge analysis for several of the test sections. For other test sections, inaccuracies in measurement of load levels could be responsible for discrepancies at some load levels.

The results of the HWD analysis showed good agreement between EBITD estimated using JDMD deflections and HWD deflections for three of the six sections. The results of the widened lane sections have a greater amount of difference between the HWD estimate and the JDMD estimate. It should be noted that the HWD data was collected several years after the 24-hour 9,000-lb. (40-kN) loaded analysis and after fatigue testing of the slabs. The estimated values of EBITD using HWD deflections ranged from -17.7 to -40.8ºF (-9.8 to -22.7ºC).

8.0 REFERENCES

1. Roesler, J. R., Scheffy, C. W., Ali, A., and Bush, D. *Construction, Instrumentation, and Testing of Fast-Setting Hydraulic Cement Concrete in Palmdale, California*. Report prepared for California Department of Transportation. Pavement Research Center, Institute of Transportation Studies, University of California Berkeley. 2000.

2. du Plessis, L. *HVS Test Results on Fast-Setting Hydraulic Cement Concrete, Palmdale, California Test Sections, North Tangent*. Draft Report prepared for California Department of Transportation. Pavement Research Center, Institute of Transportation Studies, University of California Berkeley. 2002.

3. Armaghani, J. M., Larsen, T. J., and Smith, L. L. "Temperature Response of Concrete Pavements." Transportation Research Record 1121, National Research Council, Washington, DC, 23-33. 1986.

4. Choubane, B. and Tia, M. "Nonlinear Temperature Gradient Effect on Maximum Warping Stresses in Rigid Pavements." Transportation Research Record 1370, National Research Council, Washington, DC, 11–19. 1992.

5. Yu, H. T., Khazanovich, L., Darter, M. I., and Ardani, A. "Analysis of Concrete Pavement Responses to Temperature and Wheel Loads Measured from Instrumented Slabs." Transportation Research Record 1639, National Research Council, Washington, DC, 94–101. 1998.

6. Janssen, D. J. "Moisture in Portland Cement Concrete." Transportation Research Record 1121, National Research Council, Washington, DC, 40-44. 1986.

7. Mather, B. "Reports of the Committee on Durability of Concrete – Physical Aspects – Drying Shrinkage." Highway Research News, 26-29. 1963.

8. Washa, G. W. "Volume Changes and Creep." Significance of Tests and Properties of Concrete and Concrete Aggregates, STP-169, ASTM, Philadephia, 115-128. 1955.

9. Suprenant, B. A. "Why Slabs Curl – Part I." Concrete International, March 2002, 57-61.

10. Suprenant, B. A. "Why Slabs Curl – Part II." Concrete International. April 2002, 59-64.

11. Schmidt, S. *Built-In Curling and Warping in PCC Pavements*. M. S. Thesis, University of Minnesota. 2000.

12. Rao, C., Barenberg, E. J., Snyder, M. B., Schmidt, S. "Effects of Temperature and Moisture on the Response of Jointed Concrete Pavements." Proceedings, 7th International Conference on Concrete Pavements – Orlando, Florida, USA. 2001.

13. Altoubat, S. A. and Lange, D. A. "Creep, Shrinkage, and Cracking of Restrained Concrete at Early Age." ACI Materials Journal, Vol. 98, 323-331. 2001.

14. Ytterberg, R. F. “Shrinkage and Curling of Slabs on Grade, Part I – Drying Shrinkage.” Concrete International, Vol. 9, No. 4, 22-31. 1987.

15. Ytterberg, R. F. “Shrinkage and Curling of Slabs on Grade, Part II – Warping and Curling.” Concrete International, Vol. 9, No. 5, 54-61. 1987.

16. Ytterberg, R. F. “Shrinkage and Curling of Slabs on Grade, Part III – Additional Suggestions.” Concrete International, Vol. 9, No. 6, 72-80. 1987.

17. Tremper, B. and Spellman, D. L. “Shrinkage of Concrete – Comparison of Laboratory and Field Performance.” Highway Research Record 3, National Research Council, Washington, DC, 30–61. 1963.

18. Poblete, M., Salsilli, R., Valenzuela, A., and Spratz, P. “Field Evaluation of Thermal Deformations in Undowelled PCC Pavement Slabs.” Transportation Research Record 1207, National Research Council, Washington, DC, 217–228. 1987.

19. du Plessis, L., Bush, D., Jooste, F., Hung, D., Scheffy, C., Roesler, J., Popescu, L., and Harvey, J. *HVS Test Results on Fast-Setting Hydraulic Cement Concrete, Palmdale, California Test Sections, South Tangent*. Report Prepared for California Department of Transportation. 2002.

20. Khazanovich, L., Yu, H. T., Rao, S., Galasova, K., Shats, E., and Jones, R. *ISLAB2000 – Finite Element Program for Rigid and Composite Pavements, User’s Guide*. ERES Consultants, Champaign, IL. 2000.

21. Byrum, C. R. “Analysis by High-Speed Profile of Jointed Concrete Pavement Slab Curvatures.” Transportation Research Record 1730, National Research Council, Washington, DC, 1–9. 2000.

22. Heath, A. and J. Roesler. *Shrinkage and Thermal Cracking of Fast Setting Hydraulic Cement Concrete Pavements in Palmdale, California*. Draft report prepared for California Department of Transportation. Pavement Research Center, CAL/APT Program, Institute of Transportation Studies, University of California, Berkeley. 1999.